MULTI-SCALE ASSESSMENT AND SIMULATION OF SEDIMENT BIOGEOCHEMICAL CYCLES IN COASTAL AREAS: IMPLICATIONS FOR ECOSYSTEM FUNCTIONING AND PROVISION OF SERVICES

by

Francisco J. Bravo Avendaño

Submitted in partial fulfillment of the requirements
for the degree of Doctor of Philosophy

at

Dalhousie University
Halifax, Nova Scotia
August 2017

To Martín and my family

TABLE OF CONTENTS

LIST OF TABLES

LIST OF FIGURES

ABSTRACT

Marine coastal sediments and associated communities provide benefits to humans through natural processes such as nitrate removal via denitrification (prevention or mitigation of eutrophication), burial of toxic substances (pollution control), and sediment stabilization (coastal protection). However, sediments can also have negative impacts on the environment, for example throughout the production of toxic hydrogen sulfide, and emission of greenhouse gases (CH_4, N_2O). Understanding sediment biogeochemical cycles in coastal areas and responses to natural and anthropogenic forcing can provide important insight into the functioning of marine coastal ecosystems, as well as tools to manage positive (desired) and negative (undesired) interactions with human systems.

This thesis aimed to explore the linkages and interactions among biological, geochemical and human systems in coastal sediments at sub-seasonal and meter to kilometer scales. Two major projects were conducted. The first project focused on understanding (**Chapter 2**) and predicting (**Chapter 3**) the patterns of, and controls on the C and N cycling in sediments of two shallow coastal systems of Nova Scotia, Canada. The second project focused on the study of aquaculture – sediment interactions, particularly, on the modeling and prediction of the deposition, degradation, and accumulation of organic wastes in sediments underlying fish farm cages (**Chapter 4**).

The integration of statistical and deterministic modeling, field and laboratory observations, and benthic habitat mapping provided a means to study benthic processes at multiple spatial scales. Results of **Chapter 3 and 4** highlight the important role of habitat diversity and sediment-biological interactions (e.g., autotrophic activity) on diagenetic processes in coastal sediments. **Chapter 4** provided new conceptual and modeling tools to manage aquaculture-sediment interactions in coastal areas.

LIST OF ABBREVIATIONS AND SYMBOLS USED

Abbreviation	Description
$\Delta N_2/Ar$	Saturation normalized N_2/Ar ratio
AC-O_2	Assimilative capacity based on oxygen criteria
AC-S^{2-}	Assimilative capacity based on sulfide criteria
A-MSM	photic sediment in mud to sandy-mud
Annamox	anaerobic ammonium oxidation
ANOVA	analysis of variance
A-SMS	photic sediment in sand to muddy-sand
BA	Bare aphotic sediments
BMA	Benthic microalgae
BP	Photic sediment in shallow areas
BP	Bare sediments in photic areas
C_{BMA}	Carbon in benthic microalgae
C_{EPS}	Carbon in extracellular polymeric substances
Chl-a	Chlorophyll-a
CHN	Carbon, Hydrogen, and Nitrogen
C_{org}	Organic carbon
C_{POC1}	Labile particulate organic carbon
C_{POC2}	Refractory particulate organic carbon
DIC	Dissolved inorganic carbon
DIN	Dissolved inorganic nitrogen
DIP	Dissolved inorganic phosphorus
DIR_{AM}	Depth-integrated ammonification rate
DIR_{DF}	Depth-integrated canonical denitrification rate
DIR_{NI}	Depth-integrated nitrification rate
$DIR_{OR\text{-}SR\text{-}MR}$	Depth-integrated carbon degradation rates
DNF	Denitrification
DNRA	Dissimilatory nitrate reduction to ammonium
DOM	Dissolved organic matter
DON	Dissolved organic nitrogen
EPS	Extracellular polymeric substances
FCR	Feed conversion ratio
FF	Fish farm sediments
GC-FID	Gas chromatographic flame ionization detector

GIS	Geographical Information System
HSD	Tukey's honestly significant difference test
K_v	Controlling factor of biological transport
KW	Kruskal–Wallis test
k_{waste}	Erodibility constant of organic wastes
LLWLT	Lower Low Water Large Tide
LOI	Loss on ignition
MIMS	Membrane Inlet Mass Spectrometry
N_{BMA}	Nitrogen in benthic microalgae
NEM	Net Ecosystem Metabolism
N-fixation	Nitrogen fixation
NH_3	Concentration of total inorganic ammonia expressed as nitrogen
NO_3	Concentration of total dissolved inorganic nitrate and nitrite express as nitrogen
PAR	Photosynthetically Active Radiation
PCA	Principal Components Analysis
PF_{Bac}	Partitioning factor of bacterial activity
PJ	Port Joli
PLS	Partial least squares regression analysis
P-M&S	Bare photic sediments
POC	Particulate Organic Carbon
PQ	Benthic light photosynthetic quotient
RMS	Root-Mean-Square (RMS) error
RQ	Benthic dark respiratory quotient
SB	Seagrass beds
SH	Shelburne Harbour
SL	Sediment layer
TA	Total alkalinity
τ_{ce}	Critical bed shear stress for resuspension
τ_{cd}	Critical bed shear stress for deposition
τ_u	Bed shear stress
TIN	Total inorganic nitrogen
TOE	Total oxygen exchange
u_*	Shear velocity
WC	Water column
z_0	Bed roughness
u_{WC}	Free-stream current velocity

ACKNOWLEDGEMENTS

This study was supported by funds to Jon Grant as the NSERC-Cooke Industrial Research Chair in Sustainable Aquaculture, and to Francisco Bravo by the scholarship program BECASCHILE for doctoral studies. Likewise, this research was possible due to support from the Advanced Computing Research in Atlantic Canada (ACENET).

This thesis could not be completed without the moral and logistic support of many friends, colleagues, staff of the Oceanography department, and family. I thank to Jeff Barrel, Lindsay Brager, Michelle Simone, Zeyu Zhang, Danni Harper, William Burt, Juan Antonio Manriquez, Nadine Lehmann, Kevin Sorochan, Angela Kuhn, Angela Fuentes, Myriam Lacharité, Jorge Urrego, Siggy Laupus, Berta Biescas, Anna Huguet, Raymond Garland (and his crew), Monica Bravo, Patricia Granados, Owen Brown, Robert Richards, Ross Dickson, Tamara Cantrill, Sharon Bellefontaine, Lori Lawton, Ramon Filgueira, and Bernard Boudreau, and the staff at the main office of the Department of Oceanography. I would also like to thank my parents, Eduardo and Loreto, and siblings, Eduardo y Constanza, who have supported me unconditionally through this journey. To my son, Martín, who in the distance, has been a light in my way.

Special thanks to my supervisor, Jon Grant, for allowing me to pursue my research interests, and for his unconditional support throughout all these years. I also thank my advisory committee and external reviewers for their valuable suggestions: Christopher Algar, Vladimir Kostylev, Anna Metaxas, Helmuth Thomas, Melisa Wong, and Tony Walker.

Lastly, thanks to Mariana Paludi, whom with patient provide support and care during the last stages of this Ph.D. I hope to continue walking this life in your company.

CHAPTER 1. INTRODUCTION

1.1 Dynamic of coastal sedimentary environments

Despite their tendency, natural systems are rarely at steady state. They are permanently evolving in response to variations in natural or anthropogenic forcing. The time required to reach equilibrium can be described as a function of the scale of perturbations, the capacity of the system to deal with perturbations (ecosystem resilience), and the position of the system in respect to equilibrium (Holling 1973, Gunderson 2000, Walker et al. 2004, Zirino et al. 2013).

Coastal areas are extremely dynamic environments. Compared with more stable deep-sea environments, coastal areas are characterized by varying temperature, chemistry, and hydrodynamic conditions. As a result, benthic diversity and their contribution to energy and matter cycling vary significantly in time, as well as across different sedimentary environments (e.g., estuaries, deltas, beaches, and tidal flats, etc.). Capturing relevant scales of variability of benthic activity (respiration, nutrient uptake, and regeneration, etc.) is crucial to connect local and ecosystem-scale processes, as well as to support management and protection of coastal systems. In shallow benthic environments (< 200 meters depth), this requires specific consideration of the habitat composition, sediment-biological interactions, and the benthic coupling (i.e., interconnections) with terrestrial and water column environments.

Atlantic Canada features a rich variety of structured and unstructured benthic habitats, including among others; vegetated beds (e.g., with seagrasses, macroalgae, benthic microalgae (BMA) and salt marsh plants), shellfish beds, and bare sediments of different grain size. Bare sediments are the spatially dominant habitat type, being the common in most coastal margins worldwide. Coastal features resulting from the tidal-wave action and long-shore circulation include tidal channels, sand bars, and shoals (e.g., sandbars) in intertidal and subtidal zones. Eelgrass beds are highly productive coastal habitats that provide multiple ecological functions, including nutrient cycling, carbon storage/sequestration, habitat provision, sediment stabilization, and shoreline protection (Duarte 2002). As a result of the non-substitutive nature of eelgrass (*Z. marina*) as

structuring organisms of sand/mud flats, this species is currently considered as an Ecologically Significant Species (ESS) in eastern Canada (DFO. 2009, Joseph et al. 2013).

1.2 Ecosystem services and ecological functions of coastal sediments

Marine coastal sediments and associated life (known as the benthos) provide multiple ecosystem functions and services including food production, coastal protection, nutrient cycling, and pollution control (Costanza et al. 1998, Costanza 1999, Vance-Harris & Ingall 1999, Brown, McGreer, et al. 2011). Ecological functions are the processes responsible for maintaining the structure and composition of ecological communities, and may be referred to as ecosystem properties (Hooper et al. 2005). Similarly, Noss (1990) defined a function as 'ecological and evolutionary processes, including gene flow, disturbance, and nutrient cycling.'. Ecosystem services are sets of ecosystem functions that benefit humans (Costanza et al. 1998, de Groot et al. 2002, MEA 2005). Ecosystem services and ecological functions, referred to as ecosystem processes, are central concepts in this research, as they facilitate the incorporation of ecological and oceanographic science into Ecosystem-Based Management (EBM).

1.3 Nutrient and organic carbon recycling in coastal sediments

Due to the strong benthic-pelagic coupling in coastal areas, a significant fraction of carbon and nutrient cycling, storage and sequestration are carried out in the benthic compartment. As a consequence benthos play a considerable role in coastal health and biogeochemical cycles (Jahnke 2005, Middelburg et al. 2005, Muller-Karger et al. 2005, Seiter et al. 2005).

The cycling of C and nutrients is mostly the result of the net rates of consumption and production by autotrophic and heterotrophic organisms. Heterotrophic benthic communities are responsible for the mineralization of organic matter, as well as the regeneration of nutrients, which support biological production over wider areas. In contrast, autotrophic communities in littoral sediments (e.g., eelgrass and benthic microalgae) produce and release O_2 and fix inorganic compounds (DIC, DIN, DIP, and N_2), retaining energy, and matter in the system.

Nutrient and C removal in sediments is carried out by a series of redox reactions. Under well-oxygenated conditions, organic C is oxidized mostly by aerobic respiration. Simultaneously, different anaerobic pathways operate in deeper strata where O_2 is not available. Alternative electron acceptors (NO_3^-, MnO_2, Fe_2O_3, and SO_4^{2-}) are used sequentially in order of increasing Gibbs free energy. In marine environments, sulfate reduction can be the dominant metabolic pathway of organic C oxidation due to its relatively high availability relative to other more favorable electron acceptors as nitrate and iron oxide (Welsh et al. 1996).

A number of microbial reactions and physical processes also contribute to N cycling in coastal sediments. **Figure 1** shows the major pathways of N cycling in surface sediments. Denitrification (DNF) and burial via bioturbation are the two most important internal sinks of N from coastal waters (Pätsch & Kühn 2008), while the largest source of inorganic nitrogen is organic matter mineralization.

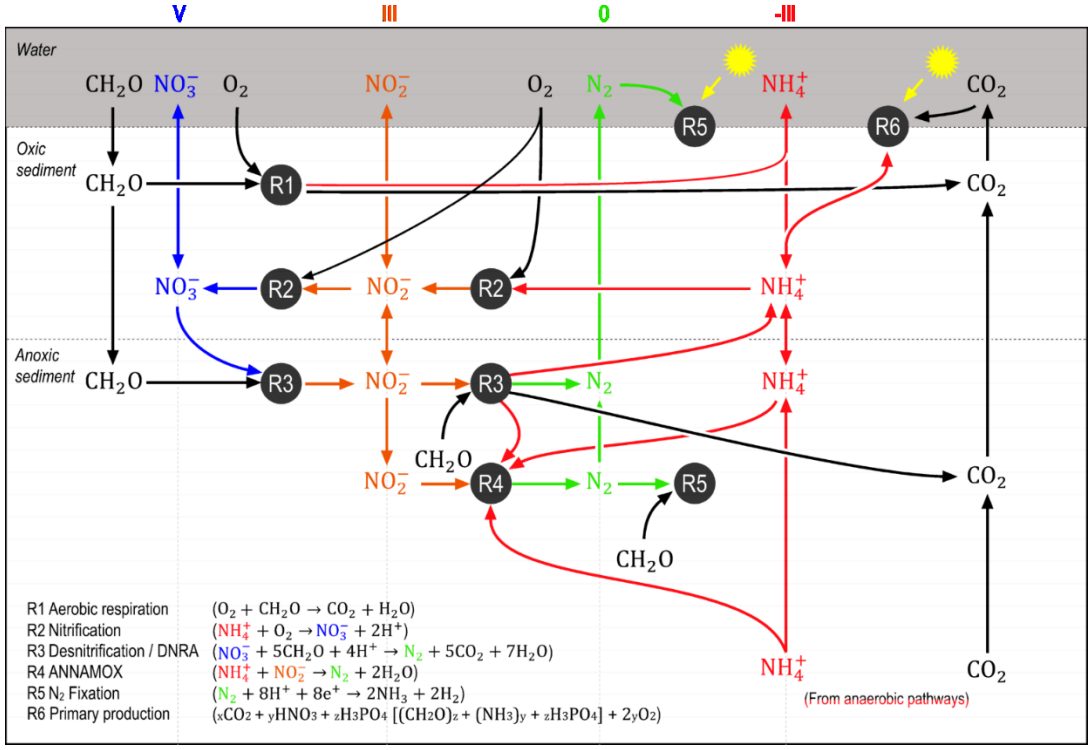

Figure 1. Biogeochemical pathways of nitrogen cycling in marine sediments. Source: own elaboration.

Major physicochemical factors controlling benthic C mineralization and DNF rates encompass (i) the input and availability of starting products (Hou et al. 2003, Seitzinger et al. 2006, Fulweiler et al. 2008, Whitehead 2012), (ii) the interaction of N species with other elemental cycles (Mn, Fe, S) which may lead to alternative pathways of N_2 production (Seitzinger 1988, Luther et al. 1997, Hensen et al. 2006, Schrum et al. 2009), and (iii) NH_4^+ adsorption in sediments (Mackin & Aller 1984, Hou et al. 2003). Sediment-biology interactions, such as sediment reworking or the microbial interactions occurring in the rhizosphere of eelgrass plants, also have a significant role on sediment biogeochemical cycles. The interactions are multiple, and an extensive review is not intended here, but a detailed review is provided by Kristensen (2005).

In aphotic sediments, a set of general patterns can be expected in the net N fluxes. Under oxic conditions (low input of C_{org}), the dominant metabolic pathways operating are oxic respiration and nitrification, with NO_3^- and NO_2^- as prevailing end products. In suboxic conditions, coupled DNF, SO_4^{2-} reduction, and anammox become dominant pathways of C mineralization and NO_3^- reduction. Under these conditions, net N removal as N_2 and N_2O is expected. The DNF efficiency, i.e., the fraction of remineralized N that goes through DNF, will depend on either an active input of NO_3^- from the water column (typical for advective dominated system), and/or tight coupling (in time or space) of nitrification and DNF. Finally, as the system becomes anoxic (e.g., due to organic matter overloading), a net efflux of NH_3 is expected, due to increased bacterial respiration and reduced nitrification rates. Annamox is also reduced or eliminated, as well as coupled DNF. The increased production and release of NH_3 to the water column may act as a negative feedback that drives further primary production and organic matter loading to the sediments (Fulweiler et al. 2008).

These patterns becomes more complex in well-illuminated shallow sediments as result of (i) phototrophic O_2 and biomass production, (ii) nutrient competition with nitrifying/denitrifying bacteria (Attrill et al. 2000), (iii) mutualistic or symbiotic relationships between primary producers and microbial communities (Cornwell et al. 1999, Miyajima et al. 2001), and (iv) biogenic stabilization of sediments (Newell & Koch 2004, Garwood et al. 2013).

The incorporation of ecological interactions and spatiotemporal heterogeneities has become essential in prediction of ecosystem processes and of human-environmental interactions, an aspect emphasized in several related studies that encourage further research (Borcard & Legendre 1994, Seitzinger et al. 2006, Fennel et al. 2009, Groffman et al. 2009, Piehler & Smyth 2011).

1.4 Upscaling and prediction of ecosystem services in coastal areas

Scaling and predicting benthic processes at larger spatial and temporal scales may greatly benefit from the combination of benthic habitat mapping and numerical simulations of sediment geochemistry. This approach provides a means for ecosystem-scale assessment of benthic processes.

Benthic habitat mapping is an essential tool for coastal researchers. Benthic maps showing the distribution of benthic physical and biological variables represent a valuable input for ecological and modeling studies, as well as for coastal management (Pickrill & Kostylev 2007, Kostylev et al. 2008).

Numerical models of carbon and nutrients cycling in sediments (also known as diagenetic models) are in a very mature state of development. The most sophisticated approaches are based on the idealized general diagenetic equation proposed by Berner (1980) (1D; depth-resolved models), which describes the mass conservation of solute and solid-phase compounds as a function of physical (advection and diffusion), abiotic chemical (redox, acid-base equilibrium, mineral precipitation/dissolution, adsorption), and biological processes (bioturbation, irrigation, respiration, etc.).

Applications target multiple environments (deep ocean, coastal, estuarine, riverine or lacustrine), as well as ecological and management-related questions, such as the quantification of global benthic fluxes and C_{org} degradation rates (Boudreau 1996, Jahnke 1996, Middelburg, Soetaert, et al. 1996, Soetaert et al. 1996, Van Cappellen & Wang 1996), benthic-pelagic coupling (Omori et al. 1994, Martin & Sayles 2004) and the prediction of the fate and impact of contaminants (e.g., excess organic matter, heavy metals, etc.) in aquatic sediments (Omori et al. 1994, Findlay & Watling 1997, Cromey, Nickell, & Black 2002, Mulsow et al. 2006, De Gaetano et al. 2008, Brigolin et al. 2009,

2014, Pastor et al. 2011). Diagenetic models are critical to connecting pore-scale processes with the macroscopic behavior of complex coastal and open ocean systems.

More recently, several efforts have been focused on modeling autotroph-sediment interactions and their effects on sediment geochemistry. Eldridge & Morse (2000) simulated the dynamic relationship between seagrass (above and below-ground biomass) and sediment geochemistry, with a description of rootzone fluxes of O_2 and DOM, and their effects on H_2S, NH_3, DIC, and C mineralization rates in sediments.

Also, a few studies have dealt with the simulation of benthic microalgae (BMA) and their impacts on sediment geochemistry (An & Joye 2001, Hochard et al. 2010). Hochard et al. (2010) used the diagenetic model OMEXDIA (Soetaert et al. 1996) to examine the impact of BMA dynamic on diagenetic pathways and benthic fluxes. BMA dynamic was modeled as a function of diel variation of PAR (including the effects of self-shading, and sediment attenuation), grazing activity by zoobenthos, and N availability. The model produced realistic situations, emphasizing the need to incorporate autotrophic metabolism in diagenetic models applied to shallow waters.

All of these studies emphasize the high variability of DNF at hour, daily, and seasonal scales in photic environments, and consequently the influence on sedimentary fluxes. The former studies provide the basis to improve the simulation of ecosystem processes at scales representative of coastal management.

1.5 Pressures on coastal areas

Humans interact in multiple ways with sedimentary environments, and many of these interactions may affect biodiversity and functioning (e.g., dredging, trawling, sediment pollution). Among them, anthropogenic nutrient enrichment constitutes a major concern in virtually all coastal and estuarine waters around the world (Bennett et al. 2001, Smith 2003, Galloway et al. 2004). The effects of nutrification on the pelagic and benthic compartments are well known and documented (Nixon 1995, Cloern 2001, Smith 2003, Orth et al. 2006, Diaz & Rosenberg 2008, Middelburg & Levin 2009). As a result, considerable efforts have been devoted to preventing and managing coastal eutrophication (GESAMP 2001).

One particular focus of this thesis is aquaculture-sediment interactions, specifically, the eutrophication of sediments underlying fish farm cages due to deposition of feces and excess feed. Sediment eutrophication is a major factor controlling productive capacity of fish farm sites. Environmental regulations in Canada, Norway, and Chile, the three largest producers of salmon worldwide, do not allow fish farms to operate under heavily eutrophicated conditions. The consequences of excessive organic loading are sediment hypoxia, accumulation of toxic sulfide, and disappearance of macrobenthic communities (Pearson & Rosenberg 1978). This condition is undesirable but difficult to avoid if the capacity of the system to degrade organic wastes is unknown. Further developments in tools for monitoring and prediction are required to reduce uncertainty in decision-making related to fish farm regulation and management.

1.6 Objectives and thesis outline

The goal of this thesis was to explore the linkages and interactions among biological, geochemical, and human systems in coastal sedimentary environments with the aim to improve understanding of sediment biogeochemical cycles. To achieve this objective, this thesis was split into three research chapters.

Chapter 2 is an empirically oriented research dedicated to the study of the spatial and temporal variability of sediment fluxes of nutrients and dissolved gases in shallow coastal environments of Nova Scotia, Canada. **Chapters 3 and 4** are modeling-based studies focused on the prediction of organic carbon and nitrogen cycling at the bay-scale **(Chapter 3)**, and locally in sediments exposed to organic enrichment from marine fish farm cages (**Chapter 4)**. Results of **Chapter 2** were used as input or in the validation of model predictions in **Chapter 3 and 4**. A summary of the main findings and recommendations for future research is presented in **Chapter 5**.

The specific objectives of each research chapter are:

Chapter 2. Benthic habitat mapping and nutrient fluxes in a shallow coastal environment of Nova Scotia, Canada

1. Estimate sediment fluxes of nutrients (NH_3, NO_3) and dissolved gases (O_2, N_2, Ar, CO_2) in representative habitat types of a shallow coastal environment of Nova Scotia, Canada.
2. Determine the relationship between observed benthic fluxes with controlling factors at the bay-scale and within major habitat types (organic matter content, temperature, O_2 availability, irradiance, mud percent, depth, etc.).
3. To characterize the spatial distribution of sediment parameters (grain size, porosity, organic content) and depth in the study area.

Chapter 3. Seasonal sediment flux modeling in a coastal bay of Nova Scotia, Canada.

4. Develop and validate a mechanistic diagenetic model to predict daily to seasonal dynamics in C and N cycling in subtidal sediments of a coastal bay of Nova Scotia, Canada.
5. Estimate the specific contribution of the major habitat/sediment types to C and N removal via mineralization and denitrification, and compare them with other significant sources and sinks of C and N in the study area.

Chapter 4. Modeling sediment assimilative capacity and organic carbon degradation efficiency at marine fish farms

6. To develop a coupled mechanistic model to predict the production, net deposition, and degradation of organic wastes in sediments underlying fish farm cages.
7. To predict the transition to hypoxic conditions as result of organic enrichment, and to determine optimal organic loads that can be degraded by sediments without leading to undesired environmental conditions.

CHAPTER 2. BENTHIC HABITAT MAPPING AND SEDIMENT NUTRIENT FLUXES IN A SHALLOW COASTAL ENVIRONMENT OF NOVA SCOTIA, CANADA

2.1 Abstract

Coastal embayments are dynamic open systems characterized by multiple sedimentary environments. Variability in sediment biogeochemical cycles is influenced by physicochemical forcing and biological processes acting at multiple spatio-temporal scales (e.g., hydrodynamics, C deposition, abiotic-chemical reactions, macrofaunal and microbial activity, etc.). The identification of relevant scales of variability is critical to determine the contribution of benthic processes to ecosystem dynamics and to inform managers on the sustainable use of coastal zones.

I determined the degree of spatial variability of benthic primary production, respiration, and denitrification in two coastal embayments in summer, and examined how these processes are influenced by organic matter content, porosity, salinity, temperature, depth, light availability, habitat, sediment type, and by the presence of fish farms.

Results showed that 11.2% to 69.3% of the total observed variance in benthic metabolic activity was accounted for the explanatory variables considered in this study. I discuss the findings in relation to 1) nonlinear and asynchronous dynamics, 2) secondary geochemical reactions, 3) non-evaluated processes, 4) ecological, observational, and analytical scales of analysis, and 5) data quality.

2.2 Introduction

2.2.1 Coastal dynamics, ecological functions, and ecosystem services

Coastal ecosystem services are recognized globally to include habitat and food provision, carbon, and nutrient cycling, and disturbance regulation, among others (Costanza et al. 1998, Costanza 1999, Vance-Harris & Ingall 1999, Brown, Smith, et al. 2011, Galparsoro et al. 2014). Due to the strong benthic-pelagic coupling in coastal areas a significant fraction of carbon and nutrient cycling, storage and sequestration are carried

out in the benthos (Jahnke 2005, Middelburg et al. 2005, Muller-Karger et al. 2005, Seiter et al. 2005). Nevertheless, the contribution of the benthos to ecosystem processes varies extensively in time and space due to either physicochemical forcing (sediment texture, gas exchange) or biological interactions including carbon deposition and bioturbation (Jones et al. 1994, Kristensen 2005). At the ecosystem scale, hydrodynamic conditions and water depth define bottom water renewal, net deposition of particulate material, and bottom sediment insolation. Biological interactions are diverse and cover multiple ecological scales from the individual organism through populations, communities, and ecosystems. In general, these interactions are driven by the presence of infaunal and epibenthic organisms, primary producers, ecosystem engineers, and microbial communities. Following Jones et al. (1994), ecosystem engineers are "*organisms that directly or indirectly modulate the availability of resources to other species, by causing physical state changes in biotic or abiotic materials*", and include for example seagrass and mussel beds.

2.2.2 Characterization of benthic habitats and valuation of benthic processes

The identification of relevant scales of natural variability is essential for a better understanding of benthic dynamics, as most benthic processes and functions are scale-dependent (Lecours et al. 2015). Fluxes of particulates and solutes have long been used to characterize benthic processes, and rates of sediment oxygen consumption or denitrification may be considered direct measures of ecosystem services. However, their spatial variation, especially with factors such as sediment type and depth, make it difficult to weigh their significance in marine ecosystems. The distribution of bottom types can only be assessed with spatially-explicit techniques such as acoustic habitat mapping. The definition of habitat is adopted from Kostylev et al. (2001) who define it as "*a spatially defined area where the physical, chemical, and biological environment is distinctly different from the surrounding environment.".* The combination of empirical measurements and benthic habitat mapping provide a means to define distinct habitat and bottom types, as well as the ecosystem-scale assessments of benthic processes including both intra- and inter-habitat variability. This approach represents an important input for ecological and modeling studies, and provide a foundation for impact assessment studies, conservation programs, and management strategies to promote sustainable use of coastal

zones within the bounds of natural variation (EU 2009, Grant & Filgueira 2011). Despite its importance, little is known about the evaluation of biogeochemical processes and the functional value of the benthos at scales relevant for coastal management (Hewitt et al. 2004, Brock et al. 2006, Harborne et al. 2006, Eyre & Maher 2011).

2.2.3 Objectives

I determined the degree of spatial variability of sediment fluxes of nutrients (NH_3, NO_3) and dissolved gases (O_2, N_2, Ar, CO_2) during summer in two coastal embayments located in the Southern Shore of Nova Scotia, Canada. Second, I determined the relationship between observed benthic fluxes and controlling factors, including the organic matter content, porosity, salinity, temperature, depth, O_2 and light availability, habitat type, and by the presence of salmon farms. Finally, I characterized the spatial distribution of sediment parameters (grain size, porosity, organic content) and depth in the study area.

I focused on three major habitat types: seagrass beds and bare sediments at euphotic and aphotic depths. Likewise, my research focussed on two important processes, C mineralization, and denitrification. Nevertheless, a broader set of benthic processes were also considered to describe the functioning of the system, including benthic primary production (gross and net O_2 and CO_2 production and consumption rates), nitrate-nitrogen (NO_3) and ammonia-nitrogen (NH_3) fluxes, and N-fixation. A major research hypotheses was proposed: the variability in sediment fluxes differs significantly across major habitat/sediment types, and consequently habitat-specificity can act as a predictor of C and N removal rates at ecosystem/bay scales.

2.3 Methods

2.3.1 Study sites

Two bays on the south shore of Nova Scotia, Canada were selected based on accessibility, benthic habitat composition, and level of human activities (**Figure 2**). Shelburne Harbour (SH, 43.71, -65.33) is a large (2291.9 ha), shallow and well-sheltered harbour (mean depth of 8.4 m, and maximum of 17.44 m), with a long history of human interactions, including fishing and fish processing, tourism, transportation, ship repair, and finfish aquaculture. A triangular peninsula divides SH into two inner bays: the eastern

Shelburne Harbour and on the western side Birchtown Bay. Water exchange with the ocean takes place through a 1250 m width channel (~14 m in the deepest points). The main source of freshwater is the Roseway River, which drains a gross area of ~495 km^2 directly into the head of Shelburne Bay (**Figure 2**). Secondary freshwater sources include Birchtown and Ackers Creeks. Daily river fresh water input in winter and spring (~1.96 and 19.4 million m^3, respectively) is less than 1.5% of the total volume of the bay (~161 million m^3). Average monthly flows fluctuate between 25.1 ± 7.4 m^3 s^{-1} in early spring (April) and 5.9 ± 5.1 m^3 s^{-1} in the late summer (August) (1915-2015 records of Water Survey of Canada). Tidal range at the head of Shelburne Harbour is 2.5 m. The water column has higher light attenuation in Shelburne Harbour due to the active input of CDOM (tannins) from Roseway River, and less turbid waters at Birchtown Bay.

Port Joli (PJ, 43.85,-64.88) is a relatively open and shallow embayment located 41 km east of Shelburne Bay. Water depths during mean tides range between 0.2–1.5 m at the sampling location. The bay has extensive eelgrass beds (*Zostera marina*) at the head of the bay (1–2 km^2), and sand flats in the outer bay. The eelgrass beds are continuous with little fragmentation and separated by a system of tidal channels. Relatively low anthropogenic impact related to coastline development is observed in the area. This site was chosen due to the presence of eelgrass beds, not found in SH. Acoustic mapping and spatial analysis concentrated on subtidal sediments of SH. In PJ, the focus was on sampling and understanding of the benthic metabolism of eelgrass beds in shallow intertidal and subtidal zones.

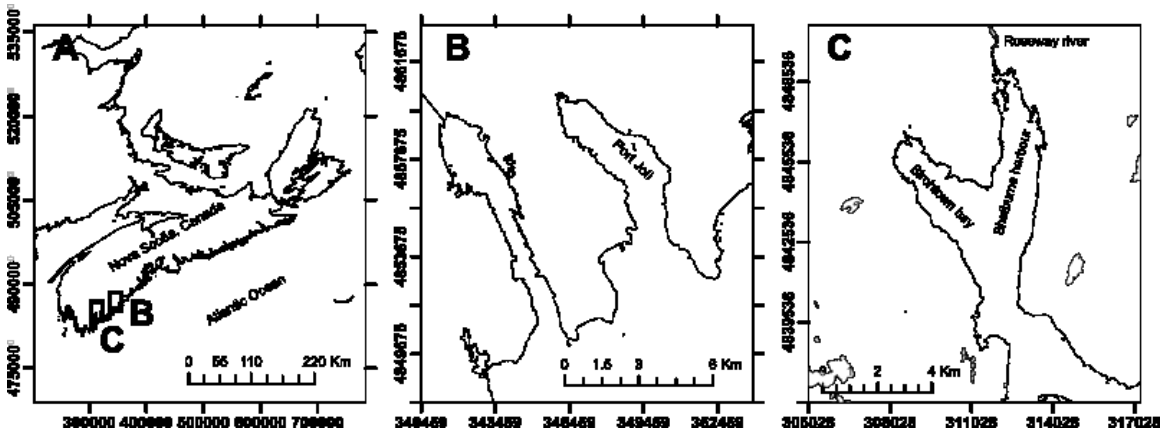

Figure 2: Study area. **A.** Nova Scotia, Canada. **B.** Port Joli, PJ. **C.** Shelburne Harbour, SH.

2.3.2 Benthic habitat mapping

Sedimentary environments were primarily classified using acoustic mapping techniques groundtruthed with benthic video as described below. A second classification scheme was generated based on pre-defined benthic habitat types, *i.e.,* areas where the physical, chemical, and biological environment are distinctly different from surrounding areas (Kostylev et al. 2001, Lecours et al. 2015). This classification generated two habitat types in Shelburne Harbour (SH): 1) bare photic sediments in shallow areas (SH-BP), and 2) bare aphotic sediments in subtidal areas (SH-BA), and two habitat types in Port Joli Bay (PJ): 1) bare photic sediments (PJ-BP), and 2) seagrass beds (PJ-SB). In addition, I consider separately fish farm sediments at SH (SH-FF). Photic sites were defined by the presence of chlorophyll-a (Chl-a) in surface sediments. Estimation of photic depth was preferable but difficult to quantify due to the high variability in water-column light attenuation (turbidity) throughout SH.

2.3.2.1 **Data collection**

Three hydroacoustic surveys following pre-defined survey lines (**Figure 3B**) were carried out in SH in July 24th, and August 15th and 21st of 2014. An MX 200 kHz aquatic habitat echosounder (Biosonics, Inc.) equipped with a DGPS sensor was used to delineate substrate composition (sand, mud, rock), and depth distribution. The system was deployed from a vessel with the transducer positioned just below the water surface. Georeferenced images retrieved from underwater video surveys and benthic grab samples were collected along the acoustic transects lines at 61 stations to support benthic habitat description and identification of sedimentological and biological features (**Figure 3A**). All data sets from remote and direct benthic sampling were input to a Geographical Information System (GIS) for further analysis.

2.3.2.2 **Acoustic seabed classification**

Post-processing of digital hydroacoustic data was done using a commercial seabed classification software (Visual Habitat Software, v1.0.6.6963, Biosonics, Inc., 2014) in combination with a GIS software (ArcMap 10.2.2 - ESRI). The process involved five major steps: (1) data cleaning, (2) analysis for acoustical classification of bottom

sediments, (3) spatial interpolation, (4) validation, and (5) application of spatial metrics to the seascape structure.

Data cleaning and correction. Bias in acoustic data associated with bottom roughness, vessel pitch and roll, and air entrainment were evaluated and data cleaned as follows. Results of the automatic bottom detection analysis were manually edited to remove artifacts associated to the presence of schools of fish, mooring systems, or steep bottom slopes. All data points closer than 0.25 meters were removed from echograms to avoid wave and bubble-induced acoustic noise associated with vessel motion and interferences from the boat propeller, usually observed at direction change between transects, and stops at sampling stations. A tidal correction, based on the datum of Lower Low Water Large Tide (LLWLT) was applied to all data sets to remove the influence of water level differences among sampling dates and time.

PCA analysis. Detection of bottom types relied on the differences in the acoustic backscatter profiles, represented in time-dependent echograms. Multiple parameters were computed based on the shape and energy characteristics of the echograms. The multivariate data set was later analyzed by Principal Components (PCA) to elucidate the contribution of echo parameters (~ 40 among spectral, wavelet, energy, fractal, and statistical parameters) to total observed variance, and identify patterns of similarity among sampled bottom beds. The number of clusters, i.e., bottom sediments categories, was defined based on groundtruth datasets (grain size and video surveys).

Interpolation and imagery of bottom types. Indicator kriging interpolation was used to quantify the spatial autocorrelation of acoustic data and to predict the distribution of bottom types. Spatial autocorrelation was examined through empirical semivariograms generated for each category identified through the PCA analysis, using a circular model with an automatic detection of parameters (range, sill and nugget effect). The adjusted function was later used to produce continuous-valued surfaces indicating the probability of unsampled points belonging to the pre-defined categories. Bottom types were finally assigned based on the highest categorical probability. No anisotropies were identified from variogram maps. The accuracy of model prediction, i.e., the degree of bias between observed and predicted values of spatial interpolations of acoustical and geochemical

variables was evaluated through cross-validation analysis. All analyses were performed in ArcMap 10.

2.3.2.3 **Spatial interpolation of sedimentary properties**

Sediment properties were interpolated at the bay-scale using the spline method (depth) and ordinary kriging technique (organic matter and porosity). As with indicator kriging (acoustic data classification), empirical semivariograms were computed for each sediment variable to determine any spatially dependent variance within the study area. The uncertainty of created surfaces was examined through the generation of prediction standard error maps.

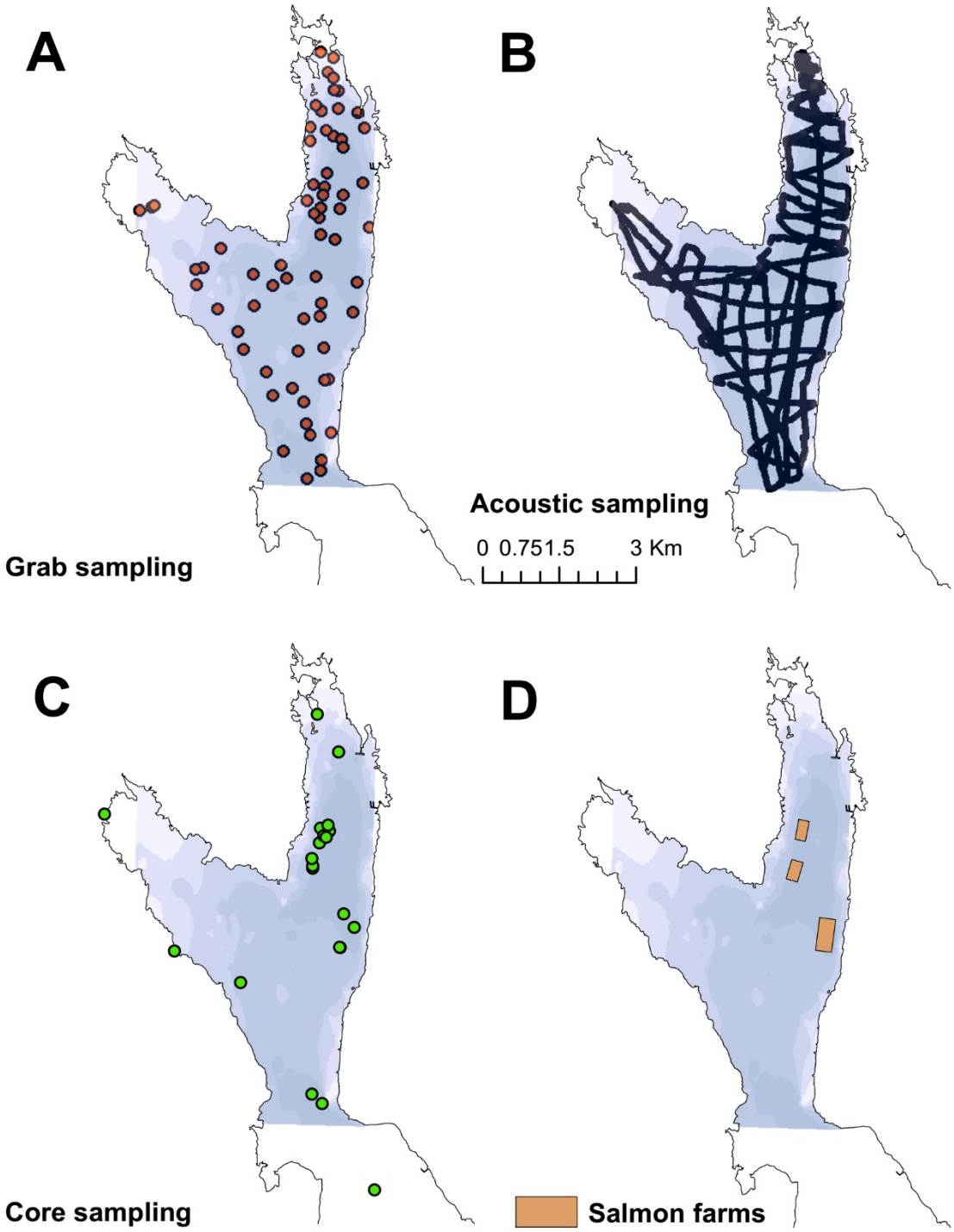

Figure 3: A. Grab sampling for LOI (n=46), porosity and grain size analysis (n=46). **B.** Acoustic tracks. **C.** Sediment core sampling (n=94). **D.** Anthropogenic activities.

2.3.3 Benthic incubations and complementary measurements

Geochemical properties of sediment and pore water, benthic fluxes, and complementary measurements were quantified at major benthic habitat types. Exchange rates of O_2, nutrient, and DIC across the sediment-water interface were quantified through *in-situ* and laboratory incubations.

2.3.3.1 **Field incubations**

Twenty-two pairs of in-situ dark/light incubations were carried out in photic sediment inhabited by eelgrass and BMA (**Table 2**). The mean water depth of photic incubations was of 1.5 meters. *In-situ* incubations were done using transparent acrylic tubes (i.d. 11.5 cm; height 30 cm), and opaque lids equipped with siphons for water sampling. At the beginning of the incubation period (t_0), bottom water samples were collected above the sediment surface to measure the concentration of O_2, NH_3, NO_3, dissolved inorganic carbon (DIC), and total alkalinity (TA). At the end of the incubation (t_1), the cores were recovered by hand and duplicate samples of overlying water and surficial sediments (upper 2 cm.) were collected for analysis of dissolved species, Chl-a, organic matter, porosity and grain size analysis. If applicable, eelgrass plants were also recovered and stored for estimations of biomass, Chl-a concentration in leaves and shoot density. The incubation time depended on slack tides that facilitated core retrieval, and the time required to reach 20% to 50% of O_2 saturation in overlying water (Eyre et al. 2002, Ferguson & Eyre 2007). If bubble formation was observed during light incubations, those samples were discarded as they may result in an underestimate of benthic production. Downwelling Photosynthetically Active Radiation (PAR) was measured with a quantum sensor (LI-COR LI-1000 data logger) place at the sediment surface close to core incubations. Salinity and temperature were recorded at the beginning and at the end of each incubation. If no PAR data was measured, modeled data for the latitude, time of the day, and day of the year was calculated according to Brock (1981), assuming a light attenuation coefficient in the water column of 0.2 m^{-1}.

In addition to in-situ incubations, sediment traps (KC Denmark, Silkeborg, Denmark) were deployed in midsummer (2014) approximately 1 m from the seabed for 48 hours at pre-selected locations in SH to characterize particle flux to sediments (**Figure**

8D). Once recovered, the trapped material was filtered with a vacuum pump (Whatman GF/F diameter 25 mm, nominal porosity 0.45 μm), at 10 kPa or lower to avoid particle damage, and the filters dried (48 hours at 60 ◦C) for subsequent loss on ignition, LOI (3 hours at 490 ◦C) and CHN analysis.

2.3.3.2 **Laboratory incubations**

Additionally, sediment core incubations were conducted under controlled laboratory conditions with the purpose of measuring denitrification rates, by removing the effects of temperature and salinity variations (i.e., occurrence of solubility-driven fluxes). N-fixation was measured based on acetylene reduction assays after saturation of overlying seawater of intact cores. Sediment cores (i.d. 6.35 cm; height 33 cm) were collected by SCUBA divers or with a multi-corer (MC-200-4 - Ocean Instruments, Inc.) and transported back to the lab in a chilled cooler filled with *in-situ* water. In the lab, cores were pre-incubated in a thermo-regulated water bath under O_2 saturation in darkness for 18 to 24 hours to allow recovery of natural faunal behavior and equilibration of temperature and solute concentration. Epifauna were removed from surface sediment prior to incubation, and as required, the sediment-water interface was adjusted to 1/3 of the core length. Once pre-incubated, aeration was removed, and duplicate samples were collected for O_2, nutrient, N_2/Ar ratio, C_2H_2 (if applicable), DIC and TA analysis. Cores were then immediately sealed with gas-tight lids equipped with a Teflon coated magnetic stirring bar. Stirring rate was adjusted to 60 rpm to prevent stratification in overlying water. The incubations were finalized and samples collected after 5.5 – 40.5 h when O_2 saturation decreased to 20 to 50%. Blank cores containing filtered seawater (0.45 μm) were incubated with the rest of the samples to account for artificial changes in solute concentrations caused by different permeabilities and solubilities of N_2 and Ar in Plexiglas. A schematic overview of the protocol of laboratory incubations is depicted in **Figure 4**. The lighting system consisted of a series of lamps (Power Spectrum T5 HO Fluorescent Bulbs) positioned on top of incubated cores.

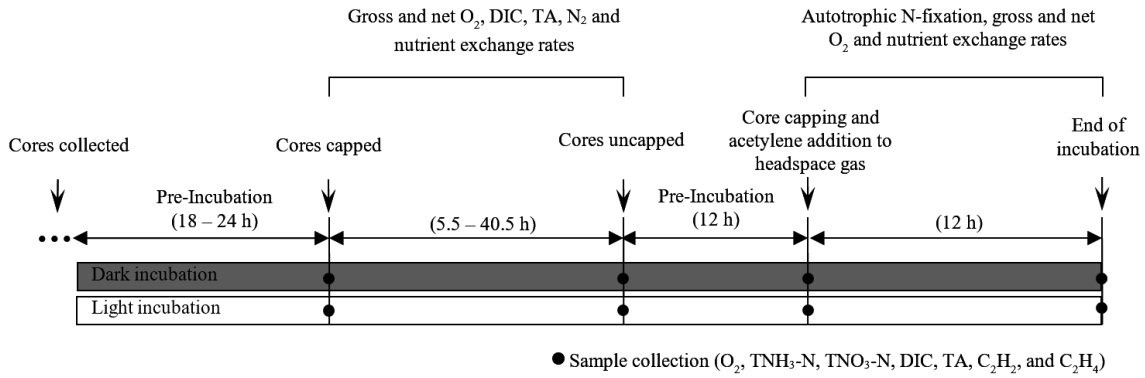

Figure 4: Incubation strategy for DNF and N-fixation rate estimation in bare sediments and seagrass beds.

2.3.3.3 **Solid and water phase analysis.**

O_2 content in overlying water was determined in the field with a fiber-optic dipping probe (PreSens GmbH, Regensburg, Germany), while NH_3, NO_3, DIC, and TA were determined in the lab from preserved samples. Water samples for nutrient content were filtered (0.22 µm) and frozen (-20◦C) in triple-rinsed (deionized water) 20 ml plastic vials until analysis in a conductivity detector (Timberline Instrument Model 550 A). DIC and TA samples were preserved using $HgCl_2$ (0.5% v/v saturated solution) and determined by coulometric and potentiometric titration respectively (Johnson et al. 1993).

Organic matter content was determined by loss on ignition at 550 °C for 4 h (Heiri et al. 2001). Sediment porosity was determined from Berner's equation (Berner 1971)

$$\varphi = \frac{W\,\rho_s}{W\,\rho_s + (1-W)\rho_w}$$

where W is the sediment water content (%), ρ_s the density of sediment assumed equal to 2.45 g cm^{-3} and ρ_w the density of porewater assumed constant and equal to 1.023 g cm^{-3}.

Grain size analyses were carried out through laser diffraction particle size analysis (Beckman Coulter LS230), following digestion of sediment samples (H_2O_2 35% v/v), and supernatant removal via centrifugation (3250 RPM for 90 min.). Mud content (< 63 µM) was also determined by wet sieving. Chl-a content in surface sediments and eelgrass leaves was quantified by fluorometric detection previous extraction with 90% acetone (Holm-Hansen et al. 1965, Welschmeyer 1994, Mitchell et al. 2002).

Dinitrogen (N_2) fluxes were quantified from excess N_2 in relation to equilibrium N_2/Ar ratio. Duplicate samples for N_2/Ar analysis were collected and stored in 12 ml gas-tight glass vials (Exetainer R, Labco) without headspace and refrigerated at sub-ambient temperature for further analysis. The analyses were performed by Membrane Inlet Mass Spectrometry (MIMS) as described by Kana et al. (1994, 1998), using a Hiden HPR-40 dissolved species gas analysis system (Hiden Analytical Ltd., Cheshire, England), and a submersible probe equipped with a silicone-based permeable membrane that allows dissolved gases to pass through and onto the mass spectrometer. A liquid nitrogen cryotrap was used to prevent water vapor and CO_2 from reaching the detector and its interference with N_2 and Ar measurements. Calibration and stabilization of the instrument signal were conducted using a pre-filtered (0.22 μm), air-equilibrated seawater sample of known temperature and salinity collected at the bottom at the time of core collection (preserved with 0,5% v/v $HgCl_2$). The accuracy of MIMS measurements of N_2/Ar ratio was evaluated by calculating the coefficient of variation of standard and actual samples (i.e., the ratio of the standard deviation to the mean).

Processing of raw mass spectrometry data involved corrections for 1) sensitivity differences of the quadrupole mass analyzer and membrane permeability to different gases based on expected N_2/Ar ratios in seawater standards, 2) electronic noise, 3) analyzer drift, 4) solubility driven-fluxes, and 5) signal stabilization in between samples analysis. The electronic noise was removed by filtering data series based on standard deviation. All values in data sets above or below two standard deviations of the mean were excluded from the analysis. As required, a correction for analyzer drift was applied by linear interpolations of measured data. Solubility driven fluxes associated with changes in temperature during sediment core incubations were evaluated through analysis of Ar data series.

The saturation normalized N_2/Ar ratio (ΔN_2/Ar) was estimated for each sample to determine if they were above or below equilibrium in relation to seawater standards. N_2 concentration in samples was calculated by multiplying the Ar concentration calculated from solubility equations, given temperature and salinity according to Hamme and Emerson 2004 by the corrected N_2/Ar ratio.

The analytical precision of the instrument (coefficient of variation) within transient data sets oscillated between 0.31 and 2.42% for standards, and between 0.6 and 5.69 % for samples. The higher precision for standards was caused by the continuous stirring of samples required to maintain equilibrium conditions, which enhanced sample homogenization and diffusion through the membrane of the dipping prove.

N_2 fixation was determined by C_2H_2 reduction (Capone 1993). C_2H_2 and C_2H_4 concentration were determined using a gas chromatographic flame ionization detector (GC-FID). N_2 fixation rates were estimated by linear regression of measured ethylene concentrations in the overlying water of core incubations. A conversion ratio of 4:1 was assumed between total moles of acetylene reduced to ethylene versus N_2 fixed into NH_4^+ + DON (Welsh et al. 1996).

Based on estimated gases and nutrient fluxes the following quantities were calculated:

i. Total exchange rates (μmol m^{-2} h^{-1}), equivalent to the net fluxes in dark and light incubations.
ii. Daily averaged fluxes calculated based on net dark/light fluxes and the number of light/dark hours (mmol m^{-2} d^{-1}).
iii. Gross photosynthetic activity for photic sediments (μmol m^{-2} h^{-1}) calculated as the difference between light and dark O_2 exchange rate (i.e., net fluxes). Gross benthic C fixation is calculated as the difference between light and dark DIC exchange rates.
iv. Net Ecosystem Metabolism (NEM), defined as primary production minus respiration.
v. Metabolic quotients including the benthic dark respiratory quotient (RQ = dark CO_2 flux: dark O_2 flux), and the photosynthetic quotient (PQ = gross O_2 production rate: gross CO_2 consumption rate). To avoid uncertainties associated with natural variability and measurement error the metabolic quotients were calculated from the slopes of linear regressions.

2.3.4 Statistical analysis

The equality of means in benthic fluxes and sediment properties in relation to independent variables (bottom types and incubation type) was tested using a one-way ANOVA. Significant main effects were examined using Tukey's HSD test. Normality and homoscedasticity were tested using the Kolmogorov-Smirnov and Levene's test, respectively. The Kruskal–Wallis (KW) test was used as an alternative nonparametric test to ANOVA.

Empirical relationships among benthic fluxes (i.e., flux ratios), and between benthic fluxes and geochemical variables, including acoustically-derived bottom types, were characterized through linear regression analyses. Heteroscedasticity, nonlinearities, and presence of outliers were analyzed from residual plots. A p-value of ≤ 0.05 in regression analysis was considered as a statistically significant difference. Means are presented with standard deviation. Pearson's correlation coefficient was used to describe the strength of the association between variables.

Finally, partial least squares regression (PLS-R) analysis was used to determine the predictive power of explanatory variables of benthic fluxes, namely LOI, salinity, porosity, temperature, depth, Chl-a, PAR irradiance, habitat and acoustic type, and O_2 availability in overlying water at the beginning of sediment incubations. Incubation time was also incorporated into the analysis to evaluate possible artifacts during experiments.

As a method of data dimension reduction, PLS-R may be considered as to yield similar information as both principal component analysis (PCA) and multiple linear regression (MLR). It is considered appropriate in defining patterns of variation when the independent factors are many and highly collinear (Carrascal et al. 2009) as observed in the data. Compared to PCA and MLR, PLS-R allows the definition of a response variable, in this case benthic fluxes, and does not require removal of collinear descriptors (e.g., using stepwise methods), with the consequent loss of predicting power.

2.4 Results

2.4.1 Habitat characterization and classification

All sediment samples from PJ were classified as sandy mud according to Folk (1957) with a median grain size 40.7 ± 7.3 μm, while SH sediments ranged from mud to coarse sand. Samples of photic sediments were muddier in PJ (BP and SB) than in SH-BP. Nonetheless, this was not confirmed statistically due to the low number of SH samples (n = 3).

A 71.7% of SH seabed (1643.04 Ha) was covered by the spatial interpolation through indicator kriging. The remaining 28% (648.85 Ha) was mostly associated with intertidal sediments inaccessible to the vessel surveys (< 4 m depth). Intertidal zones consisted mostly of muddy sediments in the eastern Shelburne Harbour, and sandy to gravel in Birchtown Bay.

Based on acoustic and geochemical analysis four major bottom types were identified in SH: 1) sand and muddy-sand, 2) mud and sandy-mud, 3) coarse sediments, and 4) hard bottoms. Representative images of each type are shown in **Figure 6**, while their spatial coverage is shown in **Figure 8C**. Sand and muddy-sand was the dominant bottom type and was observed mostly in the SH mouth and the channel connecting to the sea (54% coverage, 887.7 Ha). The second-most common bottom type was mud and sandy-mud sediments mostly associated with the deeper areas of Shelburne Harbour (26% coverage, 432.9 Ha). Finally, coarse sediments (10.6%, 174.6 Ha) and hard bottoms (9%, 147.7 Ha) cover most of the coastline and heads of SH. Deeper areas of Shelburne Harbour and Birchtown Bay were mostly dominated by fine particles, and gravel/boulders, respectively, while coarse sand dominates both heads of SH.

2.4.1.1 **Sediment properties**

LOI content, sediment porosity, and grain size. LOI content in sediment cores and grab samples varied between 0.6 and 34.6% (n = 167), while porosity ranged between 22.7 and 86.2%. The mean LOI content in SH was 13.7 ± 8.6% SD (n = 120), and in PJ samples was 14.3 ± 4.2% SD (n = 47).

The LOI content, porosity, and mud content were significantly correlated in the study area ($p < 0.05$). A significant linear relationship was observed between Ln LOI content and sediment porosity in grabs and sediment cores samples ($r^2 = 0.95$, $n = 167$, $p < 0.05$, **Figure 5A**). In addition, a positive relationship was observed between LOI and mud content in sediments excluding samples collected at fish farms ($r^2 = 0.83$, $n = 87$, $p < 0.05$), as well as between sediment porosity and mud content ($r^2 = 0.81$, $n = 91$, $p < 0.05$, **Figure 5B**).

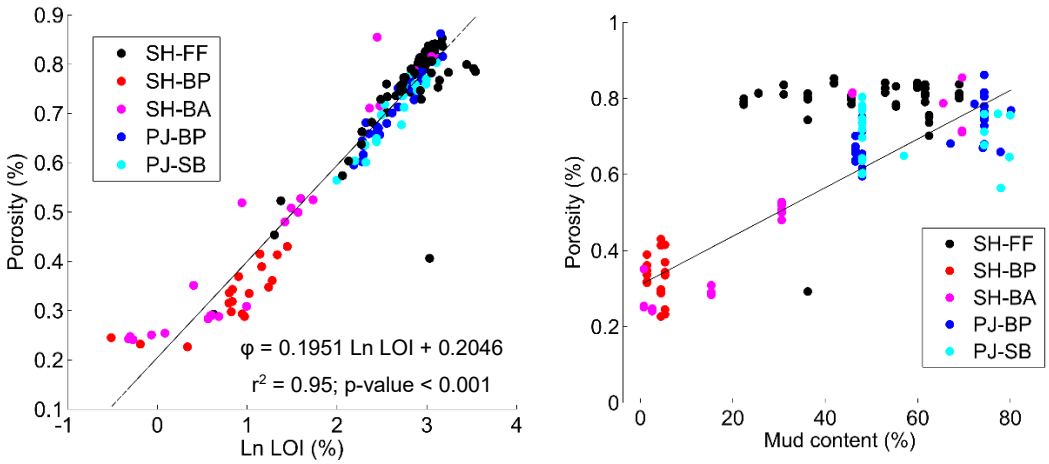

Figure 5: A. LOI content versus sediment porosity for SH and PJ sediments. **B.** Mud content versus sediment porosity for SH and PJ sediments. The regression line does not consider sediment samples from SH-FF biased by organic waste deposits. Legend key: fish farm sediments (FF), bare photic sediments (BP), bare aphotic sediments (BA), seagrass bed (SB).

No significant differences in LOI content, porosity, and median grain sizes were found among acoustic types (excluding fish farm sediments). Nonetheless, significant differences were observed among habitat types and fish farm sediments. LOI content was significantly higher ($p < 0.05$, Kruskal Wallis) in fish farm sediments (SH-FF: 20.5 ± 4.9%, $n = 50$) compared to non-aquaculture sites (SH and PJ, 10.8 ± 6.8 %. $n = 111$), most probably due to the accumulation of uneaten feed and feces below and around fish farm cages. I did not carry out macrofaunal analysis in this study. Nonetheless, azoic conditions were noted in most of the fish farm samples, as well as the presence of Beggiatoa mats and black coloration of surface sediments. The latter was most probably caused by sulfide precipitation. In pristine sediments, porosity and LOI content were significantly higher in PJ sediments, compared to SH sediments

($p < 0.05$, Kruskal Wallis). No significant differences in porosity and LOI content were observed within SH habitats (BA, BP), nor within SH habitats (BP, SB). A higher LOI content was observed in the deeper areas of the Shelburne Harbour (**Figure 8B**). The lower LOI content observed in shallow waters of SH was likely due to wave and tidal action that prevent deposition of the lighter organic matter. Similarly, mud content was significantly higher in PJ sediments (BA and BP), and SH-FF compared to SH sediments ($p < 0.05$, Kruskal Wallis). Mud content in SH sediments was slightly higher in SH-BA compared to SH-BP ($p < 0.05$, Kruskal Wallis).

Among pristine sediments, the highest LOI contents were observed in shallow photic sediments of Port Joli (PJ-BP: 14.4 ± 4.4%, n = 28), mostly due to the high content of decaying eelgrass leaves. The lowest LOI values were observed in the coarse intertidal sediments located at the head of Birchtown Bay (SH-BP: 2.6 ± 1.0%, n = 18), as well as in the sandy sediments located at the channel connecting SH to the sea.

Seagrass density and biomass. Due to a patchy distribution, seagrass shoot density was highly variable averaging 194 ± 137 shoots m^{-2} (1 and 3 shoots $incubation^{-1}$), while aboveground biomass ranged from 0.09 and 2.34 g dry weight $shoot^{-1}$ (mean of 0.58 ± 0.51 g dry weight $shoot^{-1}$). Aboveground biomass represented 64.4 ± 17.7% of total seagrass biomass, the remaining fraction being the root-rhizome system.

Chl-a content in surface sediments and eelgrass leaves. Chl-a content in eelgrass shoots was 18.2 ± 4.2 mg g^{-1} fresh weight (equivalent to 143.6 ± 32.9 µg cm^{-2}), while in bare photic sediments (PJ-BP) and seagrass sediments (PJ-SB) the mean concentration was equal to 16.2 ± 14.6 mg m^{-2} (n = 10), and 24.0 ± 10.8 mg m^{-2} (n = 6), respectively, with no significant differences among habitat types.

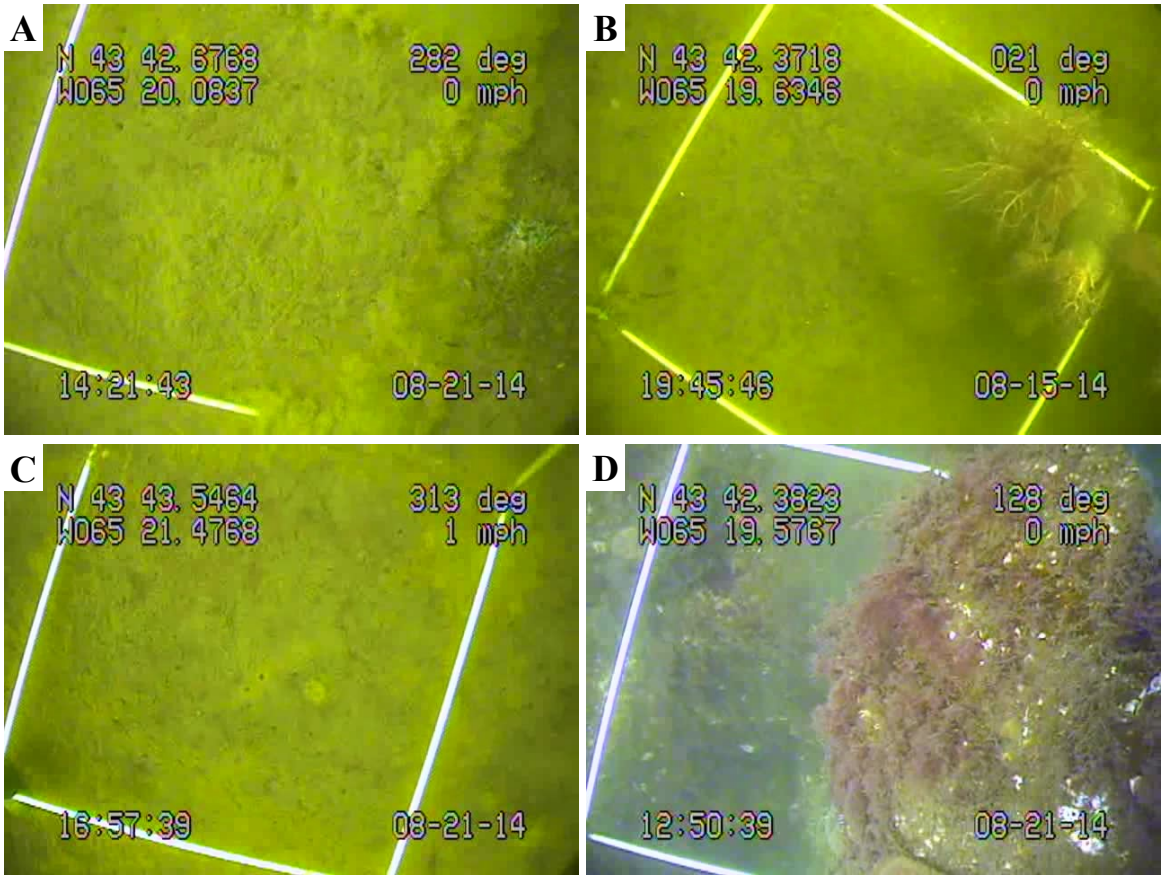

Figure 6: Underwater images of sedimentary environments. **A.** Sand and muddy sand. **B.** Mud and sandy mud sediments. **C.** Coarse sediment. **D.** Hard bottom and boulders.

2.4.1.2 **Interpolation of sediment properties**

Accuracy of interpolated surfaces. Standard error maps for each interpolated surface are displayed in **Figure 7**. The prediction standard error quantifies the uncertainty of the prediction and is calculated as the square-root of the prediction variance, which is the variation associated with the difference between predicted and observed values. If the data comes from a normal distribution, the true value will be 95 percent of the time within the interval of the predicted value ± 2 times the prediction standard error (Johnston et al. 2001).

As expected, the predicted standard error was smaller close to the acoustic track (bathymetry) and within and between sampling stations (grabs). An increase in the predicted error was observed near the shoreline in all interpolated surfaces as no data were available for those areas. Likewise, a lower predictive capability of interpolated

acoustic data was observed for the mid-bay sediments of SH, where the probability of belonging to the different acoustical categories was quite similar. Nonetheless, groundtruthing data confirm this area was dominated by medium and coarse sands.

Results of cross-validation analysis for all interpolated surfaces are shown in **Table 1**. The low accuracy of LOI interpolated surface reflected in the high RMS error (7.97) and mean prediction error (0.21) is mostly due to a low number of samples used in the interpolation (n = 62), in relation to the total SH area. The number of sediment samples from which the LOI interpolation was predicted is quite low compared to the acoustic data from which bathymetry and bottom types were predicted (>30000) which show a much higher prediction accuracy. The spatial distribution of sediment samples also affected the quality of interpolated surfaces as they were collected along the acoustic tracks, and consequently do not follow a regular grid pattern.

The mean depth of SH was 9.5 ± 4.3 m. The eastern side of SH was considerably deeper (up to 17.3 m) than Birchtown Bay (**Figure 8A**) which was dominated by a large tidal flat in the most inner area. As observed in **Figure 8A** and **B**, deeper areas of SH coincided with the higher interpolated LOI values. In contrast, the deeper areas of the channel connecting to the sea were characterized by low LOI, most probably due to high currents and low net deposition.

Table 1: Results of cross-validation analysis of interpolated sediment properties in SH using Kriging techniques.

Variable	Bathymetry	Organic matter	Bottom types	Criteria
Interpolation method	Ordinary kriging	Ordinary kriging	Indicator kriging	
Samples	31213 of 31213	62 of 62	31471 of 31471	
Mean prediction error	0.00015	0.21	-0.00061	Close to 0
Root-Mean-Square (RMS) error	0.07321	7.97	0.37187	As small as possible
Root-Mean-Square Standardized error	0.56458	0.97	0.92033	Close to 1
Anisotropy	No	No	No	

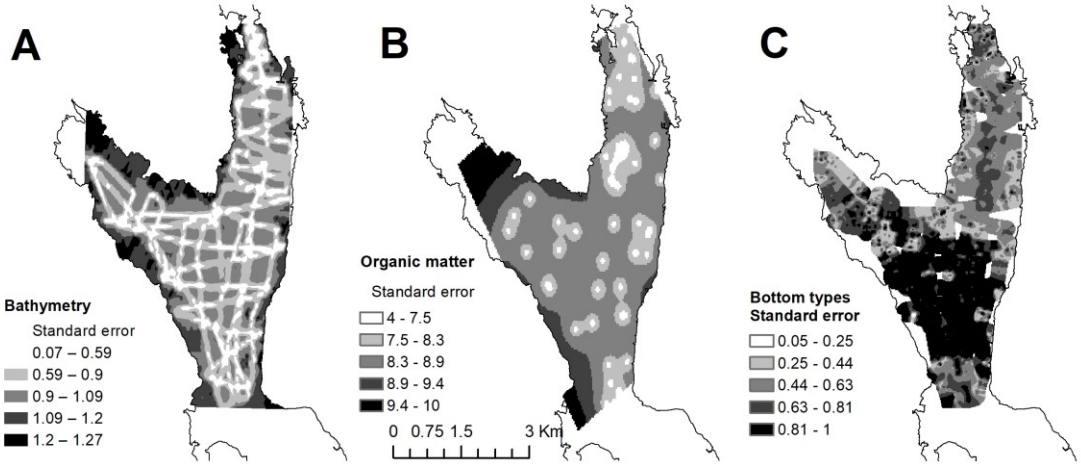

Figure 7: Standard error map of interpolated surfaces. **A.** Depth (ordinary kriging). **B.** Organic content (ordinary kriging). **C.** Sedimentary environments (indicator kriging).

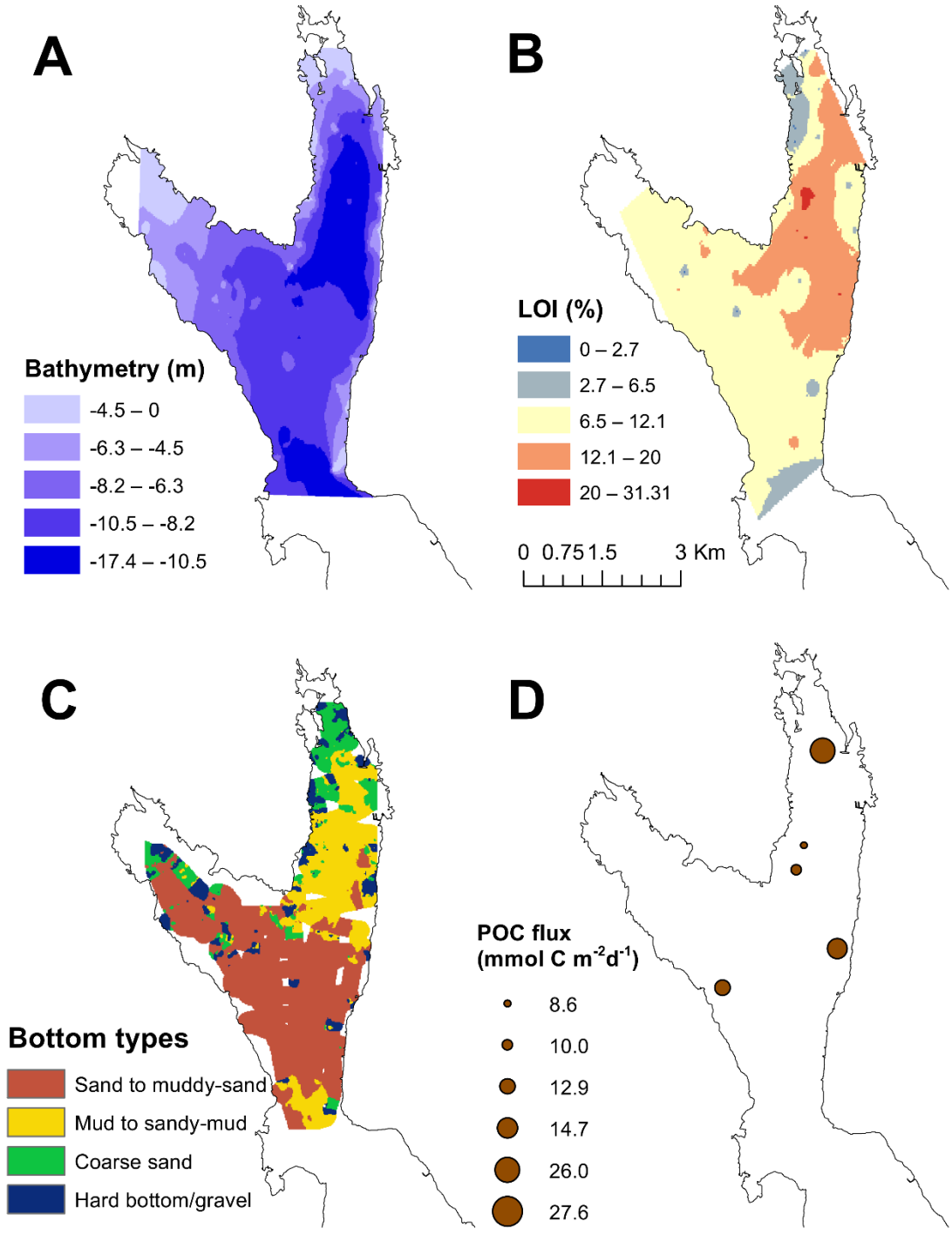

Figure 8: A. Bathymetry. **B.** Organic matter content (n=46). **C.** Bottom classification based on acoustic data. **D.** POC flux from sediment traps (n=5).

2.4.2 Benthic fluxes

2.4.2.1 General observations.

A total of 142 sediment cores were incubated *in-situ* and in laboratory conditions (**Table 2**). Incubation time varied from 2.36 to 5.98 h for *in-situ* incubations and 5.45 to 40.45 hours for laboratory incubations. Temperature in *in-situ* incubations fluctuated between 13.4 and 26.4 ºC, and between 6.3 and 10.1 ºC in laboratory experiments. Salinity oscillated between 22.5 and 30.1 ‰ in *in-situ* incubations, and between 25.9 and 31.4 ‰ in laboratory experiments. The lower salinity was recorded *in-situ* in core incubations carried out in PJ-BS in September 2013 (n = 4).

Table 2: In-situ and laboratory incubation according to habitat type and study area. Legend key: Shelburne Harbour (SH), Port Joli Bay (PJ), fish farm sediments (FF), bare photic sediments (BP), bare aphotic sediments (BA), seagrass bed (SB).

	In-situ	Laboratory	Total
Mud and sandy mud	**22**	**91**	**113**
PJ-BP	14	14	28
PJ-SB	8	12	20
SH-BA		12	12
SH-FF		53	53
Sand and muddy sand		**29**	**29**
SH-BA		11	11
SH-BP		18	18
Total	**22**	**120**	**142**
Incubation time (h)	4.03 ± 0.98	18.62 ± 6.82	
Temperature (ºC)	18.8 ± 5.4	8.7 ± 1.19	
Salinity (‰)	28.3 ± 2.3	29.8 ± 1.21	

2.4.2.2 Particulate mass flux to sediments.

Sediment trap data showed that deposition of particulate organic carbon (POC) for the summer ranged from 8.6 to 27.6 mmol C m^{-2} d^{-1} (102.9 to 331 mg C m^{-2} d^{-1}), which was in the range of oligo- to mesotrophic coastal conditions according to Eyre et al. (2009). The latter assumes a 5% of total C in sedimented material, of which 80% correspond to organic carbon (Hargrave et al. 1976, Hargrave 1980). Nonetheless, only a small number of traps were deployed at SH (n = 6), so inferences regarding spatial variability of C deposition rates cannot be provided.

2.4.2.3 **Exchange rates of solutes**

Daily average benthic fluxes and net exchange rates in light and dark conditions are reported in **Table A13** of the **Appendix A**. Results are presented disaggregated by habitat type and for fish farm sediments, and include reference values for coastal and estuarine sediments.

Observed O_2, DIC and NH_3 dark fluxes in pristine sediments were within the range reported for coastal sedimentary environments (**Table A13**). Reported O_2 consumption rates for pristine coastal sediments normally varied between 0-5000 µmol m^{-2} h^{-1} (Glud 2008), nonetheless, values as high as 24100 µmol m^{-2} h^{-1} have been reported (Hopkinson et al. 1999). DIC exchange rates were in the oligo- (< 2,000 µmol DIC m^{-2} h^{-1}) to mesotrophic range (2,000 – 4,000 µmol DIC m^{-2} h^{-1}) according Eyre & Ferguson (2009). The highest rates of O_2 consumption, DIC, and NH_3 production occurred in seagrass beds (SB) and bare sediments (BP) of PJ, where relatively higher LOI values were observed, probably as result of increased deposition of sediments on seagrass beds. O_2, NH_3, and DIC exchange rates in fish farm sediments were not significantly higher than in pristine sediments, as may be expected from higher LOI content (**Table A13**).

No statistical differences were observed in daily average fluxes (O_2, DIC, TA, and NH3) among habitat types, nor among acoustic types. Only marginal differences ($p < 0.07$) were observed in daily averaged NH_3 fluxes, which were slightly higher in aphotic incubations. Daily average fluxes of O_2 in summer were equal to -38.0 ± 29.8 mmol m^{-2} d^{-1} in bare photic sediments (PJ-BP and SH-BP, n = 23), -16.3 ± 16.0 mmol m^{-2} d^{-1} in PJ-SB (n = 9), -12.1 ± 12.9 mmol m^{-2} d^{-1} in SH-BA (n = 23), and -14.1 ± 8.2 mmol m^{-2} d^{-1} in SH-FF (n = 50). No differences in mean dark O_2 consumption rates among habitats or acoustic bottom types were observed, mostly due to the high heteroscedasticity of the data.

Benthic primary production in bare photic sediments was relatively small (max. Gross Photosynthetic O_2 production: 2621.6 µmol O_2 m^{-2} h^{-1} in PJ-BP) compared to the maximum reported values, which may reach up to 27000 µmol O_2 m^{-2} h^{-1} in organic-rich, fine-grained sediments in laboratory conditions (Revsbech et al. 1988). In seagrass beds,

the maximum observed Gross Photosynthetic O_2 production was equal to 6681.1 µmol O_2 m^{-2} h^{-1}. A 24.4 % (12 of 45) of the light sediment incubations showed a net autotrophic behavior (7 in PJ-SB, 3 in PJ-BP, and 2 in SH-BP). Nonetheless, only 3.1 % of the photic incubations had net autotrophic behavior based on the daily average O_2 consumption rates (2 in PJ-SB, 1 in PJ-BP, 0 in SH-BP). Likewise, in only three of 12 photic incubations a net influx of DIC associated with C fixation was observed (2 PJ-SB, 1 PJ-BP). Consequently, all habitat types are considered as net heterotrophic despite benthic primary production. Gross O_2 primary production averaged 678.9 ± 622.1 µmol m^{-2} h^{-1} in SH-BP (n = 9), 744.3 ± 1102.2 µmol m^{-2} h^{-1} in PJ-BP (n = 13), and 3811.8 ± 1945.6 µmol m^{-2} h^{-1} in PJ-SB (n = 9), with no significant differences among photic benthic habitats.

N_2/Ar ratios were measured in 79 sediment core incubations belonging to 18 stations located in SH. The saturation normalized N_2/Ar ratio at the beginning of incubation, considering all sediment cores, was equal to 102.2 ± 6.4 % and became more variable by the end of incubations (107.7 ± 21.2 %). After correction according to Section 2.3.3.3, 73 cores incubations (98%) showed significant differences in N_2/Ar ratios between times, but in only 65 of them (89%) the changes in N_2/Ar ratios were greater than the MIMS resolution (0.34 based on the N_2/Ar ratio of air-equilibrated standards). Net N_2 fluxes in these stations averaged -210.35 ± 781.99 µmol N_2 m^{-2} h^{-1}, and ranges between -4872.6 to 773.25 µmol N_2 m^{-2} h^{-1}. In 27 core incubations, a net efflux of N_2 probably associated with denitrification was observed. The remaining 38 core incubations showed a net N_2 uptake. No significant differences in N_2 fluxes were found among habitat types, nor among acoustic types (**Figure 9**). As well as, no significant relationships were found between LOI and denitrification rates at the bay-scale, nor at habitat-scale. The presence of negative and positive net N_2 fluxes suggest the interacting presence of N_2 fixation and denitrification in SH sediments.

Low nitrogen fixation rates (from 93.7 to 184.5 µmoles N m^{-2} h^{-1}) were confirmed in SH-BP through the acetylene reduction method. These values are within those found in similar sediments in summer (**Table A13**).

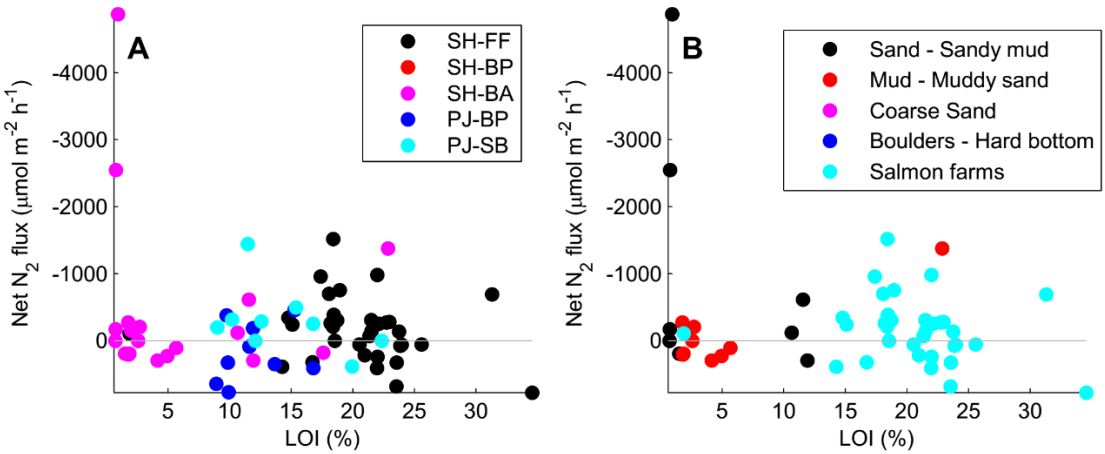

Figure 9: The empirical relationship between LOI and Net N_2 flux. Marker color represents different habitat types **(A)** and acoustic bottom type **(B)**. Legend key: Shelburne Harbour (SH), Port Joli Bay (PJ), fish farm sediments (FF), bare photic sediments (BP), bare aphotic sediments (BA), seagrass bed (SB).

2.4.3 Explained variability in benthic fluxes

Partial least squares regression (PLS) indicated that 12.6% (dark NH_3 flux) to 66.5 % (dark O_2 flux) of the total observed variance in benthic fluxes was explained by the predictor variables considered in this study (namely, LOI, salinity, porosity, temperature, depth, habitat and acoustic type, and O_2 availability at t_0) (**Figure 10**). PLS weights of single variables and component are shown for each flux in **Figure A31**. No single factor accounted for the majority of the variation in benthic fluxes. Based on the predictor's weights, the variables that contributed most to the observed variability in benthic fluxes were temperature, O_2 availability at the beginning of incubations, irradiance, and the percent mud, with minor contributions of salinity, bottom type, and acoustic bottom type. Incubation time is an experimental artifact that affected dark O_2 and DIC exchange rates. The remaining unexplained variability is distributed among non-evaluated processes and error measurements, which are discussed below.

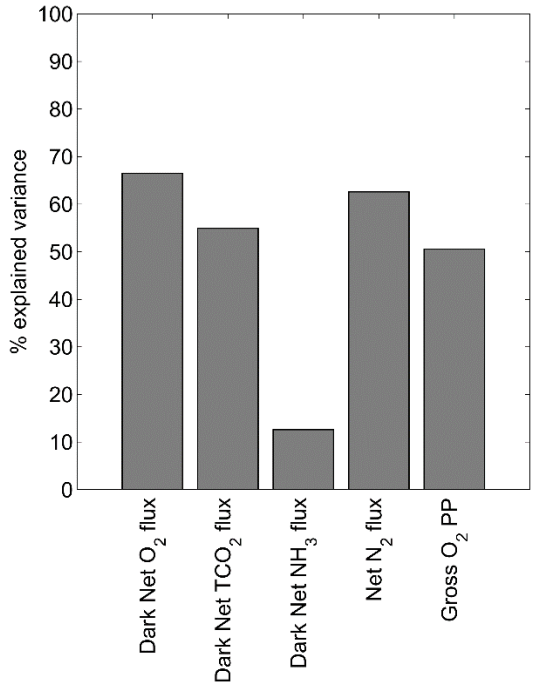

Figure 10: Partial least squares (PLS) regression analysis of benthic fluxes in relation to control variables. The plot shows the percent variance explained in benthic fluxes by predicting variables considered in this study.

2.4.4 Empirical relationships

2.4.4.1 Water depth, temperature, salinity, and incubation time

The regression analyses showed a positive relationship between temperature and benthic fluxes, particularly for dark O_2 ($n = 107$, $r^2 = 0.55$, $p < 0.05$) and DIC ($n = 35$, $r^2 = 0.37$, $p < 0.05$) exchange rates, considering all *in-situ* and laboratory incubations (**Figure 11**). Significant positive relationships were also observed between temperature and daily average O_2 ($n = 105$, $r^2 = 0.10$), DIC ($n = 25$, $r^2 = 0.46$, $p < 0.05$), and TA ($n = 25$, $r^2 = 0.28$, $p < 0.05$) fluxes. The increase in metabolic activity with increased temperature was particularly evident in PJ sediments exposed to higher isolation. The increased metabolic activity observed with increased temperature in the study area agrees with observational evidence from temperate environments (Jørgensen & Sørensen 1985, Middelburg, Klaver, et al. 1996, Wilson et al. 2013, Gudasz et al. 2015). Nonetheless, the high variability observed in the benthic fluxes also draws attention to the potential influence of other factors such as organic matter quality and primary production on this empirical relationship.

The magnitude and variability of benthic fluxes in photic sediments (PJ-BP, PJ-SB, and SH-BP) were significantly higher compared to aphotic sediments, which can be explained by the high variability in PAR irradiance, temperature, and photosynthetic biomass. I recall that most of the photic incubations were carried out *in-situ* (**Table 12**). An apparent relaxation of benthic fluxes with incubation time is suggested by regression analysis of dark O_2 ($n = 113$, $r^2 = 0.32$), DIC ($n = 35$, $r^2 = 0.35$) and TA ($n = 35$, $r^2 = 0.14$) exchange rates (**Figure 11**). This may be caused by a decrease in biological activity with incubation time. Nonetheless, regression coefficients are low ($r^2 < 0.35$) which difficult interpretation of this pattern. No significant relationships were observed between salinity and benthic fluxes.

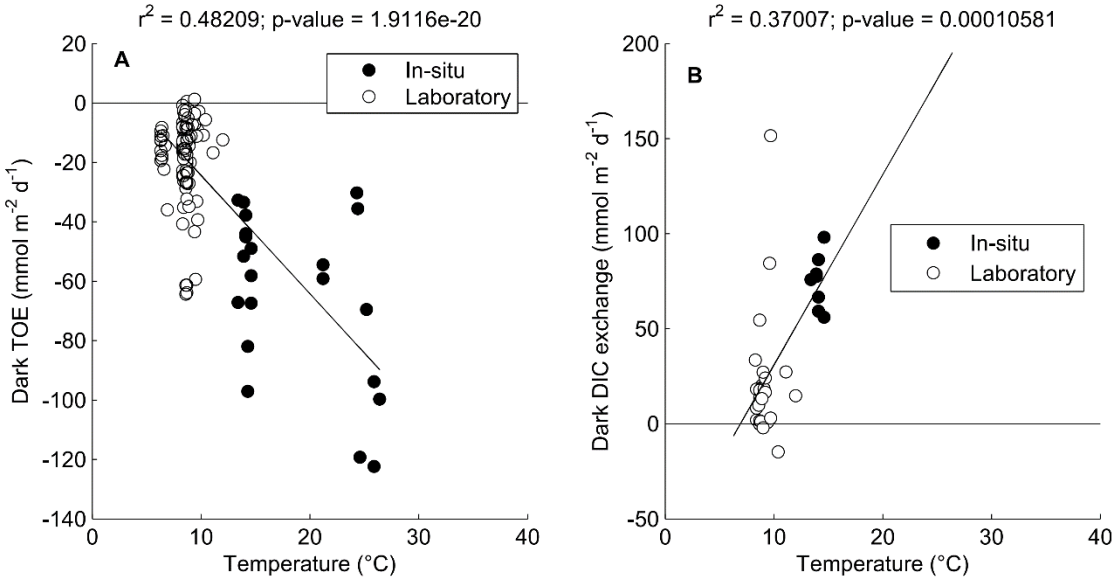

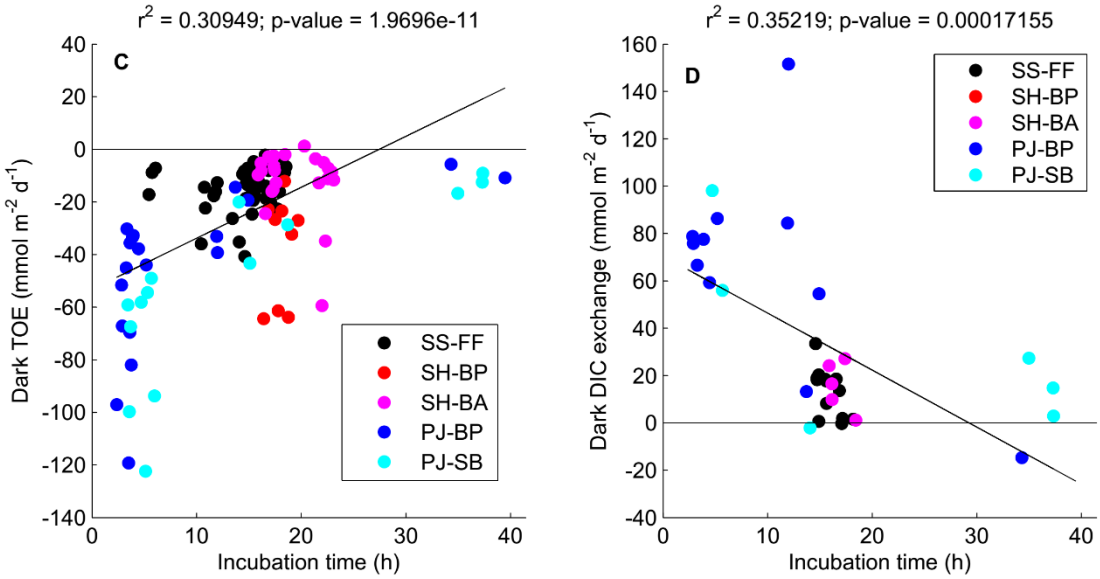

Figure 11: Empirical relationship between benthic fluxes and temperature of incubation **(A and B)**, as well as between benthic fluxes and incubation time **(C and D)**. TOE stands for Total O_2 exchange. Legend key: Shelburne Harbour (SH), Port Joli Bay (PJ), fish farm sediments (FF), bare photic sediments (BP), bare aphotic sediments (BA), seagrass bed (SB). Regression coefficients and p-values are reported on top of each figure.

2.4.4.2 **Sedimentological and acoustical variables**

No significant correlation was found between O_2 consumption rates and LOI over the entire data set (n = 192). However, significant positive correlations were found between LOI and dark-TOE in SH-FF (r^2 = 0.34, n=53) and PJ-BP (r^2 = 0.45, n=19) (**Figure 12**). Likewise, a positive correlation was observed in PJ-BP between LOI and light-TOE (r^2 = 0.34, n = 21). The daily average O_2 consumption also increased significantly with LOI in *in-situ* incubations (r^2 = 0.28, n=20), but no significant relationships were observed between both variables in the laboratory conditions.

No differences in O_2 and DIC fluxes were found between SH-FF (-561.1 ± 341.3 µmol m^{-2} h^{-1}, n = 55) and pristine sediments (-1359.9 ± 1186.9 µmol m^{-2} h^{-1}, n = 80). The highest dark TOE values were observed in PJ-BP and PJ-SG (up to 5097.3 µmol m^{-2} h^{-1}).

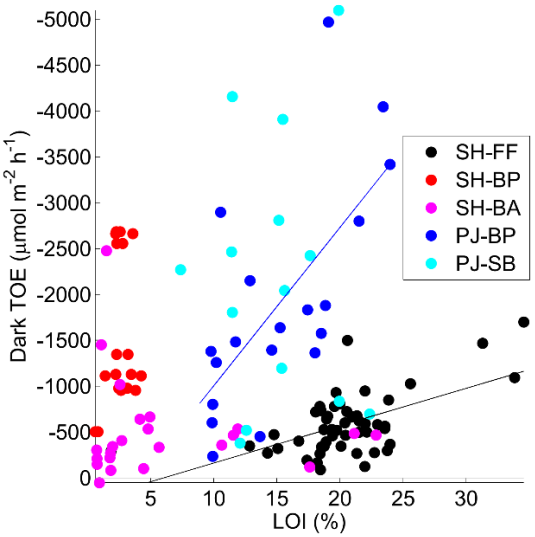

Figure 12: Dark respiration versus LOI for Shelburne Harbour (SH) and Port Joli (PJ) sediments. Legend key: Shelburne Harbour (SH), Port Joli Bay (PJ), fish farm sediments (FF), bare photic sediments (BP), bare aphotic sediments (BA), seagrass bed (SB). Except when indicated all p-values are < 0.05.

2.4.4.3 Flux ratios and metabolic quotients

Light incubations. Regression analysis indicated a significant increment of O_2 consumption rate with increasing NH_3 efflux in light incubations at PJ-BP ($r^2 = 0.41$, n = 13) and SH-BP ($r^2 = 0.72$, n = 7) (**Figure 13C**). No statistical relationships were observed between gross benthic O_2 production and DIC fluxes.

Dark incubations. Significant relationships were observed in dark fluxes at the bay-scale, i.e., when considering the entire data set. Among them, stands out the increased efflux of DIC (n = 35, $r^2 = 0.62$) and NH_3 (n = 96, $r^2 = 0.16$) with increasing O_2 consumption rates (**Figure 13A** and **B**). Likewise, a positive relationship was observed between DIC and TA exchange rates (n = 35, $r^2 = 0.75$, $p < 0.05$). At habitat-level, positive correlations were observed between dark TOE and dark DIC exchange rates in PJ-SB (n = 6, $r^2 = 0.85$, $p < 0.05$) and PJ-BP (n = 11, $r^2 = 0.39$, $p < 0.05$), as well as between TOE and NH_3 exchange rates in PJ-SB (n = 14, $r^2 = 0.51$, $p < 0.05$) and PJ-BP (n = 12, $r^2 = 0.38$, $p < 0.05$, **Figure 13A** and **B**). In SH-FF, a significant correlation was observed between TOE and TA exchange rates (n = 13, $r^2 = 0.32$, $p < 0.05$).

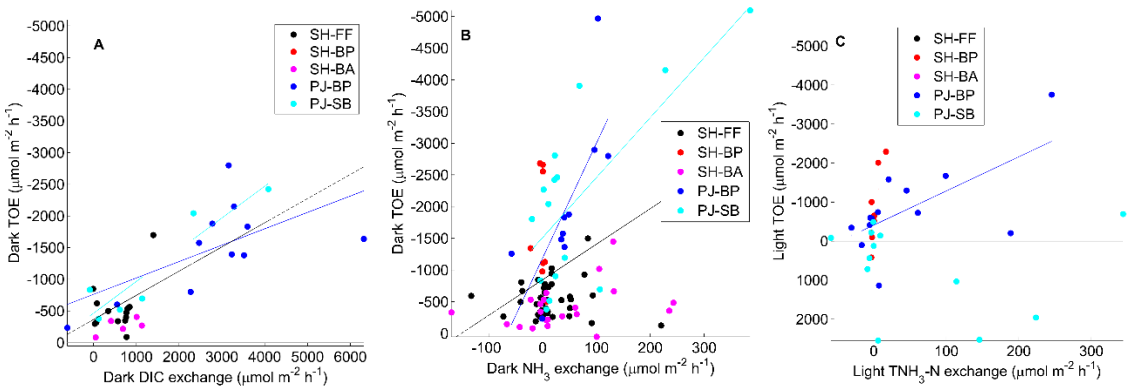

Figure 13: Flux ratios in dark and light incubations for Shelburne Harbour (SH) and Port Joli (PJ) sediments. **A.** Dark TOE vs. Dark Net DIC exchange. **B.** Dark TOE versus Dark NH_3 exchange rate. **C.** Light TOE versus Light NH_3 exchange rate. Legend key: Shelburne Harbour (SH), Port Joli Bay (PJ), fish farm sediments (FF), bare photic sediments (BP), bare aphotic sediments (BA), seagrass bed (SB). Except when indicated all p-values are < 0.05.

Average daily fluxes. Average daily fluxes in photic sediments were calculated based on net fluxes and number of light/dark hours. Light hours fluctuated during the sampling season between 11.9 and 14.2 hours (with the longest day length 15.3 hours at the summer solstice). No significant relationships were observed between the daily averaged benthic fluxes at bay-scale (i.e., considering the entire dataset). Nonetheless, several significant relationships were found at habitat-scale. A positive correlation was observed in PJ-BP between daily average DIC and TA exchange rates ($n = 8$, $r^2 = 0.97$) and between daily averaged O_2 and NH_3 exchange rates ($n = 8$, $r^2 = 0.83$). Nonetheless, these relationships should be carefully considered given the low number of samples on which they are built. Except for daily average DIC and TA exchange rates in mud and sandy-mud sediments ($n = 12$, $r^2 = 0.74$) no significant correlations between daily average fluxes were found within acoustically-derived bottom types.

Metabolic quotients. The RQ value (dark CO_2 flux: dark O_2 flux), calculated from 35 incubations where fluxes of O_2 and DIC were measured simultaneously, was 0.38 ($r^2 = 0.62$). The RQ does not change considerably after removal of SH-FF samples (RQ = 0.37, $r^2 = 0.60$, $n = 22$). In 89% of dark incubations, the O_2 uptake was lower than DIC efflux. The difference may be caused by several factors, but it is most probably associated with reoxidation of reduced compounds (NH_4^+, H_2S, Fe^{2+}, and Mn^{2+}) that consume alkalinity but produce DIC. This idea agreed with observed DIC efflux: TA efflux ratio in dark

incubations that was equal to 0.67, reflecting a relatively higher DIC efflux compared to observed TA efflux from sediment. The PQ value (gross O_2 production rate: gross CO_2 consumption rate) for light incubations in photic sediments was not calculated due to high variability in gross production rates in bare and seagrass beds.

Photosynthesis-Irradiance Relationship. PAR irradiance during *in situ* incubations varied significantly with time of the day, cloudiness, and turbidity affecting attenuation in the water column. The average PAR irradiance during in situ incubations ranged between 14.3 and 92.3 W m^{-2} (mean 30.5 ± 27.7 W m^{-2}), while in laboratory conditions it remained constant at 8.3 W m^{-2}. The lower values of PAR irradiance in laboratory conditions were due to the artificial light system. A marginal relationship was observed between gross photosynthetic O_2 production and PAR irradiance considering all photic habitats. Nonetheless, only a small proportion of total variation was explained by the PAR irradiance ($r^2 = 0.24$, n = 29). Similarly, only a marginal correlation was observed between PAR irradiance and the net NH_3 exchange rate in light conditions ($r^2 = 0.16$, n = 32). The high variability may be associated with the variable density of seagrass shoots and leaves within incubations, and spatial variations in benthic Chl-a distribution. In this regard, no correction for aboveground biomass of seagrass was applied to the benthic fluxes. Photosynthetic O_2 production can also be significantly affected by chemoautotrophic nitrification, which was not evaluated here. In this sense, an increasing daily average efflux of NO_3 was observed with increasing gross photosynthetic O_2 production (n = 12, $r^2 = 0.34$) which suggests that significant nitrification rates may be occurring in photic sediments. No correlations were detected among Chl-a content in surface sediments and benthic fluxes, except with the average NH_3 flux ($r^2 = 0.36$, n = 11).

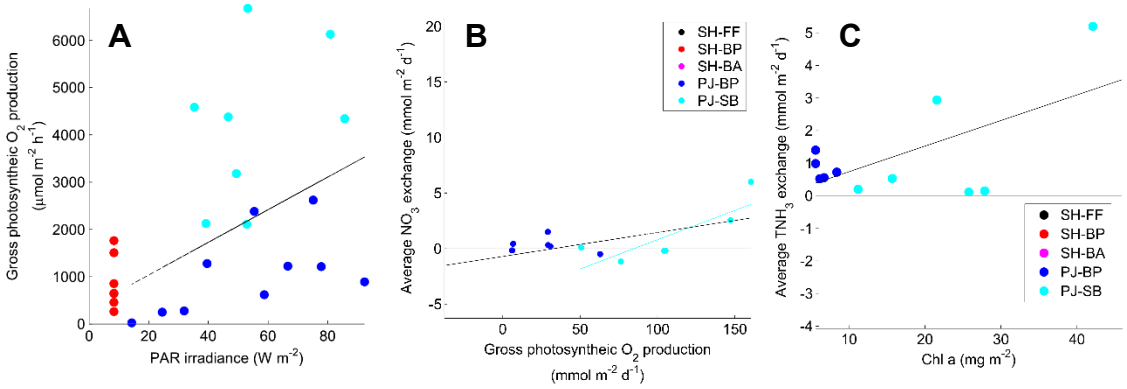

Figure 14: Empirical relationships between benthic fluxes and sedimentary variables in euphotic sediments. **A.** Gross primary production versus PAR irradiance. **B.** Gross primary production versus Average NO_3 exchange. **C.** Chl a content versus average NH_3 exchange. Legend key: Shelburne Harbour (SH), Port Joli Bay (PJ), fish farm sediments (FF), bare photic sediments (BP), bare aphotic sediments (BA), seagrass bed (SB). Except when indicated all p-values are < 0.05.

2.4.5 Integrated benthic rates

Depth-integrated remineralisation pathways of nitrogen were determined based on net dark fluxes (O_2, NH_3, NO_3, and N_2) and stoichiometric equations as described below (**Table 3**). Predicted rates include ammonification (DIR_{AM}, the heterotrophic transformation of organic nitrogen to NH_4^+), canonical denitrification (DIR_{DF}, the anaerobic reduction of nitrate to N_2 associated with organic carbon oxidation), nitrification (DIR_{NI}, the aerobic oxidation of NH_4^+ to NO_3^-), and N_2 fixation (DIR_{NF}, measured through acetylene reduction).

Table 3: Formulae used for the estimation of depth-integrated rates (DIR) of nitrification (NI), denitrification (DF), ammonification (AM), and blended carbon degradation rates by oxic respiration (OR), sulfate reduction (SR) and metal reduction (MR) for SH sediments.

Benthic rate	Unit	
$DIR_{NI} = NO_3$ dark efflux $+ N_2$ dark efflux	µmol N m^{-2} h^{-1}	**Eq. 1**
$DIR_{DF} =$ Net N_2 dark flux $+ DIR_{NF}$	µmol N m^{-2} h^{-1}	**Eq. 2**
$DIR_{AM} =$ Net NH_3 dark flux $+ DIR_{NI}$	µmol N m^{-2} h^{-1}	**Eq. 3**
$DIR_{OR-SR-MR} =$ Net O_2 dark flux $- 2 * DIR_{NI}$	µmol C m^{-2} h^{-1}	**Eq. 4**

Following Fennel et al. (2009), I estimated the nitrification rate as the sum of N_2 and NO_3 efflux from the sediment (data points with net N_2 influx were excluded from

calculation; **Eq. 1**). On average, nitrification for SH sediments equals 394.1 ± 330.0 μmol N m^{-2} h^{-1}. Likewise, from **Eq. 2**, and assuming a C:N ratio of 106:42.4, the denitrification rate for SH sediments was 1787 ± 1214 μmol C m^{-2} h^{-1}. Finally, from **Eq. 3** the average ammonification rate, as the sum of the net NH_3 flux plus nitrified nitrogen, was 425.6 ± 383.6 μmol N m^{-2} h^{-1}. Although these values are within observations for coastal temperate environments, the uncertainty in these calculations is relatively high given the high variability in benthic fluxes from which they were calculated, and the low number of N_2 fixation measurements available in the study area.

A second approach to estimate nitrification rates for SH sediments was based on diagenetic simulations reported in Chapter 3 for SH sediments. There, the rate of aerobic ammonification was estimated from observed net O_2 fluxes and model estimations of oxic respiration rates. According to simulations, and assuming Redfield stoichiometric relationships (106C: 16N: 1P), oxic respiration during summer accounts for 88% to 94% of total O_2 consumption in muddy to sandy sediments in SH. By taking an average value of 91%, the expected NH_4^+ production, associated with oxic respiration is equal to 142.1 ± 109.6 μmol N m^{-2} h^{-1}. This value is within calculated nitrification rate according to **Eq. 1**.

Finally, by assuming steady-state conditions and complete reoxidation of reduced by-products, the rate of C_{org} oxidation in sediment, except by denitrification, can be approximated as the difference between total O_2 consumption and corresponding consumption by nitrification (assuming a 1:1 ratio). The resulting C_{org} oxidation rate was equal to 246.3 ± 1.016 μmol C m^{-2} h^{-1}. Again, the large variability of measured benthic fluxes introduces a high uncertainty in this estimation.

2.5 Discussion

2.5.1 Major finding

Despite the high observed variability, significant relationships in metabolic activity were observed at habitat-scale. Among them, highlight the correlation observed between O_2 consumption rates and inorganic C production (a by-product of C degradation) in seagrass beds and BMA-rich sediments, as well as the significant increase in O_2 consumption rates with organic content observed in BMA-rich sediments and in

fish farm sediments. Sediment properties, including LOI, porosity, mud content and grain size were significantly correlated in the study area and exhibited values that differed significantly across habitat types, but not among acoustically-derived bottom types. The observed high variability in metabolic activity emphasizes the complex relationship between benthic metabolism and controlling factors. Nonetheless, the significant differences found in sediment properties among habitat types, and their relationship with benthic fluxes at habitat-scale emphasize the role that habitat diversity and sediment-biological interactions (e.g., autotrophic activity) have on diagenetic processes in coastal areas. The fact that no significant differences in sediment properties were observed among acoustically-derived bottom types may be the result of the probably continuous, rather than discrete, distribution of sediment types across SH, with transitional zones in between distinct end-members (mud, sand, gravel).

Chl-a content in eelgrass leaves was within values reported for the area (Wong et al. 2012), but up to an order of magnitude higher than values reported for *Z. marina* at different global locations, which ranged from 0.8 to 1.7 mg g^{-1} fresh weight in eelgrass leaves (Zimmerman et al. 1991, Cummings & Zimmerman 2003, Cabello-Pasini et al. 2004, Liu et al. 2011, Wong et al. 2012). Chl-a values in photic bare sediments at PJ were also within the range reported in the literature for various coastal sediments that may reach up to 560 mg Chl-a m^{-2} (MacIntyre et al. 1996). Despite the presence of benthic primary producers (BMA and seagrass), all habitat types showed a net heterotrophic behavior, with a net influx of O_2, and a net efflux of TNH_3 and DIC in the majority of sediment incubations.

The combination of benthic habitat mapping, empirical measurements, and multivariate analysis demonstrate its utility in incorporating multiple scales of variability, an aspect emphasized by several recent studies (Lecours et al. 2015), as well as in differentiating potential drivers of ecosystem functioning. However, further efforts are required to incorporate time-dependent dynamics as discussed later.

Results showed that no single variable was sufficient to explain the observed variability in benthic fluxes. In fact, only a moderate fraction of observed variability in benthic fluxes was explained by ecosystem controls considered in this study (11.2% to

69.3%). The variables that most contributed to the observed variability in benthic fluxes at the bay-scale were temperature, O_2 availability, irradiance, percent mud content in sediments and depth, while LOI only showed a significant explanatory power when data were disaggregated by habitat types.

As shown before, the O_2, NH_3, and DIC exchange rates in fish farm sediments were not significantly higher than in pristine sediments, despite the significantly higher LOI content. These observations may be explained by the fact that fish farm sediments were considerably muddier and probably dominated by diffusive transport, which may limit O_2 supply to sediments. This process may be exacerbated in azoic conditions, as observed in sediment samples, due to null bioturbation activity.

2.5.2 Sources of uncertainty

Observed variability in benthic processes results from the inherent natural variability of benthic processes and/or measurement error. Non-evaluated factors affecting natural variability in benthic fluxes include (1) nonlinear and asynchronous dynamics, and (2) secondary biogeochemical reactions. Error measurements may be related to (1) spatial (resolution and extent) and thematic (habitat and sediment type) scales of analysis, and (2) data quality (see below).

2.5.2.1 Nonlinearities and asynchronies in sediment biogeochemical cycles

In this study, I explored empirical relationships assuming linear and synchronous dependency. Nonetheless, benthic processes are known to be affected by multiple nonlinear and lagged controls. Nonlinear dynamics in sediment may occur due to the simultaneous interaction of inhibiting and limiting factors on biogeochemical processes. Nonlinearities in O_2, C and nutrient cycles has been described in empirical studies at multiple spatial and temporal scales (Omori et al. 1994, Fossing et al. 2004, Eyre & Ferguson 2009, Reid et al. 2013, Sturtevant et al. 2016), and incorporated into diagenetic models representing sediment biogeochemical cycles (Soetaert et al. 1996, Boudreau 1997).

For instance, Eyre & Ferguson (2009) suggested that denitrification rates might follow a threshold model featured by a peak in denitrification activity in suboxic conditions when sufficient inputs of organic C and nitrate occur simultaneously within

sediments. The co-occurrence of these factors may be observed in early fall, due to the accumulation of organic C during spring and summer, and the simultaneous increase in oxidant availability in fall as a result of decrease primary production and increased water column mixing.

Nonlinear time-dependent relationships have also been described for H_2S production and reoxidation in sediments (Fossing et al. 2004). The ability of sediment to reoxidize H_2S varies seasonally as a function of O_2, and metal oxides availability, which instead oscillates between periods of surplus and deficit in relation to demand and renewal.

Consequently, the analysis of time-dependent and nonlinear dynamics is an area of critical research to further understand sediment biogeochemical cycles in coastal areas. This is particularly relevant for temperate regions, such as Nova Scotia, featured by strong seasonality, severe winters, no dry season, and warm summers (Köppen-Geiger classification: Dfb). Likewise, other large-scale dynamics may also influence benthic activity. These include the occurrence of stochastic events as deep-water exchange intrusions as described for the nearby Bedford Basin (Burt et al. 2013).

2.5.2.2 **Unevaluated secondary processes**

Secondary processes not evaluated in the study that may contribute to the observed variability in benthic fluxes and empirical relationships include, among others, NH_4^+ adsorption, and the presence of alternative pathways of N_2 production in sediments. NH_4^+ adsorption into sediments can limit its availability for autotrophs and nitrifiers, affecting instead coupled denitrification rates (Mackin & Aller 1984, Hou et al. 2003). N_2 production coupled to Mn, Fe, and S cycles have also been described by Schrum et al. (2009), Luther et al. (1997), and Seitzinger (1988), among others. Other sources of uncertainty in N_2 flux measurements may be related to the incomplete reduction of NO_3^- to N_2 leading to underestimation of denitrification rates. Likewise, the quality of organic deposits may also affect mineralization rates in sediments, and observed flux ratios. Organic deposits are complex mixtures of allochthonous and autochthonous compounds of different ages and qualities. In this sense, LOI measurements reflect the total content of

organic matter but not the quality of it, which may strongly affect oxidation processes in sediments.

2.5.2.3 Spatial (resolution and extent) and thematic (habitat and sediment type) scales of analysis

Natural variability in benthic processes is embedded in multiple spatio-temporal scales. In this sense, the habitat types in this study were selected to reflect variability from habitat- to bay-scale, and considered sediment types, light irradiance, and the presence of structuring species (eelgrass). Future considerations may incorporate other bottom types or coastal features as long as they increase the explanatory power of benthic activity (e.g., tidal channels, and intertidal shoals).

2.5.2.4 Data quality

The major sources of error I detected in the data set relates with 1) the probable occurrence of unnoticed solubility- and pressure-driven fluxes during sediment incubations, 2) the interference of ion fragments during N_2/Ar detection, 3) the low precision achieved in N_2/Ar measurements, 4) bias in estimations of N_2 fixation rates based on the acetylene reduction assay, 5) dependency of incubation time, and finally, 6) uncertainties in the spatial interpolation of sediment properties.

Bias associated to solubility-driven fluxes were managed by discarding incubations were bubbles formation was observed. Nonetheless, this was rather difficult to monitor during *in-situ* incubations in shallow sediments. Likewise, the stirring conditions during incubations (i.e., rpm and height above sediment-water interface) were defined in order to avoid sediment resuspension, and a central out flushing of dissolved compounds through the sediment-water interface (60 rpm).

Denitrification studies require a precision in terms of percent coefficient of variation (% CV) < 0.05 for N_2/Ar measurements (Kana et al. 1994), however only a 0.6 to 5.7% was achieved in this study. The sample injection system based on a submersible probe proved not effective as it limits dissolved gas sampling to those areas immediately around the probe, as opposed to a flow-through membrane system as suggested by Kana et al. 1994, These measurements may also be improved by longer incubation times (> 24 hours).

The acetylene reduction assay has been extensively used in N_2 fixation studies. Nonetheless, various biases in the assay have been described, mostly in relation to the conversion rates between acetylene reduction and corresponding N_2 fixation rate. The low number of measurements also limits the capacity to extrapolate conclusion to broader scales. As well as, a considerable decrease in O_2 in the water column was observed during acetylene bubbling, which may also affect sediment metabolism under laboratory conditions.

Incubation time affected flux measurements of O_2 and DIC significantly due to an apparent relaxation of metabolic activity with incubation time. Future research is required to confirm this trend.

Finally, differences in accuracy may be explained by the natural variability of sediment types, which is a consequence of the dominant hydrodynamic regime, as well as by the intensity and spatial distribution of samples. The choice of variogram model, including search radius and the number of the closest neighboring points used for estimation, may also affect the interpolation performance.

CHAPTER 3. SEASONAL SEDIMENT FLUX MODELING IN A COASTAL BAY OF NOVA SCOTIA, CANADA.

3.1 Abstract

The integration of a one-dimensional diagenetic model of sediment geochemistry, benthic habitat mapping (depth, sediment type), and environmental time series (C_{org} deposition, temperature, PAR irradiance) was used to predict bay-scale carbon and nitrogen recycling rates in subtidal photic and aphotic sediments of an oligotrophic coastal system in Nova Scotia, Canada. Variability in benthic processes and scales of response to changes in forcing conditions were also analyzed at hourly to seasonal scales.

Model results highlight the dynamic effects of seasonal forcing (bottom temperature, PAR irradiance, and C_{org} deposition) on benthic flux variation and ecosystem functioning. Lagged responses of weeks to months were predicted in benthic primary production, C_{org} mineralization, and reoxidation of reduced by-products in relation to seasonal cycles of PAR irradiance and C_{org} deposition.

Oxidant availability decreased considerably in the summer and early fall due to increased C_{org} deposition but recovered by late winter, when accumulated reduced compounds were completely reoxidized, and oxidant availability re-established in sediments. Summer denitrification was coupled with nitrification activity that slightly intensified during winter months. Biomass of benthic microalgae maximizes in late summer, three months after the summer solstice. These patterns emphasize the need to consider daily to seasonal scales of variability in simulations of coastal diagenetic processes, where steady state conditions cannot be necessarily assumed.

Our model predicts that SH sediments play a significant role in nutrient cycling and C_{org} mineralization at the bay scale. Bay subtidal sediments behave as an active source of nutrients to the water column (NO_3, NH_3, Fe^{2+}), contributing 31.6 tonnes NO_3 y^{-1} and 83.7 tonnes NH_3 y^{-1} to the water column. Simulations suggest that denitrification was a significant sink of nitrogen in the bay, removing ~27% of total annual nitrogen

inputs to sediments (37.9 tonnes y^{-1}). Denitrification activity increased with C_{org} deposition in the range imposed in the simulations (8.9 - 28.2 mmol C_{org} m^{-2} d^{-1}).

Our model lacks many factors that control C and N recycling efficiencies, such as lateral transport within sandy sediments and alternative pathways of N_2 formation, and is therefore conservative in its prediction of C and N removal from coastal areas.

3.2 Introduction

Compared with open ocean environments, coastal areas are characterized by tighter benthic-pelagic coupling. As a result, a significant fraction of energy and matter cycling, storage, and sequestration occurs in the benthos (Jahnke & others 2005, Middelburg et al. 2005, Muller-Karger et al. 2005, Seiter et al. 2005). Despite this, the contribution of the benthos to coastal biogeochemical cycles varies extensively throughout different spatial and temporal scales. Variations come from physicochemical forcing and community, and habitat processes acting internally and externally on the system (Jones et al. 1994, Van de Koppel et al. 2012).

Defining relevant scales of variability and responses to controlling factors is crucial to further understanding of coastal biogeochemical cycles, to connect local processes with the macroscopic behavior of coastal and open ocean systems, as well as to distinguish between natural and human-induced variability. In shallow benthic environments (<200 m) this requires consideration of habitat composition, sediment-biological interactions, and coupling with terrestrial and water column environments. Sediment-biological interactions are multiple, and an extensive review is not intended here (see Kristensen (2005)). Nonetheless, community processes in shallow benthic environments are strongly driven by the presence of structural species (i.e., those that provide the physical structure of the environment, like seagrass) and macrobenthos via bioturbation, irrigation, and feeding.

Among benthic processes, seasonality in denitrification rates has frequently been reported in the literature (Nowicki et al. 1997, Tuominen et al. 1998, Cabrita & Brotas 2000, Sundbäck et al. 2000). Likewise, seasonality in the pattern of benthic C_{org} oxidation, bioirrigation intensity, solute fluxes, and benthic primary production has been

reported in coastal and shelf sediments (Berelson et al. 1998, 2003, LaMontagne et al. 2002). Little seasonality has been reported in oxygen and phosphate fluxes (Berelson et al. 2003), which can be the result of nonlinear and asynchronous processes. Nonlinear interactions mostly occur due to the presence of limiting and inhibiting factors, while asynchronous processes are usually observed due to lag responses of benthic activity to changes in environmental conditions.

Anthropogenic forcing also plays an increasing role in the state and evolution of coastal systems. Although natural variability can be considered an intrinsic component of coastal biogeochemical cycles, the rate and magnitude of variation has been significantly affected by human activities, influencing the structure, composition, and functioning of numerous coastal systems around the world (Galloway et al. 2004, Liu 2010). However, human-environment interactions are complex and may overlap in time and space resulting in additive, synergistic, or antagonistic effects. The incorporation of biological and anthropogenic interactions and the scales of response have been emphasized in multiple studies that encourage further research (Morse et al. 2003, Seitzinger et al. 2006, Fennel et al. 2009, Groffman et al. 2009, Piehler & Smyth 2011).

Approaches to predicting benthic processes such as carbon and nutrient cycling at larger spatial (local, regional, global) and temporal scales (daily, seasonal, decadal) range from simple upscaling of point measurements (e.g., mesocosm and core incubation experiments, eddy-covariance flux measurements, flow over benthic systems), to more sophisticated approaches based on nutrient budgets (Chen & Wang 1999) and diagenetic modeling (Krumins et al. 2013). Among them, the empirical parameterization of benthic processes (fluxes and rates) in relation to forcing conditions has been widely used to increase understanding of associations and to generate better predictive models. Examples of the latter include the prediction of denitrification or carbon mineralization rates in relation to total CO_2 fluxes (Middelburg, Soetaert, et al. 1996, Eyre & Ferguson 2009), sediment O_2 consumption (Glud 2008), total N inputs, sediment type (Deutsch et al. 2010), and water residence time (Seitzinger et al. 2006), among others.

In coastal areas, only a few empirical studies have focused on the prediction of benthic processes and functional value of the benthos at the bay-scale (Brock et al. 2006,

Harborne et al. 2006, Eyre & Maher 2011), with no recognized examples of numerical models applied to this spatial scale. In this sense, models of sediment geochemistry that consider the distribution of seascape features and forcing conditions represent a valuable tool for ecosystem-scale assessments of benthic processes, particularly where the coverage of biogeochemical measurements is limited, or the studied process is directly unmeasurable.

One approach to building such models is the integration of diagenetic modeling, empirical parameterization, and benthic habitat mapping. This approach provides a means of ecosystem-scale assessments of benthic processes including both intra- and inter-habitat variability. The geo-referencing of benthic physical and biological variables can be used to produce maps showing their spatial and temporal distribution, which represent an important input for ecological and modeling studies. Its development may strongly facilitate the exploration of scale-dependent, nonlinear, and asynchronous processes, and their influence on ecosystem functioning. To my knowledge, no studies based on the combination of these methods have been used to interpret measurements of whole ecosystem diagenetic processes in coastal areas.

In this research, a deterministic model of sediment geochemistry was developed with the objective of predicting daily to seasonal dynamics in C and N cycling in subtidal sediments of a coastal bay of Nova Scotia, Canada. I focused on two significant processes, C mineralization and denitrification rates, nevertheless, a broader set of benthic processes were considered to adequately represent system functioning, namely, benthic primary production, and bioturbation. Likewise, I estimate the specific contribution of major habitat/sediment types to C and N removal via mineralization and denitrification and compare them with other significant sources and sinks of C and N in the study area.

The characterization of C and N recycling rates has multiple implications, especially for those areas where denitrification and C recycling are natural mechanisms to prevent coastal eutrophication. Benthic denitrification is considered the most significant natural sink of fixed N from estuarine and open ocean waters (Cornwell et al. 1999, Groffman et al. 2006, Fennel et al. 2009), strongly influencing primary productivity, water quality, and air chemistry.

3.3 Methods

3.3.1 Study site

This study was conducted in Shelburne Harbour (SH, 43.71, -65.33), a large (24.04 km2), shallow and well-sheltered harbour (mean depth of 8.4 m, and a maximum depth of 17.44 m), located on the south shore of Nova Scotia, Canada. This semidiurnal tidal system is connected to the sea by a relatively narrow passage with a maximum depth of 14 m. Around 50 % of the bay area is shallower than 10 m. According previous studies, sheltered areas support eelgrass (*Zostera marina*) beds in the subtidal zone and saltmarsh grasses (*Spartina* spp.) in the intertidal and higher elevations (Stewart & White 2001, Bundy et al. 2014). However, at the sampling time no significant eelgrass communities were observed in the subtidal sampled areas.

The Shelburne Harbour watershed area (or Roseway, Sable, Jordan River watershed) is 1430.2 km^2 (Nova Scotia Department of Natural Resources). Watershed soils are mostly dominated by natural stands, including multiple fragments of intact forest, barren vegetation, and wetlands. No significant agriculture is developed in the watershed due to lack of productive soil. With the exception of the town of Shelburne (~7900 persons in 2015), low urban development occurs in the area.

The major fresh water source is the Roseway River located at the head Shelburne Harbour with an estimated annual discharge of 5.53 x 10^8 m^3 y^{-1} (Water Survey of Canada). The tidal/freshwater volume ratio equals 68.29 (Gregory et al. 1993). The DON export from the Roseway watershed to SH is equal 0.9 kg ha^{-1} y^{-1} (Aitkenhead-Peterson et al. 2005), or ~ 44.5 tonnes DON y^{-1} for the entire watershed (495 km^2). Based on former estimations (Gregory et al. 1993) the SH volume at low tide is approximately 140x10^6 m^3, while the tidal prism of the bay is approximately 37.2 x 10^6 m^3. Tidal range and flushing time are 1.7 m and 52.6 hours, respectively. Assuming complete mixing, the exchange rate for Shelburne Harbour at Sandy Point is ~21% (**Figure 16**).

3.3.2 Model development and data processing

The simulation of sediment biogeochemical cycles from habitat to bay-scale was based on the combination of a one-dimensional (1D) depth-resolved diagenetic model, and time-space upscaling based on benthic habitat mapping and empirical

parameterizations of forcing conditions. A summary of the numerical model is provided in **Table 4**. The model required three types of input: (1) annual time series of bottom temperature, solute concentration in bottom waters, particle deposition, solar irradiance, and sediment colonization by benthic microalgae (BMA) (2) bathymetry and sediment porosity, and (3) constant parameters that determine benthic processes (C_{org} degradation, benthic primary production, secondary reactions, etc.). The outputs of the model are time series of concentrations, rates, and fluxes of solutes and particle compounds, from which summary outputs and derived quantities are calculated.

3.3.2.1 **Early diagenetic processes**

This numerical model aimed to capture the essential features of sediment biogeochemical processes in coastal environments including:

1. the depth distribution and time evolution of particle and solute concentration in surficial sediments (20 cm)
2. the mean vertical fluxes across the sediment-water interface, and consumption/production rates at hourly to seasonal scales, and
3. the response of benthic processes to changes in boundary conditions: particulate organic carbon (POC) input, benthic primary production, and oxidant availability in bottom water

In diagenetic models, the rate of change in vertical concentration of solid and dissolved species is a function of changes due to vertical advection, diffusive processes, and transformations due to biogeochemical reactions. For depth-resolved models (multi-layer), the general diagenetic equation describing cycling of solid (S_i) and dissolved (C_i) constituents are:

$$\boldsymbol{\varphi_s \frac{\partial S_i}{\partial t}} = -\varphi_s \frac{\partial}{\partial z}(w_{sed} S_i) + \varphi_s \frac{\partial}{\partial z}\left(D_B \frac{\partial S_i}{\partial z}\right) + \sum R(S_i, C_i) \qquad \textbf{Eq. 5}$$

$$\boldsymbol{\varphi \frac{\partial C_i}{\partial t}} = -\varphi \frac{\partial}{\partial z}\left(w_{pw} C_i\right) + \varphi \frac{\partial}{\partial z}\left(D_{C_i} \frac{\partial C_i}{\partial z}\right) + \sum R(S_i, C_i) \qquad \textbf{Eq. 6}$$

In **Eq. 5** and **Eq. 6**, z is the depth below the sediment-water interface (cm), φ = sediment porosity, φ_s is the solid porosity $(1-\varphi)$, w_{sed} = sediment burial velocity (cm y^{-1}), w_{pw} = porewater advection velocity relative to the sediment-water interface (cm y^{-1}), D_B = biodiffusion coefficient (cm^2 y^{-1}), D_{C_i} = molecular diffusion coefficient of solute species i (cm^2 y^{-1}), and $\sum R(S_i, C_i)$ corresponds to the biological and geochemical reactions involving solid and solute species.

The diagenetic model was adapted from MATSEDLAB (Couture et al. 2009, Huber et al. 2014), and modified to incorporate light irradiance (Brock 1981), BMA dynamics (Hochard et al. 2010), temperature dependency (Eppley 1972), and diffusion coefficients corrected for temperature and tortuosity (Berner 1980, Ullman & Aller 1982). Further details are provided in following sections.

The reaction network included 15 chemical species and 6 primary redox reactions (**Table 5**). The diagenetic model covered the first 20 cm of sediments where most redox reactions occur. The vertical domain was divided into 32 layers with finer discretization close to the surface. This discretization was chosen as it provided the more stable (and faster) solution to the numerical model.

Table 4: Model summary.

Model structure	
Modeling aim	C and N cycling in coastal sediments.
Chemical species (15)	7 particulate (C_{POC1}, C_{POC2}, C_{BMA}, C_{EPS}, N_{BMA}, $Fe(OH)_3$, FeS). 8 dissolved (O_2, NO_3^-, NH_3, N_2, Fe^{2+}, Total S^{2-}, $SO_4^=$, Chl-a).
Transport processes (1D)	Particulate compounds → Advection, biodiffusion, bioirrigation Dissolved compounds → Advection, and molecular diffusion
Chemical reactions (10)	Oxic respiration, Denitrification, Iron reduction, Sulfate reduction, Reoxidation of NO_3, Fe^{2+}, Total S^{2-} with O_2 and $Fe(OH)_3$, Primary production by BMA, and FeS precipitation/dissolution.
Electron acceptor for organic matter oxidation	O_2, NO_3^-, $Fe(OH)_3$, SO_4^-.
Boundary conditions	O_2, SO_4^{2-}, Total $S^=$, NO_3^-, NH_4^+, N_2, and Fe^{2+} concentration in free flow bottom water. Particulate organic carbon (C_{POC1}, C_{POC2}) and $Fe(OH)_3$ deposition to surface sediments.

Forcing processes	Bioturbation, salinity, temperature, temperature-dependent solute diffusivity, depth independent sediment porosity, and PAR irradiance (at 43.865 North).
Spatial domain	
Total area of the bay (Km^2)	24.04
Resolution (m)	86.9
Cell area (m^2)	7560
Spatial grid (xyz)	140 * 108 * 35
Wet cells	3180/15120 (21%)
Depth	0-17 m
Vertical resolution	32 layers. 19.24 cm in total, including 6 layers of 0.5 mm, 10 layers of 1 mm, 5 layers of 2 mm, and 11 layers of 1.54 cm.

The description of organic matter degradation was based on the classic G-model (Westrich & Berner 1984). Three pools of organic carbon with specific degradation rates were defined in the model: labile and refractory C_{org} associated to POC deposition (0.1 and 0.001 y^{-1}, respectively) and exopolymeric substances (EPS) produce by BMA (0.26 y^{-1}). Oxidant limitation and inhibition terms of metabolic reactions were expressed through Monod type hyperbolic functions and reciprocal hyperbolic functions, respectively.

The major processes controlling the concentration of solutes and particulate compounds in the overlying water and sediments were diffusive and advective transport, C_{org} mineralization (oxic/anoxic), nitrification, primary production by microphytobenthos, burial, and mineral precipitation (FeS, FeS_2). Stoichiometric relationships in biochemical reactions were based on Redfield ratios. Canonical denitrification and burial are the unique sinks of fixed nitrogen. Not considered here are anaerobic ammonium oxidation (anammox), dissimilatory nitrate reduction to ammonium (DNRA), nor others pathways of N_2 production coupled with S, Fe and Mn cycles (Luther et al. 1997, Schrum et al. 2009). *In situ* NH_4^+ production can be nitrified, diffuse across sediments, or be taken up by BMA. NO_3 reduction to N_2 via denitrification is assumed complete with no intermediate products (nitrite, nitric oxide, or nitrous oxide).

Model parameters were taken from the literature (reaction rates, half-saturation constants, stoichiometric coefficients, diffusion coefficients, equilibrium constants, community parameters, and temperature coefficients). In order to account for

comparatively larger degradation efficiencies of C_{org} under oxic versus anoxic respiration, a dimensionless acceleration factor of 26.5 was included in the model (Canavan et al. 2006, Couture et al. 2009). The set of partial differential equations were solved using the finite difference-based solver *pdepe* in MATLAB that selects the time step dynamically.

Table 5: Idealized set of biogeochemical reactions.

Redox process		Reaction
Primary redox reactions		
R01	Aerobic respiration	$\mathrm{Org} + \mathrm{O_2} \rightarrow \mathrm{CO_2} + 0.05\,\mathrm{NH_3}$
R02	Nitrate reduction	$\mathrm{Org} + 0.8\mathrm{NO_3^-} \rightarrow \mathrm{CO_2} + 0.4\,\mathrm{N_2} + 0.05\,\mathrm{NH_3}$
R03	Iron reduction	$\mathrm{Org} + 4\mathrm{Fe(OH)_3} \rightarrow \mathrm{CO_2} + 4\mathrm{Fe^{2+}} + 0.05\,\mathrm{NH_3}$
R04	Sulphate reduction	$\mathrm{Org} + 0.5\mathrm{SO_4^{2-}} \rightarrow \mathrm{CO_2} + 0.5\mathrm{H_2S} + 0.05\,\mathrm{NH_3}$
R05	Primary production	$\mathrm{CO_2} + \mathrm{HNO_3} \rightarrow \mathrm{Org} + \mathrm{NH_3} + \mathrm{O_2}$
Secondary redox reactions		
R06	Nitrification	$\mathrm{NH_3} + 2\mathrm{O_2} \rightarrow \mathrm{HNO_3} + \mathrm{H_2O}$
R08	Fe(II) oxidation by O_2	$4\mathrm{Fe^{2+}} + \mathrm{O_2} \rightarrow 4\mathrm{Fe(OH)_3} + 8\mathrm{H^+}$
R08	S(II) oxidation by O_2	$\mathrm{H_2S} + 2\mathrm{O_2} + 2\mathrm{HCO_3^-} \rightarrow \mathrm{SO_4^-} + 2\mathrm{CO_2} + 2\mathrm{H_2O}$
R09	S(II) oxidation by $Fe(OH)_3$	$\mathrm{H_2S} + 14\mathrm{CO_2} + 2\mathrm{Fe(OH)_3} \rightarrow 2\mathrm{Fe^{2+}} + \mathrm{SO_4^{2-}} + 14\mathrm{HCO_3^-} + 6\mathrm{H_2O}$
R10	Iron sulfide oxidation	$\mathrm{FeS} + 2\mathrm{O_2} \rightarrow \mathrm{Fe^{2+}} + \mathrm{SO_4^=}$
Other kinetic reactions		
R11a	FeS dissolution	$\mathrm{FeS} + 2\mathrm{H^+} \rightarrow \mathrm{Fe^{2+}} + \mathrm{H_2S}$
R11b	FeS precipitation	$\mathrm{Fe^{2+}} + \mathrm{H_2S} \rightarrow \mathrm{FeS} + 2\mathrm{H^+}$

3.3.2.2 **Spatio-temporal forcing**

Subtidal sediments were categorized based on acoustic mapping, bathymetry, mud content, porosity, and PAR irradiance reaching surface sediments. Three large sediment categories were generated: 1) bare photic sediments in mud and sand (P-M&S), aphotic sediment in 2) mud to sandy-mud (A-MSM) and 3) sand to muddy-sand (A-SMS). From field observations the mean porosity of each category was 0.63 ± 0.11, 0.76 ± 0.08, 0.52 ± 0.08, respectively (**Figure 16B**). These values were used in diagenetic simulations as representative of each category. The critical depth used to separate photic from aphotic sediments was equal to the depth at which modeled PAR irradiance (see details in following sections) at the sediment-water interface was equal to 10% of its value at the water surface. Details of acoustic surveys and sediment analysis are described in Chapter 2.

The spatial domain contains 3180 wet cells, each one representing 0.76 Ha of the bay (horizontal resolution of 86.9 m) (**Table 4**). Gravel and bedrock (G&R) substrates were identified by acoustic mapping as reported in Chapter 2 and accounted in bay-scale predictions. Intertidal sediment was not included in simulations due to complexities of parameterising benthic activity during exposure and inundation periods in the study area. Intertidal flats, located mostly at the westernmost arm (Birchtown Bay), are particularly prone to tidal and wave action, sediment reworking, dewatering (by evaporation and drainage), gas stripping (Chanton et al. 1989), and disturbance by shore ice formation, all factors not included in the diagenetic models.

Only daily to seasonal variability in forcing conditions was incorporated in the model (POC deposition, solutes concentration in bottom waters, PAR irradiance, temperature, BMA colonization). Consequently, simulations were run until dynamic steady state conditions, with no interannual variations, were achieved in state variables.

3.3.2.2.1 Net POC deposition

Time-dependent fluxes of particle species were imposed at the upper boundary, except for reactive Fe(III) for which a constant flux of 0.255 mmol m^{-2} d^{-1} was assumed based on Brigolin et al. (2009). Net C_{org} deposition (gross deposition – erosion) was forced using a sinusoidal function fitted to time-series of bottom C_{org} deposition reported for Southern Nova Scotia (Webster et al. 1975, Hargrave 1980, Hatcher et al. 1994) as well as point data collected at SH in the late summer of 2014 (**Figure 15A**). The maximum depositional flux measured at SH in this study was 8.8 g (dry wt.) m^{-2} d^{-1}, equivalent to 29.3 mmol POC m^{-2} d^{-1}, after assuming a 0.4% C_{org} in total particle mass flux (5% of total particulate mass flux corresponds to particulate C, of which 8% is organic C). Average annual deposition calculated from these observations was 19.27 mmol m^{-2} d^{-1} (min. 8.9 mmol m^{-2} d^{-1}, max. 28.2 mmol m^{-2} d^{-1}), considered within the range of oligotrophic coastal systems according to Eyre & Ferguson (2009). The fitted function for all data is shown in **Eq. 7**

$$C_{org}(t) = \frac{a}{2} * \cos\left(2\pi * \frac{t + TL}{365}\right) + Average\ annual\ deposition \qquad \textbf{Eq. 7}$$

where *a* is the amplitude of the sinusoidal function , *t* is time in day units, and *TL* (100 d) is a coefficient used to position the annual peak of POC deposition. From **Eq. 7** annually integrated C_{org} deposition equals 6766.4 mmol m^{-2} y^{-1} (81.3 g m^{-2} y^{-1}). The input of dissolved organic matter is not considered in the current formulation.

C_{org} deposition varies across the bay in time but not in space. Nonetheless, spatial differences in benthic fluxes were expected as result of differences in sediment porosity and BMA activity. Only seasonal variability in C_{org} deposition was considered in the simulations, and do not consider shorter variability caused by tidal actions, or other stochastic events affecting gross deposition. Two-thirds of deposited C_{org} was labile, the remainder refractory material.

3.3.2.2.2 Boundary conditions for solutes and temperature

Similar to C_{org} deposition, a sinusoidal function was fitted to temperature data series collected at nearby Liverpool Bay in 2016 (**Figure 15C**). Temperatures in bottom water vary significantly throughout the year between 1.6 °C in mid-winter (~day 62) to 11.9 °C in mid to late summer (~day 245). Higher variability was observed in summer months probably due to deep-water intrusions from offshore. Drops in temperature were also accompanied by decreases in O_2 concentration in bottom water. This stochastic variability was not considered in SH simulations. O_2 and N_2 concentration in bottom water were calculated from solubility equations (Garcia & Gordon 1992, Hamme & Emerson 2004), while bottom water concentration of Fe^{2+}, FeS, Total S^{2-}, and C_{EPS} were set to zero. Time-series of bottom water concentrations were not available for the study area, and NO_3 and NH_3 were assumed constant in overlying bottom waters (NO_3 = 40 μM, NH_3 = 3.45 μM), based on measurements available for SH (Canadian Council of Ministers of the Environment 2007) and others coastal systems (Hatcher et al. 1994, Hochard et al. 2010, Dias et al. 2016). Zero concentration gradients were imposed at the lower sediment boundary for all solid and dissolved species. The effects of temperature on primary reactions, and particle mixing (enhanced bioturbation) were incorporated based on Q_{10} formulation (Eppley 1972), while temperature dependence of diffusion coefficients was modeled as in Fossing et al. (2004).

3.3.2.2.3 Sediment biological interactions

The impact of microphytobenthos, *i.e.,* the effects of biomass and O_2 production, excretion of extracellular polymeric substances (EPS), and nutrient uptake were incorporated into the model following Hochard et al. (2010). The model formulation remains unchanged except by the incorporation of time-dependent temperature and PAR irradiance. Likewise, a sinusoidal forcing function was introduced to simulate annual BMA colonization of surface. Based on this function, BMA colonization peaks in midsummer to a value 1.03 mg Chl-a m^{-2} h^{-1}, which was defined according to Grant et al. (1986). In Hochard's model, the maximum growth rate is described as a function of light, cell quota (internal C/N ratio) and T°. N uptake is a function of external concentration and cell quota, and Chl-a synthesis is controlled by light availability (photoacclimation) and the maximum Chl-a/N ratio allowed. Respiration, grazing and EPS production is proportional to fixed C. Following Hochard et al. (2010), bioturbation of solid C_{BMA} and N_{BMA} was equal to half of the biodiffusion coefficient (D_b). The latter choice was made to account for vertical migration of BMA within sediments. The model does not consider sediment resuspension, nor the effects of sediment stabilization by exopolymeric substances produced by BMA. Grazing was not explicitly included in the model, but grazing and respiration were assumed proportional to fixed C. C_{EPS} production was also assumed proportional to fixed C.

3.3.2.2.4 Light

Simulations of photosynthetically active radiation (PAR) reaching the sediment-water interface were produced as a function of water depth, light attenuation, cloudiness (sinusoidal function), and zenith angle, the latter dependent on the time of day, the day of the year and latitude. The hourly PAR radiation (I_0) annual cycle was simulated from Brock (1981) as:

$$I_0 = SC * ECC * C_\theta * PAR_{frac} * Cloud \qquad \textbf{Eq. 8}$$

where SC is the solar constant (1366.1 W m^{-2}), ECC is the eccentricity correction (between 0.9 and 1.1 approx.), C_θ is equal to the cosine of the solar zenith angle, PAR_{frac} the photosynthetic active radiation fraction (equal to 0.43 of total incoming light), and $Cloud$ the fraction of light after cloud attenuation. This last, was assumed constant and

equal to 0.4. Maximum light intensities follow the seasonal cycle of the Northern hemisphere (43.865 °N). I_0 was attenuated in the water column and within sediment assuming exponential decrease, with attenuation coefficients equal to 0.2 and 2000 m^{-1}, respectively. Daily maximum PAR irradiance at surface P-M&S sediments (2.5 m depth) was 195.1 W m^{-2} by the summer solstice (~day 168) and decreased to a daily maximum of 86 W m^{-2} by the winter solstice (~day 355).

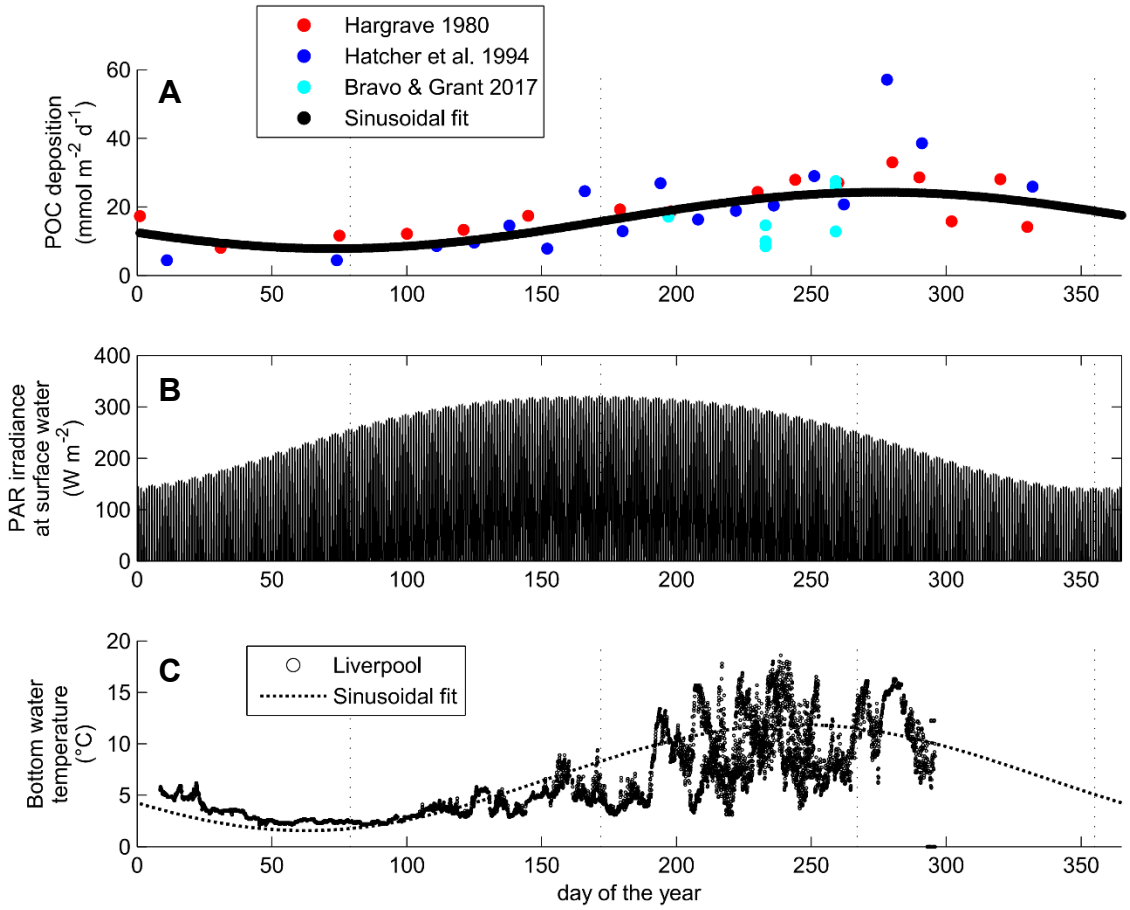

Figure 15: Time-dependent forcing. **A.** Particulate organic carbon deposition time-series measured at multiple coastal areas of Southern Nova Scotia, Canada. A sinusoidal function was adjusted to observations and used as forcing in diagenetic simulations. **B.** Simulation of PAR irradiance at the sea-water surface at hour scale according to Brock (1981). **C.** Bottom water temperature at nearby Liverpool Bay and corresponding sinusoidal fit used as model forcing. Time expressed as Julian days.

3.3.2.3 **Geochemical indexes**

Daily, seasonal, and annual mean rates and fluxes (±1 standard deviation) were calculated from diagenetic simulations for each sediment type. Spatio-temporal scaling was carried out by integrating rates vertically within the sediments (20 cm), as well as in time (daily or seasonally). Estimates were made assuming astronomical seasons, i.e., assuming days 79 (March equinox), 172 (June solstice), 267 (September equinox) and 355 (December solstice) as the first day of spring, summer, fall, and winter. Later, based on spatial coverage of sediment categories, mean and integrated biogeochemical rates and fluxes were calculated at the bay-scale.

From prognostic variables (fluxes) the following indices were calculated:

i. Denitrification efficiency, *i.e.,* the percentage of the total inorganic nitrogen released from the sediments as dinitrogen gas (N_2-N / (DIN + N_2-N) * 100%) (Berelson et al. 1998, Eyre et al. 2002).
ii. C_{org} degradation efficiency, defined as the ratio between daily-averaged C_{org} degradation rates and gross deposition rates. Resuspension is not modeled in this study.
iii. Oxidation capacity (O_{cap}) was calculated as:
$O_{cap} = [O_2] + 0.8\ [NO_3] + 0.25\ [Fe(OH)_3]$ mmol O_2-eq. m^{-2}

Where $[O_2]$, $[NO_3]$, and $[Fe(OH)_3]$ denote the depth integrated concentration of oxygen, nitrate and oxidised iron in bulk sediment (mmol m^{-2}, upper 2 cm) and 0.8 and 0.25 are a factor converting NO_3 and $Fe(OH)_3$ into stoichiometric oxygen equivalents, respectively.

3.3.3 Functional value

Simulations focused on the state and evolution of benthic processes as result of natural variability from diel to seasonal scales. Predictions of nitrogen removal at bay scale were contrasted with other bay sinks (i.e., nitrogen burial, and plant uptake) and sources of nitrogen (municipal discharges, riverine inputs, atmospheric deposition, and net bay-ocean exchange). Net ocean-bay exchange was also calculated from tidal flushing and time series of Total Inorganic nitrogen (TIN) concentration at the Scotian shelf and within SH.

Annual reports for the Shelburne wastewater treatment facility were used to estimate municipal discharges to the bay (Ontario Clean Water Agency 2016). No data were available to estimate nitrogen inputs for Roseway River. Instead, I estimated riverine inputs by combining mean annual discharge ($m^3\ y^{-1}$) (Water Survey of Canada) and average reported N concentration from rivers belonging to the same drainage area (Southeastern Atlantic Ocean Drainage Area, NS) (Environment Canada 2011). Atmospheric inputs were calculated from estimations from northeastern United States (Gao et al. 2007, Howarth 2007). Validation of model results was carried out by comparison with observed fluxes at SH (Chapter 2) and other coastal systems in Nova Scotia, Canada.

3.4 Results

3.4.1 Sediment distribution and species concentration

Based on depth, PAR irradiance and mud content, a 56.4% of SH subtidal sediments were classified as A-MSM (13.7 km^2), 21.6% as A-SMS (5.3 km^2), and 13.9 % as P-M&S (3.4 km^2) (**Figure 16A**). Hard bottom coverage was 1.9 km^2 (8.1%). Mean depth of photic sediments was 2.5 ± 1.5 m, while mean depth for aphotic sediments was equal to 11.0 ± 3.0 m. Spatial interpolation of sediment porosity is shown in **Figure 16B**.

According to model results, total C_{org} content (C_{POC1}, C_{POC2}, C_{EPS}) in surface sediments (1 cm) across the bay fluctuated throughout the year between ~3.6 and 14.4 g m^{-2} (**Figure 22a)**. Expressed as % solids (g C_{org} g dry $sediment^{-1}$ * 100) the mean surface C_{org} content for surface sediments ranged between 0.007 and 0.07 % solids. The latter estimate assumes a sediment density of 2.45 g cm^{-3}. Lowest values were predicted in late spring (P-SMS, ~day 123) and the highest in late fall (A-MSM, ~day 313, **Figure 22A**). The bay-averaged concentration of C_{org} throughout the year was 7.7 ± 3.5 g m^{-2}. The contribution of labile C_{org} and C_{EPS} was low relative to total C_{org} (<10%). Nonetheless, labile C_{org} and C_{EPS} showed the highest variability in concentration throughout the year.

In all sediments types, suboxic conditions (0 > vertically weighted mean O_2 < 63 µM in upper 1 cm) were predicted in surface sediments during months of higher C_{org} deposition. O_2 penetration was higher in winter months and decreased from late spring to late fall due to increased demand by C_{org} oxidation and reoxidation processes. Minimum

predicted O_2 concentration in surface sediments was 36.4 µM (late summer, ~day 258, A-SMS) and the maximum equal to 95.8 µM (early spring, ~day 83, A-MSM). Despite seasonal hypoxia, sulfide concentrations in surface sediments (2 cm) were always lower than 300 µM, considered within the range of oxic conditions (Hargrave et al. 2008).

Predicted sediment C_{org} concentration peaked about 3 months after the annual peaks in C_{org} deposition (**Figure 15C** and **Figure 22A**). Similarly, bay-averaged sulfide concentration peaked ~23 days after the annual peak in C_{org} deposition. Sulfide accumulated despite decreasing rates in sulfate reduction, which were in close synchrony with C_{org} deposition rates. Maximum sulfide values were predicted in A-SMS at ~day 288 (~230 µM).

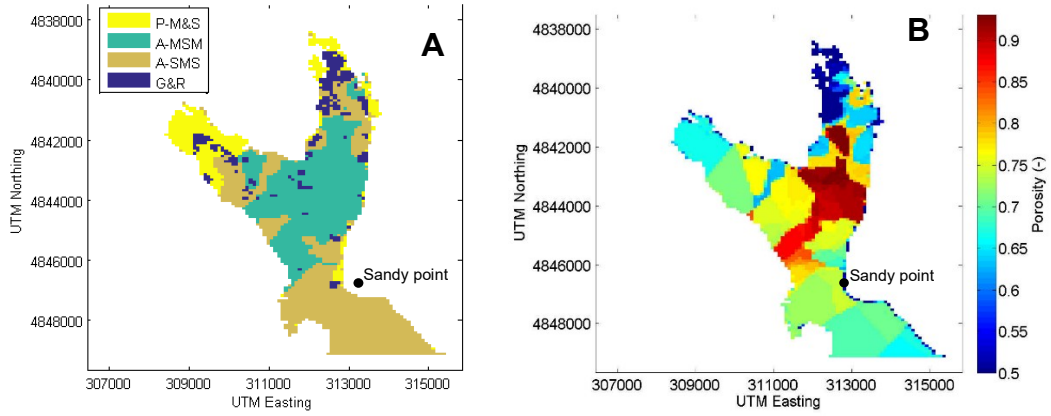

Figure 16: Bottom classification based grain size data **(A)**, and sediment porosity **(B)**. Legend key: bare photic sediments (P-M&S), aphotic sediment in mud to sandy-mud (A-MSM), sand to muddy-sand (A-SMS), and gravel and rocks (G&R).

3.4.2 Solute and particle cycling

3.4.2.1 Benthic fluxes

Mean benthic fluxes of solutes and particles predicted from season and sediment category are shown in **Table 6** and **Table 7**. Average time-series of benthic fluxes, DNF efficiency, and C_{org} concentration are shown in **Figure 22**. These values were obtained once simulations reached a dynamic steady state with no interannual variations in state variables.

A periodic idealized cycle in benthic fluxes was predicted as result of seasonally imposed variations in C_{org} deposition (**Figure 22**). Predicted fluxes were within

observations reported at SH in **Chapter 2** and other coastal inlets and shelf sediments of Nova Scotia, Canada. Nonetheless, observed variability was considerably higher than predicted by model simulations (**Table 6**). This is because the simulations represent averaged conditions for major sediment types and boundary conditions and not specific cases. Based on predicted O_2 and NH_3 fluxes all sediment types showed a net heterotrophic behavior throughout the year, including photic sediments. The predicted net O_2 flux was always negative (i.e., net consumption), even in photic sediments, and ranged between -4.2 (early spring, ~day 87, A-SMS) and -13.8 mmol m^{-2} d^{-1} (late summer, ~day 264, A-MSM). Likewise, a net efflux of NH_3 was always predicted despite seasonality, including P-M&S. NH_3 efflux ranged between 0.13 mmol m^{-2} d^{-1} (~day 85, A-SMS) and up to 1.57 mmol m^{-2} d^{-1} (~day 264, A-MSM). Reported net O_2 fluxes of SH sediments ranged between -64.3 and 61.0 mmol m^{-2} d^{-1} in dark and light incubations, respectively (Bravo & Grant 2017). Nonetheless, this range includes data from light incubations carried out in intertidal sediments, not considered in this study. O_2 consumption rates reported for coastal environments in Nova Scotia are as high as 43 mmol m^{-2} d^{-1} (Hargrave 1978, 1980). Observed NH_3 fluxes for estuarine and coastal marine sediments average around 3 mmol m^{-2} d^{-1}, but may reach up to ~65 mmol N m^{-2} d^{-1} (Bailey 2005), while NO_3 fluxes across the sediment-water interface fluctuated between -0.07 and 0.48 mmol N m^{-2} d^{-1}. A net NO_3 uptake was predicted in P-M&S (~day 251), while the highest efflux was predicted in A-MSM (~day 46). A small but constant efflux of Fe^{2+} to bottom waters was predicted all year long in all sediment types (max. of $6x10^{-5}$ mmol m^{-2} d^{-1}).

3.4.2.2 C_{org} degradation

Predicted C_{org} degradation rates by season and sediment category are summarized in **Table 6, Table 7** and **Figure 17**. Total degradation peaked in early fall (~265 d) in synchrony with POC deposition, and decreased by late fall and winter. Annually averaged C_{org} degradation rates for SH was 18.1 ± 5.2 mmol m^{-2} d^{-1}, with no considerable differences among sediment types (**Table 7**). Due to seasonal differences in C_{org} deposition, oxic respiration was higher in summer and fall through all sediment types (up to 25.7 mmol m^{-2} d^{-1}, P-M&S, ~day 264) and decreased considerably by winter and early spring to values as low as 11.0 mmol m^{-2} d^{-1} in P-M&S (~day 87). C_{org} respiration was also significantly influenced by bottom temperature; winter respiration was attenuated by

a 47.4% as result of lower temperatures. The contribution of aerobic and anaerobic pathways of C_{org} degradation was relatively constant throughout the year, with no significant differences among seasons. Oxic respiration dominated C_{org} degradation in all sediment, accounting for 72.9 ± 0.9 % (A-SMS) to 78.9 ± 0.6 % (A-MSM). Sulfate reduction dominated anaerobic respiration (74.9 ± 2.7 % in A-MSM, to 80.5 ± 2.5% in A-SMS), followed by nitrate reduction (18.5 ± 2.5 in A-SMS to 23.8 ± 2.7 in A-MSM).

C_{org} degradation rates closely agreed with seasonally imposed C_{org} deposition rates. In agreement with depositional patterns, two-thirds of degraded organic matter corresponded to labile C_{org}, and the remaining to refractory C_{org}. The degradation efficiency was equal 100% when calculated on an annual basis. Slight seasonal differences in degradation efficiency were predicted between periods of high (summer-fall) and low (winter –spring) organic deposition. C_{org} degradation was 8.3% lower than deposition in summer and fall, while in winter and spring it was a 6.1% higher (**Table 6**). This implies that the oxidative capacity of sediment may be surpassed during summer and fall in SH sediments as result of increased demand for oxidants (O_2, NO_3, FeIII). Accumulation of C_{org} and reduced by-products (H_2S, NH_3) was predicted to occur even after the annual peak in C_{org} deposition (for about three months).

C_{EPS} degradation only represented 1.7% of annually integrated C_{org} degradation rates in photic sediments. As a result, C_{EPS} production does not significantly affect degradation efficiency in P-M&S, nor the production of exudates by grazers.

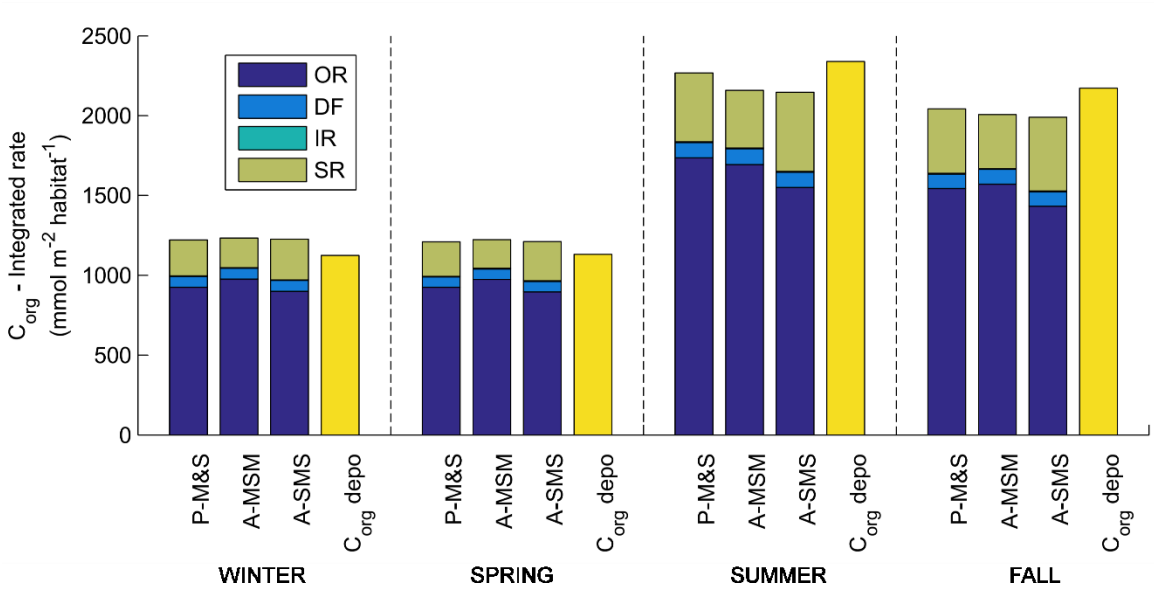

Figure 17: Seasonally integrated C_{org} degradation and deposition rates by season and sediment type (mmol m^{-2} $habitat^{-1}$). Legend key: OR (oxic respiration), DF (denitrification), IR (iron reduction), SR (sulfate reduction), C_{org} deposition (yellow bar), bare photic sediments (P-M&S), aphotic sediment in mud to sandy-mud (A-MSM) and sand to muddy-sand (A-SMS).

3.4.2.3 **Oxidation capacity**

Sediment oxidative capacity depends on an active supply of oxidant from the water column, as well as on the potential demand by reduced compounds within sediments. According to simulations, the oxidative capacity varied considerably throughout the year but averaged 62.7 ± 20.8, 80.8 ± 28.8, and 49.0 ± 17.1 mmol O_2 eq. m^{-2} d^{-1} in P-M&S, A-MSM, and A-SMS, respectively. Oxidative capacity was the greatest in early spring and decreased considerably by late summer in all sediment types, the latter due to increasing C_{org} deposition, and therefore oxidant demand. On average, O_2 and $FeOH_3$ contributed almost equally and with the largest percentage to the oxidative capacity (max. 84% at ~day 142, A-MSM), followed by NO_3 (max. 20.1%, at ~day 263, A-MSM), with no substantial differences among sediment types. O_2 contribution to oxidative capacity varied between 31.1 to 50% throughout the year, while $Fe(OH)_3$ varied between 30.5 and 55.3% across all sediment types.

The net O_2 flux ranged between -4.8 mmol m^{-2} d^{-1} (~day 87, A-SMS) and -13.8 mmol m^{-2} d^{-1} (~day 265, A-MSM) (**Figure 22**). Sediment O_2 demand was largely dominated by oxic respiration (> 80%) in all sedimentary environments and all seasons,

but particularly in summer and fall (**Figure 18**). Labile C_{org} was responsible for 61.3% (~day 87, P-M&S) and 94.9% (~day 274, A-SMS) of total O_2 consumption. Secondarily, nitrification contributed with 3.6% (~day 249, P-M&S) to 12.0% (~day 78, P-M&S) to O_2 demand, being the largest contribution predicted in winter and spring (**Figure 18**), when oxic respiration decreased in sediments. Oxygen production in photic sediments significantly ameliorates O_2 uptake from bottom water in the summer and fall (**Figure 20B**). O_2 uptake decreased up to 37% during daylight hours, when primary production (~day 250) peaks in surface sediments. Minor sources of O_2 consumption were reoxidation processes (H_2S, Fe^{2+}) and respiration by benthic grazing. The continuous efflux of H_2S predicted in all sediment types throughout the year reveals a potentially low capacity of SH sediments to prevent it from escaping to bottom waters, either by precipitation (FeS, FeS_2) or reoxidation to $SO_4^{=}$ (in the presence of O_2 or $FeOH_3$).

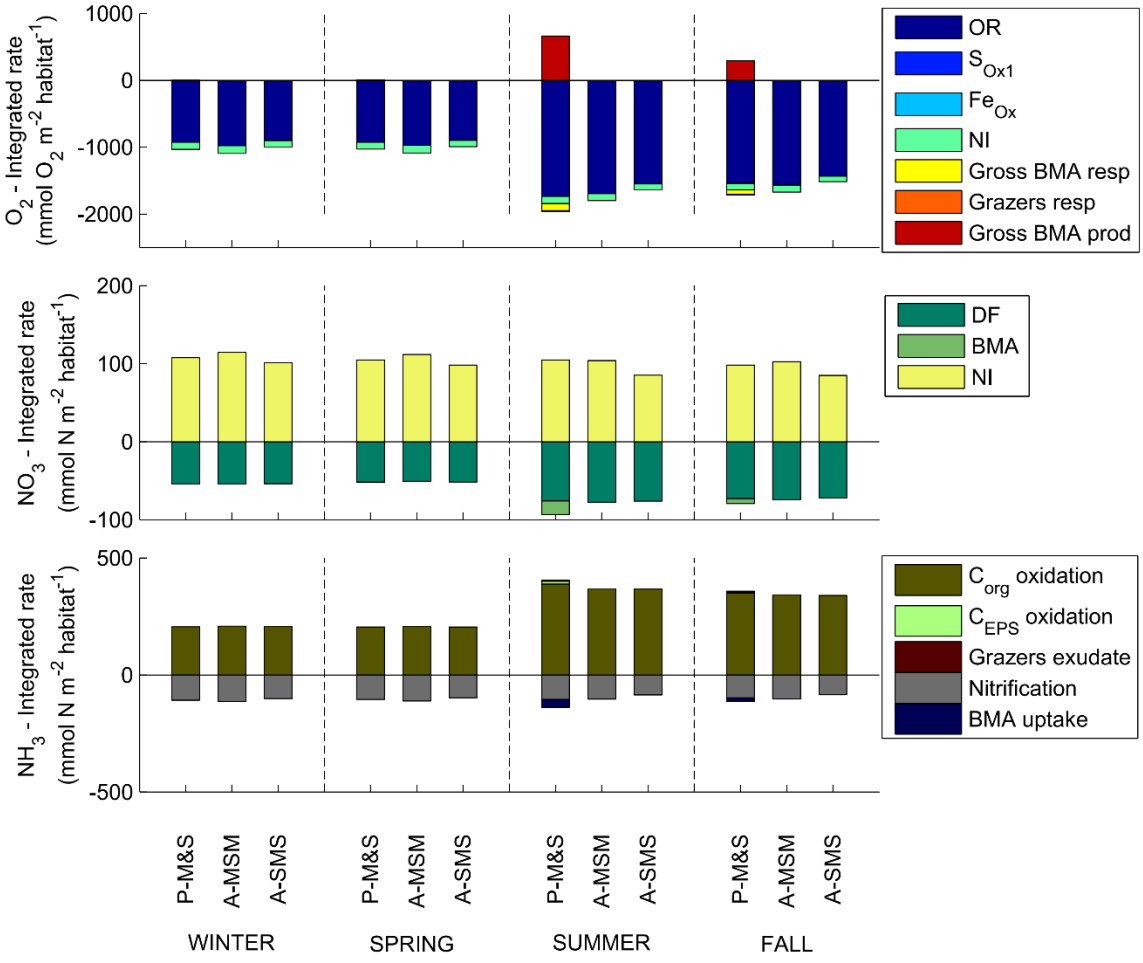

Figure 18: Seasonally integrated O_2, NO_3, NH_3, and N_2 consumption rates (mmol m^{-2} $habitat^{-1}$) by season and sediment type. Positive values mean production while negative values mean consumption. Legend key: OR (oxic respiration), DF (denitrification), NI (Nitrification), S_{Ox1} (H_2S oxidation with O_2), FeOx (Fe^{2+} oxidation with O_2), Benthic microalgae (BMA), bare photic sediments (P-M&S), aphotic sediment in mud to sandy-mud (A-MSM) and sand to muddy-sand (A-SMS).

3.4.2.4 **Nitrogen cycling**

Nitrogen cycling in sediments was controlled by several processes, including organic matter degradation, denitrification, nitrification, BMA uptake, and exudate production by grazers.

3.4.2.4.1 Nitrate cycling

SH sediments behave most of the year as a source of NO_3 to overlying water, especially in periods of low C_{org} deposition. Nonetheless, the magnitude and direction of NO_3 fluxes varied significantly throughout the year. In the three sediment types, a net NO_3 efflux is predicted in winter and spring, while a significant decreased or a net uptake is predicted in summer and fall when C_{org} degradation was comparatively higher (**Figure 22**). A net influx was only predicted in photic sediments in late summer due to increased denitrification and BMA uptake. I recall that constant boundary conditions (NO_3, NH_3) were assumed in bottom waters due to lack of data for the study area. This assumption should be carefully considered, as more realistic boundary conditions may affect net N fluxes at the sediment-water interface.

In winter and early spring, the NO_3 demand by denitrifiers and BMA activity diminished considerably as result of decreasing C_{org} deposition and PAR irradiance (**Figure 18**). In parallel, nitrification activity was slightly stimulated as result of increasing O_2 availability, allowing some NO_3 to escape out of sediments. The opposite condition, i.e., inhibition of nitrification, was predicted in summer and early fall as result of increasing O_2 and NO_3 demand associated with C_{org} oxidation and BMA uptake. Nitrification in winter and spring was on average 5% higher than in summer and fall, reaching up to 0.8 mmol NO_3 m^{-2} d^{-1} (~day 250, A-SMS). Maximum predicted nitrification rates were ~1.3 mmol NO_3 m^{-2} d^{-1} in late winter (~day 14, A-MSM). Nonetheless, significant peaks in nitrification activity (up to 1.5 mmol NO_3 m^{-2} d^{-1}) were predicted in photic sediments, specifically in daylight hours in late summer.

3.4.2.4.2 Ammonium cycling

Ammonia flux was always positive, *i.e.,* into the water column (**Figure 18**) and consistent with the timing of increased rates of C_{org} deposition, decreasing considerably in early spring and increasing by the end of the summer due to increase C_{org} degradation (**Figure 22**). In general, NH_3 production increase significantly in summer and fall in all sediment types due to increased C_{org} oxidation, with no considerable differences between sediment types. Despite nitrification and BMA uptake, physical diffusion out of sediments was the dominant factor controlling NH_3 concentrations throughout the year.

3.4.2.4.3 Dinitrogen production

N_2 fluxes were strongly influenced by C_{org} deposition and O_2 availability in sediments. Both processes indirectly controlled nitrification-denitrification activity, which showed a strong seasonal coupling throughout the year. Likewise, C_{org} deposition and N_2 production were positively correlated within the range of C_{org} deposition rates imposed on sediments (8.9 - 28.2 mmol C_{org} m^{-2} d^{-1}).

N_2 production via denitrification was promoted in summer and fall and decreased by winter and spring as result of lower C_{org} deposition rates and prevailing oxic conditions in sediments (**Figure 18**). Temperature influenced denitrification mostly through effects on O_2 solubility in bottom waters. Imposed temperatures decreased significantly in winter favoring O_2 availability and uptake by sediments.

Accumulated by season, N_2 production was 41% higher in summer compared to the annual average. Predictive diffusive N_2 fluxes at the sediment-water interface, expressed in µmol m^{-2} d^{-1}, fluctuated between 156.2 mmol N m^{-2} d^{-1} (~day 65, A-SMS) and 605.5 µmol N m^{-2} d^{-1} (~day 243, A-MSM). These values were relatively low compared to maximum reported values in the literature, which may reach up to ~6000 µmol N m^{-2} d^{-1} (Seitzinger 1988, Joye & Anderson 2008, Eyre & Maher 2011, Piehler & Smyth 2011). Annually averaged denitrification rates fluctuated between 263.7 ± 77.7 in A-SMS to 414.2 ± 132.4 µmol m^{-2} d^{-1} in A-MSM. Nitrification activity was comparable to that of denitrifiers, the former a major factor controlling NO_3 availability (via NH_4^+ reoxidation) throughout the year. In this model, NO_3 was only consumed by denitrifiers and BMA. Competition for nitrate between denitrifiers and benthic primary producers

was only significant in summer and early fall, where BMA uptake represented up to 33% of NO_3 consumption rates.

3.4.2.5 **Primary production**

Benthic primary production was a significant driver of C and nutrient cycling at hour- to daily-scale. Nonetheless, the variability imposed by BMA activity on benthic processes was well within seasonal variability imposed by C_{org} deposition. As a result, benthic primary production does not affect the daily average rates and fluxes significantly when compared to aphotic sediments.

As observed in **Figure 19**, BMA production increased steadily throughout spring to peak in late summer (~day 250), after which it rapidly decreased until ceasing altogether during winter months. These results suggest that growth conditions were favorable during most of the summer despite declining levels of PAR irradiance. The maximum daily-averaged depth-integrated production rate was 6.87 mmol C_{BMA} m^{-2} d^{-1}. The annually accumulated primary production for photic sediment was equal to 519.7 mmol C_{BMA} m^{-2} y^{-1} (6.24 g C_{BMA} m^{-2} y^{-1}).

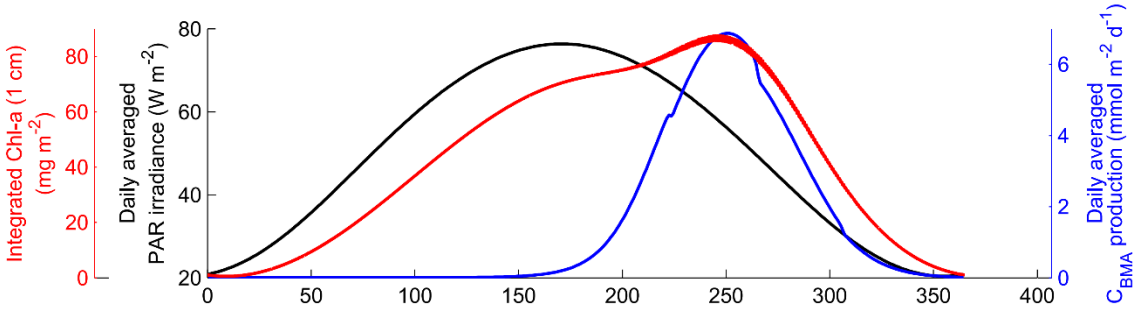

Figure 19: Annual predicted BMA dynamic in photic sediments.

Figure 20 shows the influence of BMA activity on sediment C_{org} degradation, O_2 consumption and N removal at the hourly scale, around day 250 (late summer) when the highest annual BMA production was predicted in simulations. At the peak of benthic primary production, oxic respiration and nitrification were notoriously stimulated during daylight hours due to BMA O_2 production. Oxic respiration peaked at mid-day reaching up to 24 mmol C_{org} m^{-2} d^{-1}. This value was 15% higher than corresponding rates for aphotic sediment. Maximum O_2 production predicted through the year was equal to 16.5

mmol O_2 m^{-2} d^{-1}. Denitrification was attenuated in daylight hours due to O_2 production but stimulated at the onset of dark hours, when the optimal concentration of limiting NO_3 and inhibiting O_2 coincide in sediments. Peak DNF efficiency was predicted in dark hours (up to 20.4%).

The diffusional O_2 flux across the sediment-water interface was reduced by up to 26% by mid-day due to BMA primary production (from around 10.5 mmol m^{-2} d^{-1} at midnight to 7.7 mmol m^{-2} d^{-1} at midday) (**Figure 20**). Similarly, the NO_3 flux to the water column was significantly reduced or switched toward the sediment in daylight hours as result of BMA uptake (**Figure 21**). Net NH_3 fluxes were not affected by benthic primary production, which was largely controlled by oxidation of organic matter (**Figure 21**). No O_2 supersaturation associated with BMA activity was predicted in the most active layer, 0.5 mm below the sediment surface.

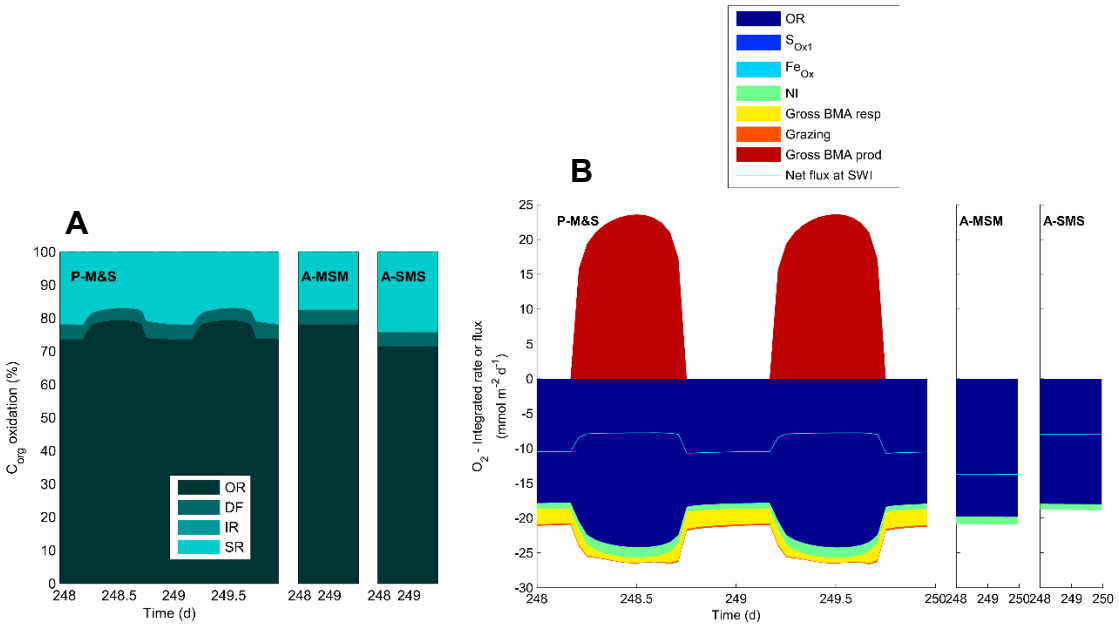

Figure 20: Predicted summer dynamics in benthic processes in photic (P-M&S) compared to aphotic (A-MSM, A-SMS) sediments. The stacked colored areas represent the contribution of depth-integrated consumption (negative) and production (positive) rates to C_{org} oxidation (**A**) and O_2 consumption (**B**) in sediments. The light blue line in figure B represents the corresponding net flux at the sediment-water interface. Simulations correspond to 48 hours, starting midnight of day 248 when the annual peak of benthic primary production is predicted. Time expressed as Julian days.

Integrated Chl-a concentration in surface P-M&S sediments (1 cm) ranged between 123.4 and 166.5 mg m^{-2}. Predicted Chl-a concentrations were up to an order of magnitude higher than observed values in intertidal sediments at SH and nearby Port Joli, which averaged 16.2 ± 14.6 mg m^{-2} (n = 10) at midsummer (maximum of 46.4 mg m^{-2}). Nonetheless, the low number of observations make difficult to compare these observations with model results.

Predicted Chl-a concentration were higher than steady state predictions of integrated Chl-a concentration (1 cm) by Hochard et al. (2012) for shallow muddy sediments at Florida Bay (~60 mg m^{-2}), being the difference caused by differences in depth, porosity, PAR irradiance, temperature, and NO_3^- and NH_3 in bottom water. Except for NO_3 and NH_3 concentration in bottom water, all former variables were time-dependent in this study. Nonetheless, when assumed parameters of Hochard et al. (2010) and steady state conditions the same BMA activity was predicted, confirming no errors in model formulation.

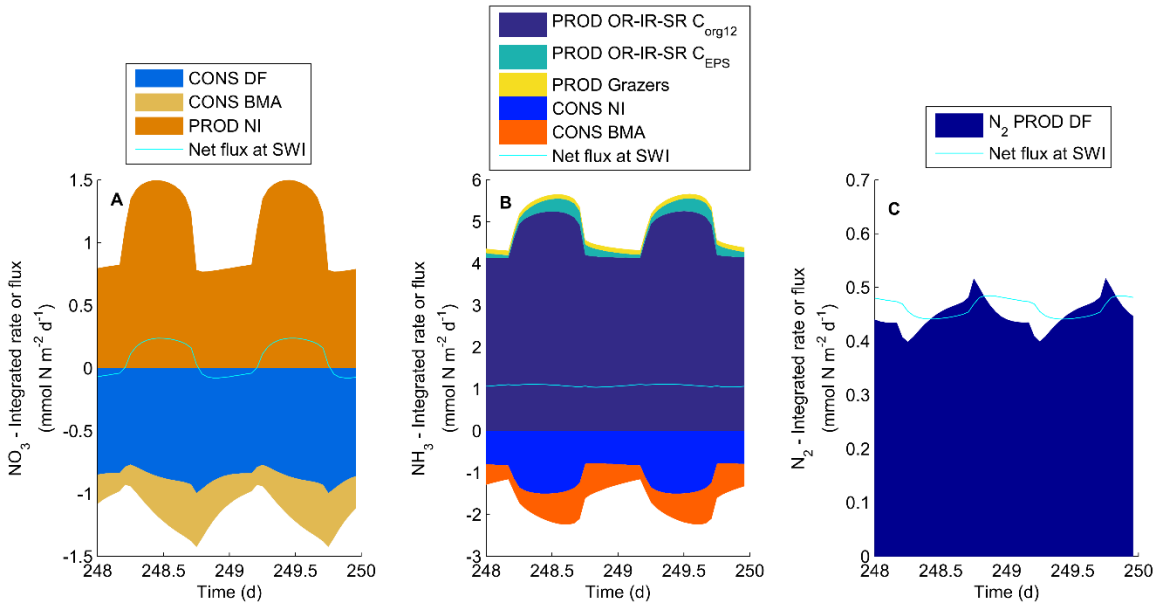

Figure 21: Predicted summer dynamic in NO_3 (**A**), NH_3 (**B**), and N_2 (**C**) cycling in photic sediments (P-M&S). The stacked colored areas represent the contribution of depth-integrated consumption (negative) and production (positive) rates. The light blue line in each figure represents the corresponding net flux at the sediment-water interface. Simulations correspond to 48 hours, starting midnight, at the annual peak of benthic primary production. Time expressed as Julian days.

3.4.3 Integrated processes

Bay subtidal sediments behave as an active source of nutrients to the water column (NO_3, NH_3, Fe^{2+}). Total annual C_{org} degradation at SH was 1816.9 tonnes (average 0.22 g C m^{-2} d^{-1}), while the net production of NO_3 and NH_3 released to bottom water was predicted to be 31.6 and 83.7 tonnes per year, respectively. As result of increase C_{org} deposition, most of the N_2 produced through the year (37.9 tonnes y^{-1}) was attributed to summer and fall (63.5%) (**Figure 22**). Nonetheless, the highest denitrification efficiency, that is to say, the percentage of the total inorganic nitrogen released from the sediments as N_2 was predicted during spring months, followed by summer (**Table 6**). The annual denitrification efficiency for the bay was of 27.5%.

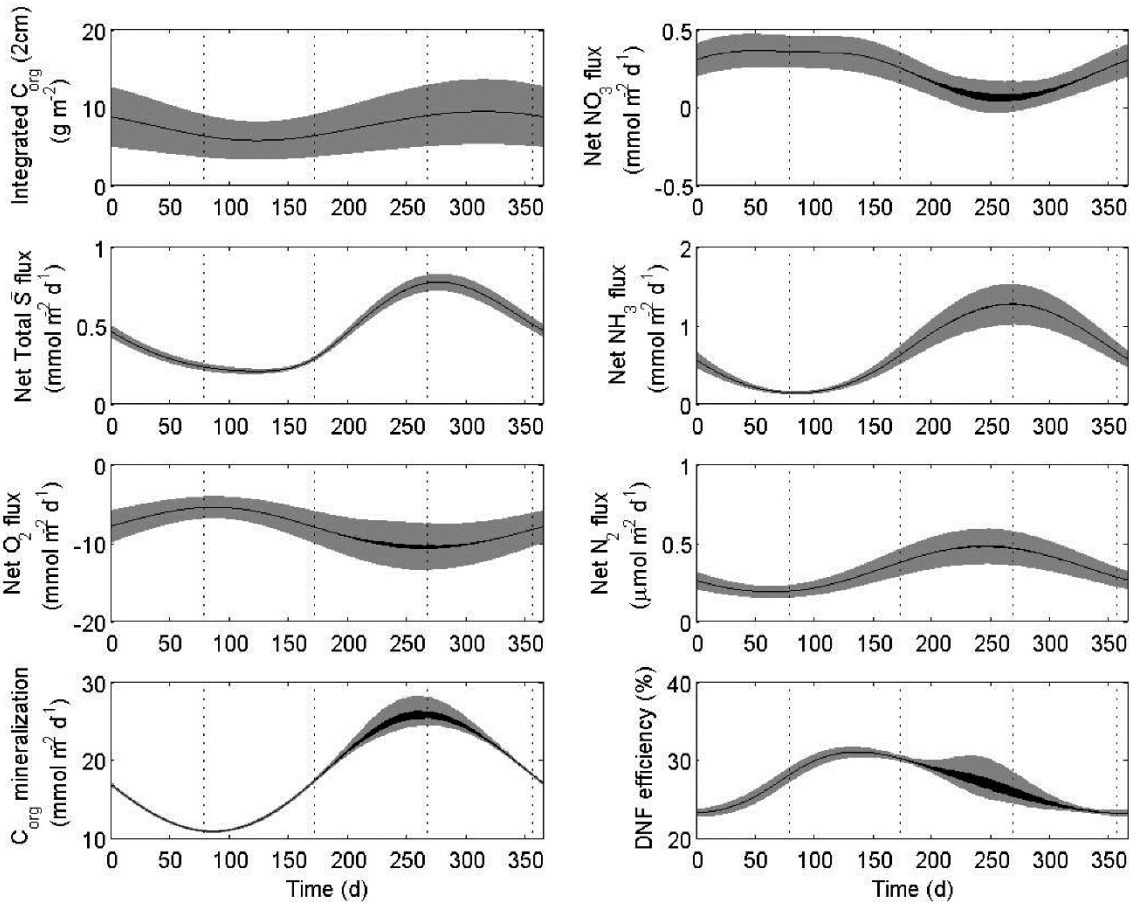

Figure 22: Bay-averaged benthic processes predicted from diagenetic simulations and weighed by areal coverage of different sediment types (P-M&S, A-MSM, A-SMS). Mean (black line) ± 1 standard deviation (gray area) are shown for each process or state variable. Positive and negative fluxes indicate uptake and release from sediments, respectively. Julian day is used for the dependent axis. Changes in standard deviation

(thickness of gray area) are caused by differences in benthic processes among different sediment types as well as due to dial variations in benthic processes in photic sediments.

Table 6: Annually- and seasonally-averaged benthic fluxes predicted for SH. Fluxes and rates in mmol m^{-2} d^{-1} except for nitrogen fluxes (µmol N m^{-2} d^{-1}). Observed values from Bravo & Grant (2017) correspond to summer and fall observation (2012-2014). Positive values denote efflux from sediments, while negative values denote influx.

	Annual	Winter	Spring	Summer	Autumn	Observed
C_{org} deposition	18.5 ± 6.8	12.6 ± 3.0	12.2 ± 2.9	24.6 ± 3.1	24.7 ± 2.9	8.5 – 27.6
C_{org} oxidation	18.2 ± 5.2	13.8 ± 2.1	13.1 ± 2.0	22.9 ± 2.7	22.8 ± 2.3	–
Degradation efficiency (%)	100	109.4	107.8	92.9	92.5	
Net O_2 flux	-8.1 ± 1.8	-6.7 ± 0.9	-6.3 ± 0.8	-9.6 ± 0.8	-9.7 ± 0.7	-2 – -64.3
Net NO_3 flux	235.2 ± 112.1	341.9 ± 25.0	329.6 ± 29.6	124.7 ± 62.4	147.0 ± 66.9	-6276 – 5824
Net NH_3 flux	676.1 ± 404.3	330.1 ± 155.6	291.6 ± 143.7	1035.0 ± 201.3	1045.0 ± 188.1	-4073 – 3178
Net N_2 flux	332.2 ± 102.1	218.2 ± 28.4	270.3 ± 55.1	450.9 ± 30.3	384.9 ± 55.1	-18558 – 116942.4
Denitrification efficiency (%)	27.0 ± 2.7	24.9 ± 1.5	30.4 ± 0.8	28.2 ± 1.3	24.4 ± 0.8	–

Table 7: Annually averaged benthic fluxes predicted for each sediment type. Fluxes and rates in mmol m^{-2} d^{-1} except for nitrogen fluxes (µmol N m^{-2} d^{-1}). Positive values denote efflux from sediments, while negative values denote influx.

	P-M&S	A-MSM	A-SMS
C_{org} deposition	18.5 ± 6.8	18.5 ± 6.8	18.5 ± 6.8
C_{org} oxidation	18.5 ± 5.8	18.1 ± 5.2	18.0 ± 5.1
Net O_2 flux	-7.7 ± 1.6	-10.5 ± 2.4	-6.2 ± 1.4
Net NO_3 flux	231.6 ± 116.2	336.2 ± 136.1	149.8 ± 94.1
Net NH_3 flux	636.3 ± 363.1	818.4 ± 507.6	567.2 ± 329.7
Net N_2 flux	326.55 ± 97.5	414.21 ± 132.4	263.68 ± 77.7
Denitrification efficiency (%)	27.5 ± 3.1	26.5 ± 2.6	27.2 ± 2.8

3.4.4 Functional value of benthos

As observed in **Figure 23**, estimated N inputs from Roseway River, municipal discharges and atmospheric deposition equal 11.97, 14.30, and 10.33 tonnes N y^{-1}, respectively. The net N bay-ocean exchange rates can be approached based on tidal flushing and time series of TIN concentration on the Scotian Shelf and within SH. Based on reported flushing time (52.6 h) and tidal volume ($3.7x10^7$ m^3) (Gregory et al. 1993), the flushing rate (or water renewal rate) at the SH channel connecting to the sea approximate 707,224 m^3/h. The daily tidal flushing volume was equal 1.7×10^7 m^3 d^{-1}. TIN concentration in offshore surface waters of the Western Scotian Shelf varies seasonally as in most temperate regions. In general, winter nitrate concentrations offshore are the highest (max of ~20 µM) and became largely depleted during spring and summer due to increased phytoplankton activity. Nitrate concentration remains low all through the summer and recovers in the fall. Annually averaged nitrate concentration for the Western Scotian Shelf is 3.4 ± 3.5 µM (Petrie et al. 1999). No time series of TIN or nitrate concentration were found for SH, but reported single measurements fluctuated between 0.85 (1 m depth) and 2.28 µM at 13 m depth, respectively (Canadian Council of Ministers of the Environment 2007). According to these data, the net bay-ocean exchange is -7.94 tonnes y^{-1}. Gross N export is 25.46 tonnes y^{-1} while the import is 33.41 tonnes y^{-1}. From calculation, SH seems to behave as a net importer of N from offshore. However, the confidence in the estimated net bay-ocean exchange is very low, due to scarce nutrient data available for SH, and uncertainties in the water exchange calculations based on the tidal prism. In addition, these estimations do not account for potential deep-water intrusions from offshore into SH as described for nearby Bedford Basin by Platt et al. (1972) and Burt et al. (2013).

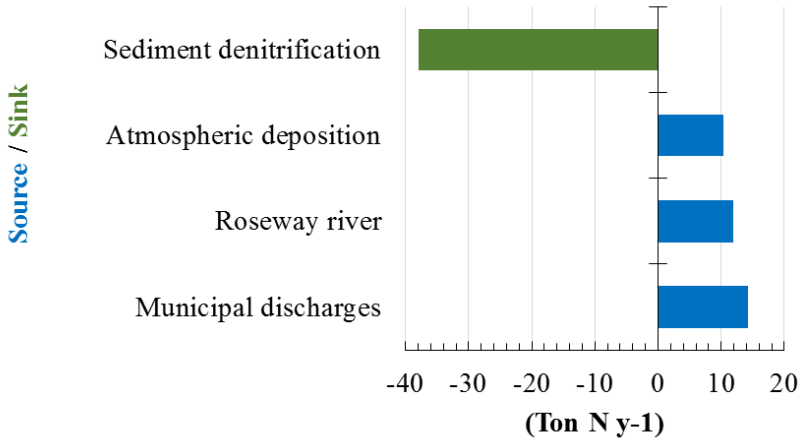

Figure 23. Nitrogen budget in Shelburne Bay, NS, Canada.

3.5 Discussion

3.5.1 Sources of uncertainty, model assumptions, and limitations

This is the first effort of combining diagenetic modeling and benthic habitat mapping to assess sub-seasonal and bay-scale dynamics in benthic processes and sediment ecosystem services (C and N removal). Nonetheless, as in any ecosystem model, uncertainties are present in the model structure, parameterization, and forcing conditions.

Concerning model formulation, the main source of uncertainty is most probably associated with the incomplete representation of the N cycle. In the model, heterotrophic DNF is assumed as a unique source of N_2 production. No anammox or alternative pathways of N_2 formation coupled with S, Mn, and Fe cycles were considered in the model (e.g., autotrophic sulfur denitrification). Although extensively studied (Seitzinger 1988, Luther et al. 1997, Schrum et al. 2009), none of these reactions have been parameterized in diagenetic models, and therefore further work is required to evaluate these reactions and their incorporation into the model.

Although formulations are avaiable, DNRA, NH_4^+ adsorption into sediments, and N_2 fixation were not considered in the model formulation. Nonetheless, as demonstrated by Hardison et al. (2015) and Hardison et al. (2015), DNRA can affect significantly NO_3 reduction pathways in sediments. Likewise, sediment NH_4^+ adsorption may strongly limit

its availability for nitrifiers and autotrophs, affecting consequently coupled DNF (Mackin & Aller 1984, Hou et al. 2003).

Physical transport of solutes at the sediment-water interface (advection – diffusion) is always relevant to matter and energy cycling in sediments. Solute transport across the sediment-water interface greatly depends on sediment type, more specifically porosity and permeability, as well as of hydrodynamic conditions, that defines overlying water shear and renewal of solutes above sediments (Huettel et al. 1998, Santos, Eyre, & Huettel 2012). Biological activity also plays a significant role through bioturbation and sediment irrigation (Kristensen 2005).

A major limitation of 1D diagenetic models is the assumption of no lateral transport of substances within sediments. This assumption is valid in fine-grained sediments but does not always hold in permeable sediments, where lateral advection related to wave and tidal pumping may be significant. It also does not consider flow- and topography-induced advection, the latter caused by ripples or other surface heterogeneities (Forster et al. 1996, Fennel et al. 2009, Santos, Eyre, & Huettel 2012, Huettel et al. 2014). The associated uncertainty is mostly restricted to A-SMS sediments, which compressed 21.6% of subtidal areas according to benthic mapping. Further complexities may arise due to potential fluxes associated with bubble formation and release (*i.e.,* gas stripping). Decreased solubility caused by changes in temperature and hydrostatic pressure may significantly affect gas fluxes at the sediment-water interface (Chanton et al. 1989). Tidal fluctuation is a major driver of bubble formation and of sediment degassing (CH_4, O_2, and N_2). The significance of this process for benthic processes in SH sediments is unknown in this study.

The model includes 82 parameters, 10 biogeochemical reactions, and 5 elemental cycles. Among all parameters, the most sensitive are those associated with decomposition of organic matter (Tromp et al. 1995). In this study, maximum degradation rates for labile and refractory organic carbon were defined based on reported values for coastal and continental shelf sediments according to Hochard et al. (2010) and Luff & Moll (2004). Overall degradation rates of organic matter (by all pathways) vary from 10^{-7} to 10^{3} y^{-1}. In

this sense, a better characterization of organic matter degradability based on other studies conducted in Nova Scotia may contribute to increasing confidence in model results.

The largest uncertainty in the model forcing is in C_{org} deposition rates. POC deposition measured in the east coast of Canada ranges two orders of magnitude between 10^2 to 10^4 mg C m^{-2} d^{-1} in coastal embayments, continental shelves, and slope (Hargrave 1995). Relatively high seasonal variability in sedimentation rate in coastal embayments has been reported for eastern Canada (Hargrave & Taguchi 1978, Hatcher et al. 1994). This variability may be explained by the interaction of multiple factors acting at minutes (wind-wave interactions), hours (tidal periodicity), weeks to months (river flow or phytoplankton dynamics), and years to decade scales (climate-induced changes) (Hargrave 1995). Major factors controlling sedimentation include water column structure (mixing depth, seasonal stratification, etc.), lateral transport from offshore waters, and biological production. Despite the variability, a distinctive increase in material deposition has been observed in early fall in inshore waters of Southern Nova Scotia (Hargrave 1980, Hatcher et al. 1994). For nearby Bedford Basin, POC deposition is ~ 4 times greater in early fall (Oct-Nov) compared to winter (Feb-Mar).

In this study, sediment traps were deployed at three different locations of SH in the late summer of 2014. The maximum depositional flux measured at SH was 29.3 mmol POC m^{-2} d^{-1}. This value is relatively low compared to maximum depositional rates reported by nearby embayments, including Lunenburg Bay (up to 1873.4 mmol POC m^{-2} d^{-1}), St. Margaret's Bay (up to 516.2 mmol POC m^{-2} d^{-1}), South Broad Cove (up to 29.6 mmol POC m^{-2} d^{-1}) and Bedford Basin (~49 mmol C m^{-2} d^{-1})(Hatcher et al. 1994, Hargrave 1995). Nonetheless, the collected data agreed with mean annual C_{org} deposition rates reported for the same inlets, which range between 17.3 and 26.92 mmol C m^{-2} d^{-1} (Webster et al. 1975, Hargrave et al. 1976, Hargrave & Taguchi 1978, Taguchi & Hargrave 1978, Hargrave 1995, Burt et al. 2013). The former averaged values are all considered within the range of coastal oligotrophic (< ~45 mmol m^{-2} d^{-1}) conditions according to Eyre & Ferguson (2009). As a reference point, POC deposition on the Scotian Shelf and slope regions are up to ~150 mg C m^{-2} d^{-1} (12.48 mmol m^{-2} d^{-1}) (Hargrave 2001).

The quality of interpolated surfaces (depth and porosity) also introduces uncertainties in model predictions due to the approximation of unsampled points (Jager & King 2004). Upscaling uncertainties include the assumption of no spatial variation in temperature and C_{org} deposition, as well as the existence of discrete rather than continuous gradients in sediment distribution. In this study, I fitted a curve to observations of C_{org} deposition from the South Shore of Nova Scotia, and I imposed this time series to the entire bay assuming no spatial differences. Future efforts should consider spatial forcing either by coupling the diagenetic model with a spatially-explicit pelagic ecosystem model or by empirical parameterization of C_{org} deposition rates to representative sediment variables (e.g., LOI, grain size, etc.). The need to incorporate lateral variability is highlighted in this study, as well as in former ones (Seitzinger et al. 2006, Woelfl et al. 2006, Fennel et al. 2009, Groffman et al. 2009, Piehler & Smyth 2011). The same logic applies to POC resuspension from sediments. As explained before, the same time-series of C_{org} deposition was imposed in all sediment types (P-M&S, A-MSM, A-SMS), which implies no lateral variations across the bay. Nonetheless, net deposition (gross deposition – erosion) is expected to vary significantly across the bay, particularly in the more dispersive environments (sand) located toward the Harbour's mouth. As results, the model may be over-predicting C_{org} and N mineralization rates in these areas and their contribution to bay dynamics. Future coupling with a water column model should improve simulation of forcing conditions.

A constant light attenuation is assumed in the water column and sediments. Nonetheless, increased water attenuation is often observed in summer to fall due to riverine inputs of colored dissolved organic matter (CDOM). The potential effects on benthic activity, including BMA production, were not considered in the model.

The assumptions associated with bottom water concentrations of solutes, including O_2 and nitrogen species are important in model forcing. Time-series of bottom water concentrations of O_2 and nitrogen species were not available for the study are such that saturated values were assumed for O_2 and N_2 according to temperature and salinity. Likewise, a constant concentration of NO_3 and NH_3 were assumed in bottom waters based on single measurements available for SH. These forcing conditions assume no variation

in the lateral catchment and atmospheric loads (not represented in the model) which may significantly vary throughout the year. Nonetheless, no large variations in land-based nutrient loads are expected in SH, as any agriculture or other significant human-related sources of nutrients to the bay are observed in the drainage area (Southeastern Atlantic Ocean Drainage Area, NS).

3.5.2 Scales of response

Scales of response are important as they define the sensitivity of the system to changes in boundary conditions (e.g., organic carbon deposition, oxygen availability in bottom waters, nutrient enrichment, etc.). Lagged responses are frequently observed in nature, and they cover multiple spatio-temporal scales. Examples in pelagic environments include the lagged predator – prey relationships between seasonal phytoplankton and zooplankton production (Riley & Bumpus 1946), as well as between bacterioplankton and phytoplankton production in coastal (Hoch & Kirchman 1993) and offshore environments (Ducklow et al. 1993). Lagged patterns between physicochemical and biological processes are also observed for example between spring-tide resuspension event and peaks of nutrients and Chl-a in coastal seas (Su et al. 2015). In benthic systems, examples include the time lag between production and release of reduced substances (Jørgensen 1977), seasonal lags between C_{org} deposition and mineralization (Hargrave 1978, Rudnick & Oviatt 1986, Rudnick 1989), and the lagged recovery of eutrophic ecosystems due to accumulation of reduced species in the system (Brady et al. 2013).

While some simulated processes in this study (O_2, NO_3, NH_3 and H_2S fluxes) were quite consistent with the timing of C_{org} deposition, others showed lags in relation to seasonally-changing forcing conditions (i.e., light, temperature, C_{org} deposition, O_2 concentration). Among them, highlight the lagged response of benthic primary production to the annual cycle of PAR irradiance. The time required for microphytobenthos to reach its maximum annual biomass and production was delayed by about 78 days respect to the summer solstice. Evidence of this phenomenon, although not always explicitly recognized in the literature, can be observed at hourly (Spilmont et al. 2007) to seasonal scales (Meyercordt & Meyer-Reil 1999, Wolfstein et al. 2000, van der Wal et al. 2010).

Nonetheless, further analyses are required to validate this prediction and associated model parameterization.

As C_{org} deposition increased in summer, an increased supply of oxidants was required to oxidize organic inputs and reduced by-products (sulfide and NH_3). Accumulation of reduced compounds is expected when oxidant demand surpasses the supply. Accumulation of C_{org}, H_2S, and NH_3 was predicted for about three months after the annual peak in C_{org} deposition, which occurred in late summer. The oxidant deficit accumulated in this period was re-established later in the fall and winter when C_{org} deposition rates decrease, and reduced compounds were completely oxidized. As indicated by O_2 and $FeOH_3$ concentrations in surface sediments, oxidative capacity recovered completely by early spring (~day 110). Similar lagged patterns in C_{org} accumulations and H_2S production have been described by Fossing et al. (2004) for Aarhus Bay sediments. Model predictions by Luff & Moll (2004) for North Sea sediments also showed similar patterns.

According to model results, heterotrophic activity was considerably attenuated during winter due to decreasing temperature (~47%), while reoxidation of reduced products accumulated throughout the summer was complete in the same period. These model predictions contrast with mesocosm observations by Rudnick (1989) in Narragansett Bay. In his study, a net accumulation of C_{org} was observed during the winter and spring, while the opposite situation (i.e., consumption greater than deposition) was observed during summer. The observed lag in detrital mineralization during winter and spring (of ~1 month) was attributed to attenuation of heterotrophic activity and benthic grazing by low temperatures. These apparently contradictory results highlight the interplay between C_{org} deposition and temperature, and their influence on patterns of benthic mineralization. Enhanced sub-surface preservation mediated by sediment bioturbation was also described as a potential factor affecting the timing of C_{org} mineralization and accumulation in sediments (Rudnick & Oviatt 1986).

As an oligotrophic coastal environment, SH is characterized by low C_{org} deposition rates. The low deposition translate in a relatively lower O_2 demand by C_{org} mineralization, which instead promotes nitrification, and an active recycling of NO_3 back

to the water column. Accordingly, C_{org} deposition rates above ~28 mmol m^{-2} d^{-1} in A-SMS sediments have the potential to change the flux direction of NO_3 into the sediment, while a slightly higher deposition is required in A-MSM sediments to change the net flux. This C_{org} and O_2 dependent reversal of net NO_3 fluxes has been previously described by Middelburg, Soetaert, et al. (1996) in coastal to abyssal sediments. The implications of this 'switch' on ecosystem functioning, particularly on N removal, are difficult to predict for other depositional scenarios given nonlinear and time-dependent interactions involved.

Major factors controlling benthic denitrification encompass the input and availability of starting products as C_{org} and NO_3 (Hou et al. 2003, Seitzinger et al. 2006, Fulweiler et al. 2008, Whitehead 2012), the presence of metabolic inhibitors (O_2), the interaction of N species with other elemental cycles as Mn, Fe, S (Seitzinger 1988, Luther et al. 1997, Schrum et al. 2009), and NH_4^+ adsorption in sediments (Mackin & Aller 1984, Hou et al. 2003). These factors instead, are strongly affected by sediment type, the dominant hydrodynamic regime, as well as by temperature affecting metabolic activity. Enhanced advective porewater exchange in permeable sediments has been suggested to stimulate coupled nitrification–denitrification (Santos, Eyre, & Glud 2012, Eyre et al. 2013). Santos, Eyre, & Glud (2012) suggested that intermediate pore water advection flows in porous carbonate sands may enhance the development of microniches (i.e., steep oxygen gradients), and conditions for coupled nitrification-denitrification. Extensive work on the effect of porewater advection on benthic metabolism has also been reported in Huettel et al. (2014), Precht & Huettel (2004), Santos, Eyre, & Huettel (2012), Huettel et al. (2003), and Forster et al. (1996), among others. In the simulations, porewater advection was constant (time- and depth-independent) and proportional to the solid burial velocity (1.048 cm y^{-1}). Although the latter is a common assumption in diagenetic modeling (Boudreau 1996, Couture et al. 2009), a better formulation is required to account for the effects of advective pore water flow on sediment oxidative capacity and benthic metabolism.

In a gradient of C_{org} deposition, it is expected that denitrification activity will display a threshold-like behavior, increasing with C_{org} deposition until reaching a

maximum value after which it is expected to decreases as reducing conditions became dominant and NO_3 availability limiting in surface sediments. Evidence of this threshold behavior has been provided by Webster & Harris (2004), and Eyre & Ferguson (2009), but it was not predicted within the range of C_{org} deposition observed at SH.

In addition, future efforts should focus in the parameterization of heterotrophic and autotrophic N fixation pathways, which are not included in the model, but may be significant in coastal sediments (Welsh 2000, Fulweiler et al. 2007). To my knowledge, no models of benthic N-fixation (autotrophic and heterotrophic) in sediments have been developed. Its incorporation is essential to balance sources and sinks of N, particularly in euphotic sediments, including seagrass beds, where high rates of heterotrophic N-fixation have been reported (Welsh et al. 1996, Welsh 2000, Fulweiler et al. 2007).

3.5.3 Bay-scale prediction of benthic processes and functional value of benthos

While quantitative conclusions are uncertain given model assumptions, the development, and improvement of bay-scale diagenetic models may contribute significantly to the prediction of benthic processes and ecosystem services, as well as to assess the effects of local (e.g., eutrophication) and global (e.g., ocean warming) stressors.

According to model results, a net efflux of NO_3, Fe^{2+}, and NH_3 to bottom waters was predicted all year long in all sediment types. Heterotrophic production may represent an important source of nutrients for autotrophic communities, including, saltmarsh grasses (*Spartina* spp), and eelgrass (*Zostera marina*) in the subtidal, intertidal and higher elevations (Stewart & White 2001, Bundy et al. 2014). Nonetheless, the fate of this source of nutrient in the water column was not predicted in this study given uncertainties in the estimation of net exchange of nutrient between the bay and offshore waters. Consequently, further analyses are required to quantify how much of sediment nutrient inputs are consumed locally within the bay or advected away.

Our model predicts that SH sediments play a significant role in nutrient cycling and C_{org} mineralization at the bay scale. Denitrification removed ~27% of annual nitrogen inputs to sediments. Predicted annual N removal via sediment denitrification was equal to 37.9 tonnes y^{-1}, which was around 3.2 times greater than riverine inputs (11.97 tonnes y^{-1})

and 2.6 times greater than the effluent discharge of the town of Shelburne wastewater treatment plan (14.30 tonnes y^{-1}).

A more detailed budget of N in SH should also consider the contribution of intertidal sediments (Cabrita & Brotas 2000, Jickells & Rae 2005, Faber et al. 2012), diffuse runoff (e.g., storm water, forest runoff, etc.), industrial point sources, particularly from local fish farms, plant uptake associated with shore communities (macroalgae, eelgrass, salt marsh grasses, etc.), and sediment N_2O production.

CHAPTER 4. MODELLING SEDIMENT ASSIMILATIVE CAPACITY AND ORGANIC CARBON DEGRADATION EFFICIENCY AT MARINE FISH FARMS

4.1 Abstract

The eutrophication of sediments underlying marine fish farms is one of the major environmental concerns of the industry and regulatory agencies. In this study, a mechanistic model of sediment geochemistry was developed with the following objectives: (1) to determine maximum organic loads that can degraded without leading to undesired benthic conditions, (2) to predict the transition to suboxic conditions as a result of organic enrichment, and (3) to predict sulfide levels in surface sediments, a key regulatory variable in Canada. I propose a new definition of assimilative capacity (AC) applicable to marine fish farms, as the gross deposition rate of organic wastes that maximizes total respiration rates while preventing sediment sulfide accumulations in surface sediments (upper 2 cm) above regulatory limits (AC-H_2S).

Model results were consistent with empirical observations and highlight the influence that organic loading history, hydrodynamics, and benthic bacteria, have on assimilative capacity. AC-H_2S varied between 0.49 to 22.7 g C_{org} m^{-2} d^{-1} in poorly-flushed environments, with no upper limit defined in environments exposed to mean tidal currents > 9.5 cm s^{-1} (DISP scenarios), where most fish farm organic wastes are dispersed to the far-field or resuspended after deposition below fish cages. The combination of diagenetic modelling and geochemical indicators may contribute significantly to the development of more effective tools for selection and environmental management of marine fish farms. At this stage, the model should be considered as a proof of concept, developed with the purpose of verifying the utility of assimilative capacity for real-world application. Further validation is still required.

4.2 Introduction

Ensuring sustainable aquaculture production in coastal areas requires careful attention to environmental interactions with the benthos and water column. Among near-field interactions, the eutrophication of sediments underlying fish farm cages due to deposition of organic-rich solid wastes (feces, uneaten feed) represents a major factor influencing productive capacity and social licence to operate marine fish farm sites. The generation and release of organic wastes to the environment mostly depend on the farm size and husbandry practices (e.g., feed conversion rates, feeding strategies, fish biomass, etc.). Their dispersion in the water column and deposition to sediments depends on physical conditions, including hydrodynamics and water depth. Once at the bed, wastes can accumulate, be degraded, buried or resuspended to the water column. Degradation of organic wastes (also referred to as respiration or mineralization) is a function of the supply of oxidant to surface sediments and the composition and successional stage of benthic communities carrying out degradation. These factors also define the recovery rate of fallowed sites and the return of geochemical and biological indicators to the bounds of natural variation.

The consequences of excessive organic loading are sediment hypoxia and prominence of anaerobic diagenetic processes, notably sulfate reduction and release of sulfides toxic to infauna. Visual signs of this transition include the appearance of sulphur-oxidizing bacterial mats, shallowing of the redox potential discontinuity layer (RPD) (Mulsow et al. 2006), and progressive loss of macrobenthic and meiofaunal communities due to reducing conditions (Pearson & Rosenberg 1978, Mazzola et al. 2000, Meyer-Reil & Köster 2000, Nilsson & Rosenberg 2000, Buschmann et al. 2006, Wilding et al. 2012).

Due to the benthic response to organic loading, a cost-effective indicator used to monitor and research benthic impacts of salmon farming is the total sulfide (S^{2-}) concentration (Wildish et al. 2001, Hargrave et al. 2008) which increases with organic loading as demonstrated by Holmer et al. (2005), Hargrave et al. (2008), Hargrave (2010), Brooks & Mahnken (2003) and Brooks (2001). Its application in monitoring programs currently includes Maine (USA), Canada, Australia, and others. Unfortunately, this measure belies the complexity of sulfur dynamics in sediments and its interactions with

organic wastes. In ambient conditions (no farm), O_2 availability alternates between periods of surplus and deficit in relation with major consumptive processes (aerobic respiration and oxidation of reduced substances), a dynamic that can be observed naturally at daily to seasonal scales. Sulfide produced by sulfate reduction can be reoxidized in the presence of O_2 or precipitated to elemental sulfur (S^0) and sulfide minerals (mostly FeS, FeS_2). Precipitation of sulfide minerals is an important mechanism that prevents sulfide diffusion and re-oxidation into the aerobic zone of sediments, which mostly occurs under O_2 deficiency and low concentrations of metal oxides. The restoration of oxic conditions may occur either by increased renewal and oxygenation of bottom waters, decreased organic carbon (C_{org}) loading, or reworking of surface sediments. The accumulation of precipitated sulfur and other reduced compounds (NH_3, Fe^{2+}, Mn^{2+}) occurs naturally (Fossing et al. 2004), but it may strongly intensify in fish farm sediments.

Given the complexity of sediment biogeochemical interactions, and the wide range of coastal environments in which fish farms are located, the transition to anoxic conditions occurs neither at fixed wastage rates (i.e., fish cage output of organic wastes) nor at fixed deposition rates to sediments. The ability of sediments to digest organic input and remain oxic is referred to as assimilative capacity, and is an important criterion for maintaining ecosystem sedimentary services (Omori et al. 1994). However, 'remain oxic' is a qualitative term that must be calibrated in terms of both oxygen and sulfide thresholds. Despite its importance, site-specific considerations of benthic assimilative capacity of organic wastes and dependencies on the local history of mineralization (Zirino et al. 2013) are barely considered in managing and selection of fish farm sites. Based on observations, C_{org} loading rates causing significant changes in benthic community structure and geochemical parameters, particularly sulfide, vary by an order of magnitude from 0.36 to 11.4 g C_{org} m^{-2} d^{-1} (Cranston 1994, Hargrave 1994, Findlay & Watling 1997, Gillibrand et al. 2002, Fisheries and Oceans Canada 2004, Chamberlain & Stucchi 2007, Environment Canada 2009, Chang et al. 2012).

The relationship between organic deposition and benthic response is inherently a problem of sediment diagenesis. Previous models used to reproduce dynamics of fish

farm sediments range from simplified depth-integrated models (Omori et al. 1994, Silvert & Sowles 1996, Stigebrandt et al. 2004, De Gaetano et al. 2008) to more sophisticated approaches combining simulations of fish growth at fish farms, particle dispersion and deposition, and benthic degradation (Brigolin et al. 2009, 2014). Omori et al. (1994) and Stigebrandt et al. (2004) have proposed steady-state models to predict threshold of organic loading to sediments. I build on this work and extend it to consider temporal dynamics, bacterial activity, and bottom water renewal.

In this study, a coupled mechanistic model simulating the production of organic wastes, its dispersion, deposition, resuspension, and degradation in sediments underlying fish cages was developed with the aim of investigating aquaculture-environment interactions and local assimilative capacity. After assessing the performance of model predictions with field observations, the model was specifically used to (1) investigate the evolution of total dissolved sulfide concentrations in organically enriched sediments and its value as an indicator of sediment quality, as well as (2) to predict the capacity of sediments to degrade organic wastes while avoiding undesired benthic conditions in a broad range of hydrodynamic conditions. The sensitivity of state variables to model parameterization was analyzed to constrain the contribution of major early diagenetic processes.

4.3 Material and methods.

4.3.1 Numerical model

The numerical model is composed of three modules representing a marine salmon farm, the surrounding water column, and the benthos. Together, they simulate the production of organic wastes at the fish farm and their fate once released to the environment (dispersion in the water column, deposition, degradation and accumulation in sediments). A detailed description of model equations and analytical forcing functions is provided in the supplement (**Table A14** to **Table A18**). A schematic of the model is provided in **Figure A32**. The model was implemented in MATLAB (MATLAB R2013a, The MathWorks Inc., Natick, MA, 2000). Time stepping was conducted using the forward Euler method, with a fixed time-step of 10 seconds.

4.3.1.1 Fish farm operation and organic waste production

The production of organic wastes, including lost (uneaten) feed and feces assumes a representative fish farm production cycle with parameters in **Table 8**. Feeding practices of salmonids, including feeding frequency, ration size, and diet composition, vary considerably with body weight and length, and with growing conditions (culture density, temperature, and O_2 renewal within cages) (Stead & Laird 2002, Kaushik 2013). Feeding frequency of adult fish in net cages varies from to 2-7 times per day, with twice-per-day the most representative of current farming practices. Feeding times are usually adjusted to avoid ebb/flood maximum as most of fish activity is concentrated in maintaining position, as well as during slack tides, which may induce suboxic conditions due to low water renewal and increased metabolic activity. Organic carbon content in feed pellets and feces ranges between 49.6% and 57%, and between 27.6% and 33%, respectively (Brigolin et al. 2014, Chang et al. 2014). Diet composition may vary from high protein content in summer to favor muscle growth, to high energy content in winter to ensure muscle maintenance. Fish farm densities range between 10 and 17 Kg m^{-3} depending on salmonid species, but may reach up to 30 kg m^{-3}. Typical salmon grow-out period ranges between 14 and 24 months for eastern Canada. Based on these data, I forced the simulations by assuming 1) a twice-per-day feeding schedule (20 minutes each, starting when the tidal currents was decreasing and lower than mean current speed, $u_{WC,mean}$), 2) an average carbon content of 52.3% and 27.9% in feed pellets and feces, respectively, and 3) a

salmon grow-out period of 18 months. Fish were assumed to be adults and size dependence of fecal output was not incorporated at this stage. Due to this last assumption, a conservative culture density of 8 Kg m^{-3} was assumed in all simulations.

Feed wastage, as a percent of feed supplies, currently averages ~3%, but may be as high as 8% (Cromey, Nickell, & Black 2002, Stucchi et al. 2005, Chang et al. 2014). Assuming parameters of **Table 8**, the wastage rate of feces and lost feed coming out at the base of the fish cage varies between 15.8 and 27.3 g C_{org} m^{-2} d^{-1} for a feed wastage of 3% and 8%, respectively. Total waste produced during the entire production cycle is 163 Kg (3% feed wastage) and 234 Kg (8% feed wastage) per tonne of fish produced. Both values are within the range reported in the literature that may reach up to ~ 1 tonne of organic waste per tonne of fish produced (Silvert & Sowles 1996). Feces represent the majority of aquaculture wastes (76%) assuming 3% feed waste, while it decreases to 53% assuming an 8% feed wastage. Feed conversion ratio (FCR, dry feed used per wet biomass of fish produced) is estimated to be ~1.2 due to improvements in feeding technology and feed ingredients (Wang et al. 2012). The FCR calculated from **Table 8** (1.45 and 1.47, for the 3 and 8% feed wastage rates, respectively), was higher than expected for current farming practices, nonetheless, these values are only referential, as they do not consider fish size dependencies of feeding rates and feed properties.

Table 8: Parameters required for estimation of wastage rate (lost feed plus feces) for a single representative salmon farming cycle based on Stucchi et al. (2005), Petersen et al. (2005), and Chang et al. (2014). Digestion coefficient represents the proportion assimilated of ingested feed.

Parameter	Value
Cage volume (m^3)	6000
Cage depth (m)	15
Cage side length (m)	20
Net pen bottom area (m^2)	400
Weight of salmon smolts (Kg ind^{-1})	0.09
Harvest weight of salmon (Kg ind^{-1})	4.5
Culture density (Kg m^{-3})	8
Harvested biomass (Kg)	60000
Grow-out period (d)	540
Lost feed / Feed wastage (%)	3 – 8%
Percent mortality (individual based)	12%

Digestive coefficient for salmon	0.9
Organic C content in feed (dry weight)	52.3%
Organic C content in feces (dry weight)	27.9%
Settling velocity of feed pellets (cm s^{-1})	10.9
Settling velocity of feces (cm s^{-1})	3.0

4.3.1.2 **Dispersion of organic wastes in water column and deposition to sediments**

Dispersion of organic wastes in the water column is controlled by water depth, free-stream current velocity (u_{WC}), and settling velocities of faeces and feed pellets (**Eq. 24**, **Table A18**) (Stucchi et al. 2005). The free-stream bottom current (u_{WC}) followed a semidiurnal tidal cycle (12 hours and 25 minutes, **Eq. 21** of **Table A18**), and does not include local variations due to waves or coastal currents, nor more extreme events like storms. I assumed a constant depth of 35 meter in all simulations, no vertical changes in current speed with depth above the benthic boundary layer, and waste particles homogenously released at the base of the fish cage (20 m side and 15 m vertical).

Once at the bottom, the net deposition of organic wastes was controlled by bed shear stress, and critical shear stress for erosion (τ_{ce}) and deposition (τ_{cd}) (**Eq. 22**, **25** and **26** of **Table A18**), assumed equal to 0.0179 and 0.004 N m^{-2}, respectively (Cromey, Nickell, Black, et al. 2002), with no distinction between feces and lost feed. The erosion rate of organic wastes was calculated as a function of the erodibility constant (k_{waste}) and the excess shear stress. Resuspension of organic fish wastes occurred when bed shear stress (τ_u), was higher than the critical shear stress (τ_c) defined for organic wastes. Only particles accumulated at the sediment surface (i.e., first layer of the depth-resolved model) were subject to erosion, not the material within the sediments. Ambient POC deposition was incorporated directly to sediments as described below, but no resuspension was assumed after deposition unlike aquaculture waste.

4.3.1.3 **Diagenetic processes in sediments**

A one-dimensional transport-reaction model was developed to simulate the response of fish farm sediments to organic enrichment. The biologically-active sediment layer, where C_{org} degradation takes place, was assumed equal to 50 cm. The model domain was divided vertically in 60 layers (from the surface down: 20 layers of 0.25 cm,

10 of 0.5 cm, 20 of 1 cm, and 10 of 2 cm). A finer discretization was defined close to the surface to allow description of strong concentration gradients expected in fish farm sediments.

The general diagenetic equations for solutes (C_i, µmol cm^{-3} $_{solid}$, **Eq. 9**) and solid (S_i, µmol cm^{-3} $_{porerwater}$, **Eq. 10**) species is described as follow:

$$\varphi_s \frac{\partial S_i}{\partial t} = -\varphi_s \frac{\partial}{\partial z}\left(w_{sed} S_i - K_v D_b \frac{\partial S_i}{\partial z}\right) + \sum R(S_i, C_i) \qquad \textbf{Eq. 9}$$

$$\varphi \frac{\partial C_i}{\partial t} = -\varphi \frac{\partial}{\partial z}\left(w_{pw} C_i + D \frac{\partial C_i}{\partial z}\right) + K_v \nu\left(\mathrm{C_{i,0}} - \mathrm{C_i}\right) + \sum R(S_i, C_i) \qquad \textbf{Eq. 10}$$

In the above equations, z is the depth below the sediment-water interface (cm), and φ = porosity [dimensionless] (assumed to be constant in depth and time), w_{sed} = sediment burial velocity [cm d^{-1}], w_{pw} = porewater advection velocity relative to the sediment-water interface [cm d^{-1}], $\mathrm{C_{i,0}}$ = concentration of solutes at sediment-water interface [µmol cm^{-3}], D_b = bioturbation coefficient [cm^2 d^{-1}], D = molecular diffusion coefficient of solutes [cm^2 d^{-1}], ν = the exchange velocity of solutes due to bioturbation [cm d^{-1}], and $\sum R(S_i, C_i)$ = the net rate of reactions involving solid and solute species [µmol cm^{-3} d^{-1} in bulk sediment (porewater + solid)]. The complete reaction network is described in **Table A14**.

External forcing was imposed as variations in tidal current speed ($\mathrm{u_{WC}}$), concentration of solute compounds in bottom waters, and solid deposition rates ($POC_{flux,SWI}$, $Waste_{flux,SWI}$, $Fe(OH)_{3,dep}$). Bottom water concentration of O_2 and SO_4^{2-} was calculated at every time step based on the current speed and the concentration difference between the boundary value representing far-field water and the bottom water immediately above sediments (T1-3, **Table A16**). The far-field water column had O_2 saturation according temperature and salinity, constant SO_4^{2-} concentration (28 mM) and no reduced compounds (Total S^{2-}, Fe^{2+}). At the lower boundary, flux of solutes was set to zero, while solids (C_{org}, FeIII) were permanently buried according burial speed (w_{sed}) and the solid concentration at depth. The reaction network includes twelve chemical species, four elemental cycles (C, O, S, and Fe), and nine redox reactions (**Table 9**). Two

C_{org} pools with specific degradation rates were considered; natural particulate organic carbon (POC) and aquaculture organic wastes (feed pellets and feces). Production and dispersion of feces and lost feed in the water column were calculated separately, but once in sediments they were considered as a single degradable pool (feed pellets + feces).

C_{org} degradation is carried out by oxic respiration (R2, **Table A15**), sulfate (R3) and iron reduction (R4). Maximum degradation rates of POC and aquaculture wastes were equal to 0.1 and 1 y^{-1}, respectively. The values were chosen based on reported decay rates by Cromey et al. (1998), Brigolin et al. (2009), and Paraska et al. (2014). Denitrification was omitted from the model as its contribution to organic waste degradation is expected to be mostly restricted to initial stages of organic enrichment. Reduced metabolites can be either re-oxidized (R5-6) or precipitated (R7-9). Sulfide may precipitates with iron to S_0, FeS, or FeS_2, with all precipitates being permanently sequestered within sediments. Iron oxides act as intermediates in H_2S oxidation (R7), but O_2 was the terminal electron acceptor (R5-6). In the model, iron oxide deposition to sediments was assumed constant (175.2 µmol m^{-2} d^{-1}, Fossing et al. (2004)), and only affected by biogeochemical processing, not by resuspension.

Table 9: Idealized set of biogeochemical reactions.

Primary redox reactions	
(R1-R2)	$CH_2O + O_2 \rightarrow\ CO_2 +\ H_2O$
(R3)	$CH_2O + \frac{1}{2}SO_4^{=} + \frac{1}{2}H^+ \rightarrow CO_2 + \frac{1}{2}HS^- + H_2O$
(R4)	$CH_2O + 4FeOOH + 8H^+ \rightarrow CO_2 + 4Fe^{2+} + 11H_2O$
Secondary redox reactions	
(R5)	$H_2S + 2O_2 \rightarrow 2SO_4^{=} + 2H^+$
(R6)	$4Fe^{2+} + O_2 \rightarrow 4FeOOH + 8H^+$
(R7)	$H_2S + 2FeOOH + 4H^+ \rightarrow S^0 + 2Fe^{2+} + 4H_2O$
(R8)	$Fe^{2+} + H_2S \rightarrow FeS + 2H^+$
(R9)	$FeS \rightarrow FeS_2$

The simplification of the reaction network compared to more sophisticated 1D diagenetic models (Boudreau 1996) is consequence of the long-term goal to perform manageable calculations for decision-makers. Stoichiometric relationships in C_{org} degradation were based on Redfield ratios. Oxidant limitation and inhibition terms in redox reactions were expressed through Monod-type hyperbolic functions and reciprocal hyperbolic functions, respectively (**Table A17**). Concentration of solutes (O_2, Total S^{2-})

and particles (C_{org}) are reported as mean values for the upper two centimeters of sediments. This distinction is required as monitoring programs of fish farm sites in Canada report sulfide and organic matter content only for this layer (Chang & Page 2011, New Brunswick Department of Agriculture & DAAF) 2012, NSDFA 2014, Fisheries & Canada 2015).

Bioturbation. The biologically-mediated transport of solutes across the sediment water interface was simulated according Hammond & Fuller (1979). Their formulation of exchange across the sediment-water interface is calculated as a function of the difference in solute concentration between sediment and overlying bottom water times the exchange velocity (ν) (**Eq. 10**). I choose this formulation, to reduce uncertainty of separately modelling biodiffusion and bioirrigation (non-local exchange) processes. Bioturbation of solids was simulated using a biodifussion coefficients (Db).

In addition, a controlling factor of biological transport (K_v) was added to account for detrimental effects of toxic H_2S concentration on macrofaunal activity (**Eq. 27**, **Table A18**). In the model, macrofaunal communities become inactive with no bio-transport at sulfide concentrations in sediments > 5000 μM, considered lethal for benthic infauna (Brigolin et al. 2009). The K_v factor (0 - 1) expresses the current state of faunal bioturbation and how quickly they recover or become inactive according to benthic stress.

Bacterial dynamics. Bacterial activity (B_{SL}) was explicitly simulated in the model. Its incorporation was required to account for the expected increase in bacterial activity in fish farm sediments. According to Vezzulli et al. (2002) and La Rosa et al. (2001), bacteria abundance may increase up to three times in sediments beneath fish farm cages has been observed. Bacterial activity in sediments, including aerobic and anaerobic metabolism was explicitly modeled assuming facultative metabolism and a discrete logistic growth model according to Talin et al. (2003). Growth rate was jointly determined by the intrinsic growth rate (d^{-1}), which is proportional to C_{org} respiration (R2 to R4, **Table A15**), and a variable carrying capacity which depends on C_{org} availability (**Eq. 20**, **Table A14**). The relative change in microbial activity is reduced as its biomass increases, approaching zero as the carrying capacity is reached. Formulation of Talin et al. (2003) was unchanged except by the incorporation of a partitioning factor of bacterial

activity (PF_{Bac}) among different metabolic pathways (see R2-4 of **Table A15** and **Eq. 28** to 33 of **Table A18**). B_{SL} in equation R2 to R4 is dimensionless, and may be viewed as an enhancement factor of C_{org} degradation. $\frac{\partial Bact}{\partial t}$ have units of d^{-1}.

Parameterization. Most model parameters were taken from the literature (reaction rates, half-saturation constants, stoichiometric coefficients, and temperature dependence coefficients), and some adjusted manually within the range of published data, in order to correctly reproduce field observations (**Table A19**).

4.3.1.4 POC production and export to bottom waters.

Ambient POC deposition was assumed constant and equal to 0.42 g C_{org} m^{-2} d^{-1}. This value is within reported range for shallow coastal environments in eastern Canada (Hargrave 1994, 1995, Hatcher et al. 1994, Burt et al. 2013), and is considered typical of oligotrophic to mesotrophic coastal systems (Eyre & Ferguson 2009).

4.3.1.5 Sensitivity analysis

The sensitivity of state variables to changes in model parameters and forcing conditions was evaluated following Jørgensen & Bendoricchio (2001) and Chapelle et al. (2000). The parameters tested include the boundary conditions, transport and reaction parameters, saturation and inhibition coefficients, sedimentary coefficients, and those related with benthic activity. A sensitivity index was calculated as:

$$S\% = \frac{100}{p} * \frac{1}{n} \sum_{i=1}^{n} \frac{x_i - x_i^{ref}}{x_i^{ref}} \qquad \textbf{Eq. 11}$$

where $IS\%$ is the normalized standard deviation index, p is the percentage of parameter variation (±10%), and $(x_i - x_i^{ref})$ represents the change in the state variable (x_i) in relation to a reference value (x_i^{ref}). State variables incorporated in the analysis were O_2 consumption (total, oxic respiration, and chemical demand) and Total S^{2-} concentration. Main results of the sensitivity analysis are reported in section 4.1, and complementary data is presented in the supplement section (**Figure A33** and **Table A20**). In addition, a mass balance calculation of POC, O_2, H_2S and Fe(III) at steady-state was calculated to ensure mass conservation.

4.3.2 Geochemical indices

Two geochemical indicators were monitored in simulations: *total sulfide* (*Total* S^{2-}) concentration in sediments, and the *degradation efficiency*, defined as the ratio between daily-averaged C_{org} degradation rates and gross deposition rates (expressed as percent when multiplied by 100). C_{org} degradation efficiency was calculated by integration of time series of gross deposition (*i.e.,* particles arriving at the sediment surface) and depth-integrated degradation rates for the periods of interest (*e.g.,* throughout the fish farm cycle). Values that are lower than one can be explained either by accumulation of organic wastes in non-dispersive conditions or by erosion in dispersive conditions.

4.3.3 Assimilative capacity of fish farm organic wastes

The assimilative capacity of sediments was determined based on their ability to oxidize organic carbon, and prevent the development of reducing conditions, as shown conceptually in **Figure 24**. It is assumed that total respiration (oxic + anoxic, black line) increases with increases in C_{org} deposition. As waste net deposition increases, the relative contribution of oxic respiration (dotted black line) to total C_{org} degradation is expected to decreases as result of increased anoxic respiration. In this study, assimilative capacity was defined as the gross C_{org} deposition rate (g m^{-2} d^{-1}), that can be degraded in a particular sedimentary environment without leading to sulfide concentration above acceptable levels according environmental regulations in Canada (sulfide > 1500 µM in the upper two centimeters of sediments; AC-H_2S (Hargrave et al. 2008, Fisheries & Aquaculture 2011, [CSL STYLE ERROR: reference with no printed form.], NBDENV 2012).

Based on the former definition and associated criteria, environmental management of aquaculture sites is considered successful if gross deposition of C_{org}, including ambient and fish farm loading, is below the local sediment assimilative capacity. I report assimilative capacity using gross instead of net deposition (deposition – erosion) to be able to compare model results with empirical and model estimations of sediment assimilative capacity and waste deposition.

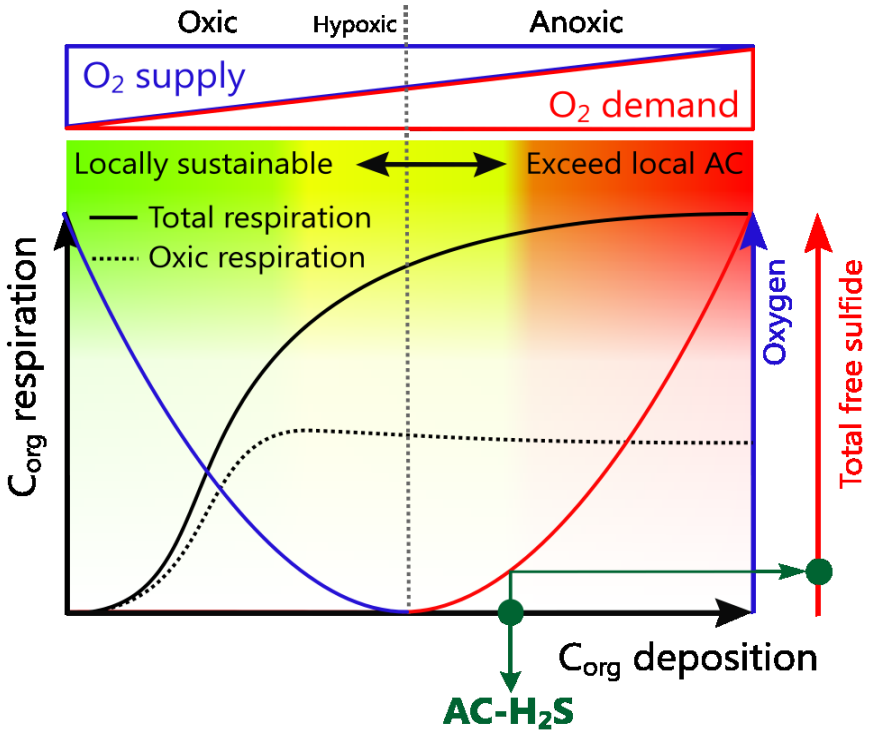

Figure 24: Conceptual representation of assimilative capacity (AC) of organic-rich solid wastes in sediments underlying fish farm cages. Total and oxic respiration are represented by the black filled, and dashed line, respectively, while O_2 and Total S^{2-} concentration are represented by blue and red lines, respectively. The green dots represent the highest C_{org} loading rate (POC + organic wastes, net value) feasible to be assimilated by benthic communities while preventing toxic sulfide above predefined threshold by environmental regulations in Canada.

Assimilative capacity was predicted based scenarios analysis, but also more formally using constrained optimizations. Optimization analysis consisted of the iterative adjustment of wastage rates (fish cage outputs) to produce gross deposition at assimilative capacity. I stress that although anaerobic respiration also removes organic matter through decomposition, this criteria allow for some anaerobic degradation without exceeding AC-H_2S.

The estimation of AC-H_2S throughout constrained optimization implies that benthic communities, more specifically bacterial activity (B_{SL}), have steady growth to reach their maximum capacity for degrading organic wastes. To investigate the

implications of the latter assumption I compared constrained values with results of scenario analysis.

4.3.4 Scenario simulations

Simulations were carried out in four hydrodynamic scenarios covering poorly-flushed (low shear stress) to well-flushed conditions (high shear stress). **Table 10** specifies the hydrodynamic conditions and the sediment parameters for each scenario, identified as high and low deposition (H-DEPO and L-DEPO), and low and high dispersion (L-DISP and H-DISP), respectively. Average free-stream bottom currents ($u_{WC,mean}$) were equal to 3, 5, 9 and 11 cm s^{-1}, respectively (**Table 10**). Maximum current speeds exerted by tides were equal to 6.2, 10.3, 18.5, and 22.6 cm s^{-1}, respectively. I distinguish dispersive from non-dispersive (depositional) sites based on the mean tidal current ($u_{WC,mean}$), being the threshold 9.5 cm s^{-1}, the free-stream speed at which resuspension of solids wastes initiates (corresponds to $\tau_c > \tau_u$). On average, u_{WC} was above the threshold current speed for resuspension during 0% (H-DEPO), 17.6% (L-DEPO), 49.1% (L-DISP), and 55.1% (H-DISP) of a full tidal cycle. Water column depth bellow the fish cage (Z_{WC}) was 20 m in all scenarios (35 m in total) and sediment porosity constant 0.8 in all simulations.

Simulations of fish farm activities and deposition of organic wastes were initiated once steady state conditions were achieved in sediments exposed to ambient C_{org} deposition. Total waste production for the entire farming cycle (g C_{org} m^{-2}), and its fate once released to the environment (deposition, erosion, degradation, burial, and accumulation in surface sediments) was calculated by integration of resulting time series. In order to represent the broad spectrum of husbandry practices at the fish farm, I run simulations assuming feed wastage between 3% (highly efficient) and 8% (inefficient), and either a constant wastage rate (i.e., no diel variation in feeding rate, in constrained optimizations) or twice-per-day feeding for 20 minutes each (in scenario analysis). In the latter case, lost feed to the environment only occurs during feeding time.

Table 10. Hydrodynamic and sedimentary parameters for scenario analysis.

	H-DEPO	**L-DEPO**	**L-DISP**	**H-DISP**
Average free-stream bottom current (cm s^{-1})	3.1 ± 2.2	5.1 ± 3.6	9.2 ± 6.5	11.3 ± 8.0

Maximum bottom current (cm s^{-1})	6.2	10.3	18.5	22.6
Porosity, φ	0.8	0.8	0.8	0.8
Percent dispersion based on $u_{WC,mean}$ and Z_{WC}				
Non consumed feed pellets	74.1	85.3	93.4	95.1
Feces	95.0	97.9	99.2	99.5
Ambient deposition (g C_{org} m^{-2} d^{-1})	0.42	0.42	0.42	0.42

4.4 Results

4.4.1 Mass conservation and sensitivity of variables to model parameterization

The model is stable, that is to say do not collapse due to error such as round-off, truncation, or discretization, and provides reasonable results across a wide range of environmental conditions and to rapid changes in C_{org} deposition. Mass conservation was achieved for solutes and particulate compounds in steady state conditions. I tested the sensitivity of changes in model parameterization on two key variables; O_2 consumption rates (chemical and biological) and sulfide concentration in surface sediments. Results showed that O_2 consumption rates, particularly chemical demand, were highly sensitive to the rate constant for sulfide oxidation by O_2 ($k_{\text{Total } S^{-2}_{SL,ox1}}$) (**Figure A33**, **Table A20**). The high sensitivity to this parameter is due to the wide range of values described for it in the literature, from 10^5 - 10^{15} 1/(M yr) (Katsev et al. 2004). As expected, O_2 consumption rates were also sensitive to the O_2 concentration in bottom water ($[O_{2,WC,BC}]$), the maximum decay rates of C_{org} in sediments ($R^{max}_{POC,SL}$, $R^{max}_{Waste,SL}$), and the burial rate of particles within sediment. Total S^{2-} concentration was sensitive to the specific oxidation rate of POC ($R_{max,POC}$), and the half saturation rate for sulfate reduction ($K_{s,SR}$). Except for $k_{\text{Total } S^{-2}_{SL,ox1}}$, the sensitivity of the state variables in all cases was lower than 5%, which indicates the robustness of the model to changes in forcing conditions and parameterization (Hochard et al. 2010).

4.4.2 Sediment metabolism in ambient conditions

The same ambient POC deposition (non-farm) was imposed in all hydrodynamic scenarios described in **Table 10** (0.42 g C_{org} m^{-2} d^{-1}), and no resuspension of POC was assumed in the simulations. Similarly, sediment properties, including porosity and burial velocity, were assumed constant among scenarios. Only the O_2 concentration in bottom waters was free to vary as described in the methods. Under ambient deposition, model

predictions show that sediment O_2 demand does not affect the O_2 concentration significantly in bottom water in any scenario. As result, no differences were predicted in the benthic processes among scenarios when exposed to ambient deposition. The Total O_2 Uptake (TOU) at steady state was equal to 3.7 mmol m^{-2} d^{-1}, dominated by aerobic respiration (61%). Chemical O_2 demand (COD) contributed with the remaining 39% being largely dominated by sulfide reoxidation (97%). Degradation efficiency was equal to 84%, being the remaining fraction buried within sediments (16%). Sulfate reduction dominated C_{org} degradation (85%), followed by oxic respiration (14%). Sulfide concentration predicted in surface sediments (upper 2 cm) was equal to 859 uM. Expressed as % solids (g C_{org} g dry $sediment^{-1}$ * 100), C_{org} concentration in ambient conditions was equal to 0.82%.

4.4.3 Sediment dynamics during fish farm operations

The impact of organic enrichment on TOU, the accumulation of reduced by-products (H_2S, Fe^{2+}), and depletion of oxidants in sediments varied depending on the hydrodynamic conditions (H-DEPO to H-DISP), and the wastage rate from the fish cage.

4.4.3.1 Transient dynamics

Figure 25 exemplified the transient response of sediments exposed to fish farm wastes in the L-DEPO scenario. The simulation was initiated from ambient deposition and assuming a single fish farm cycle according **Table 8**, twice-per-day feeding, and a 3% feed wastage. The daily-accumulated wastage rate under these conditions was equal to 19.4 g C_{org} m^{-2} d^{-1}, of which a 75% correspond to feces and 25% to lost feed. As observed in **Figure 25A**, gross deposition of organic wastes varied significantly within the day as result of changes in dispersion due to tidal currents, as well as, due to variations in waste production, particularly during feeding time (from 0 to ~34 g m^{-2} d^{-1}).

TOU increased significantly after exposure to organic wastes (up to 15.8 mmol m^{-2} d^{-1}). As observed in **Figure 27B**, oxic respiration contributed with the majority of O_2 consumption throughout the farming cycle. This occur at the expense of the chemical oxygen demand (COD) which decreases during the same period, from ~1.4 mmol m^{-2} d^{-1} in ambient conditions to less than 0.5 mmol m^{-2} d^{-1} under fish farm operation. Two reactions contribute in the model to COD: Total S^{2-} and Fe^{2+} oxidation. Similar to the

sediments exposed to ambient deposition, COD in fish farm sediments was largely dominated by sulfide oxidation.

Expressed as % solids (i.e., g C_{org} g $solid^{-1}$ * 100), the C_{org} concentrations (POC plus organic wastes) in surface sediments by completion of the fish farm cycle was equal to 1.5% in the L-DEPO scenario (**Table 11**).

Table 11: Benthic processes at fish farm sediments under four hydrodynamic scenarios (H- and L-DEPO, L- and H-DISP). Simulations were carried out assuming a representative fish farm production cycle according to **Table 8**, including a feed wastage of 3%, twice-per-day feeding (for 20 minutes each), and a constant water depth of 20 m below the fish cage (35 m in total). Wastage rate including feces and lost feed was equal to 19.4 g C_{org} m^{-2} d^{-1}. Degradation efficiency was calculated based on daily averaged C_{org} degradation and gross deposition rates (i.e., prior resuspension). Gross C_{org} deposition rates represent the flux that reaches sediments prior resuspension, but after dispersion in the water column. Surface concentration of C_{org}, O_2, and Total S^{2-} are reported for the upper 2 centimeters of sediments. Values of waste production, deposition and degradation in fish farm sediments are accumulated values for the entire fish farm cycle.

	H-DEPO	**L-DEPO**	**L-DISP**	**H-DISP**
Waste production (kg m^{-2})	10.5	10.5	10.5	10.5
Gross waste deposition (kg m^{-2})	2.3	1.6	1.1	0.9
Organic waste degradation (kg m^{-2})	0.6	0.0	0.0	0.0
Degradation efficiency (%)	26.2	0.5	0.3	0.3
Mean Total S^{2-} (μM)	3930.6	788.0	803.9	813.9
Maximum Total S^{2-} (μM)	5528.2	825.5	836.0	843.8
Mean C_{org} (% solids)	1.3	0.6	0.6	0.7
Mean O_2 (μM)	1.5	24.6	23.2	22.4
Minimum O_2 (μM)	0.5	21.1	20.1	19.4

After cessation of organic waste deposition (fish harvest), sediment recovery was characterized by a slow decrease of oxic respiration, and of the content of sulfide and organic matter. The recovery of oxic and chemical O_2 demand to background levels in the L-DEPO scenario lasts more than a year according simulations; nonetheless, this model does not consider the occurrence of stochastic events, like winter storm that may accelerate sediment recovery.

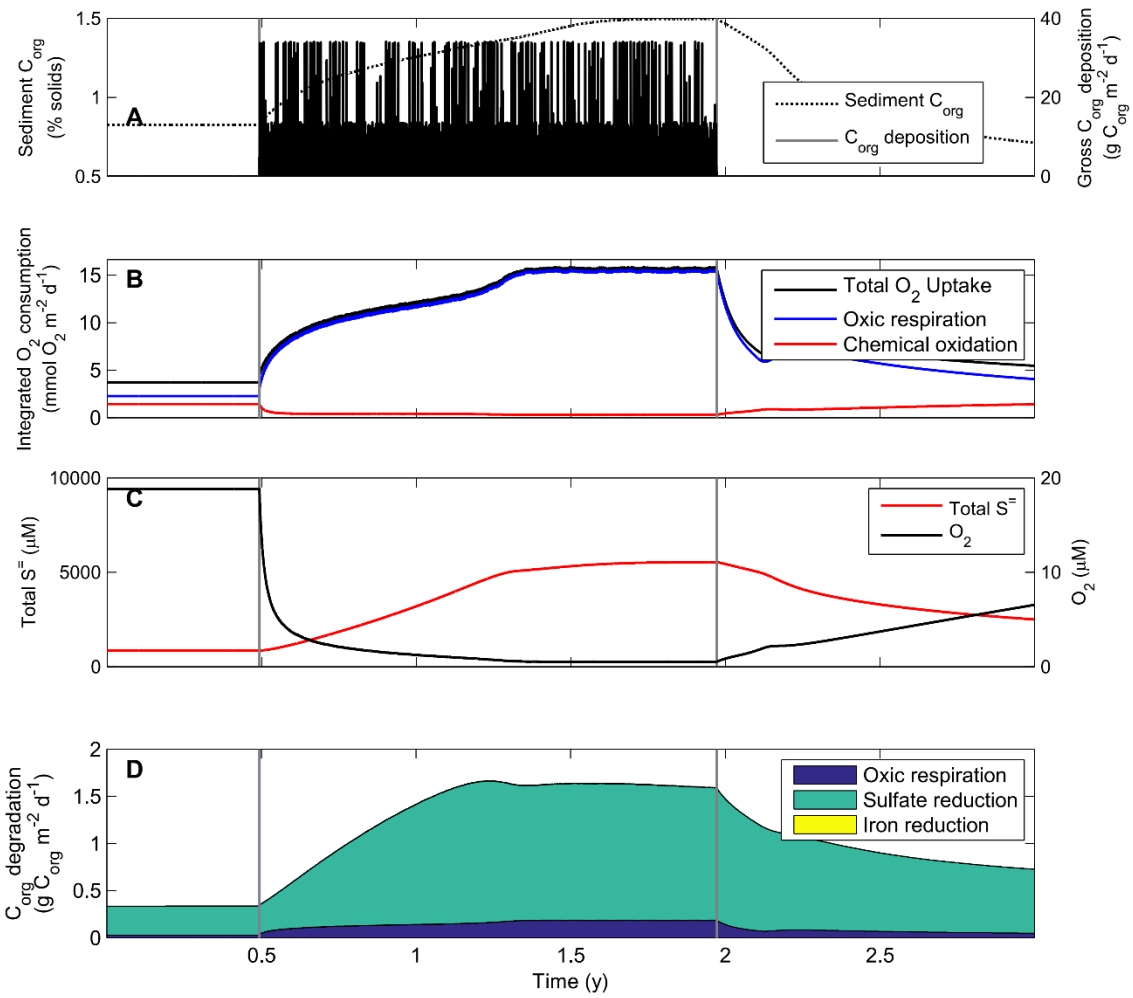

Figure 25: Forcing and state variables in a temporal simulation of organic waste processing in sediments underlying a fish farm cage according parameters of **Table 8** and assuming a feed wastage of 3%. Vertical gray lines at 0.5 and 1.97 years delineates the farming cycle. This simulation corresponds to the high deposition case (H-DEPO) defined in the text. Parameters of the simulation are as follow: length of fish farm production cycle: 18 months, mean free-stream bottom current: 3.1 ± 2.2 cm s^{-1}, daily accumulated wastage rate (feces plus lost feed): 19.4 g C_{org} m^{-2} d^{-1}, average daily organic waste deposition (gross value): 2.3 g C_{org} m^{-2} d^{-1}. **A.** Gross C_{org} deposition and C_{org} concentration in sediments (POC + organic wastes). Peaks observed in deposition rates are caused by increased wastage rate during feeding time. **B.** Contribution of oxic respiration and chemical O_2 demand to vertically-integrated O_2 consumption rates. **C.** Sulfide and O_2 concentration in surface sediments (upper 2 cm). **D.** C_{org} degradation in sediments and contribution of oxic and anoxic mineralization pathways.

The degradation efficiency, defined as the ratio between organic waste degradation and gross deposition, increased significantly throughout the farming cycle as a result of sustained increases in bacterial activity and sedimentary C_{org} (**Figure 26A**).

This increase in degradative capacity over time occurred despite detrimental effects of organic enrichment on bioturbation activity. The greatest changes in degradation efficiency of organic wastes were predicted in H-DEPO from values close to zero at the beginning of the farming cycle to 26.5 ± 11.2 % at completion. Degradation efficiency was close to zero in L- and H-DISP due to almost null net deposition of organic wastes.

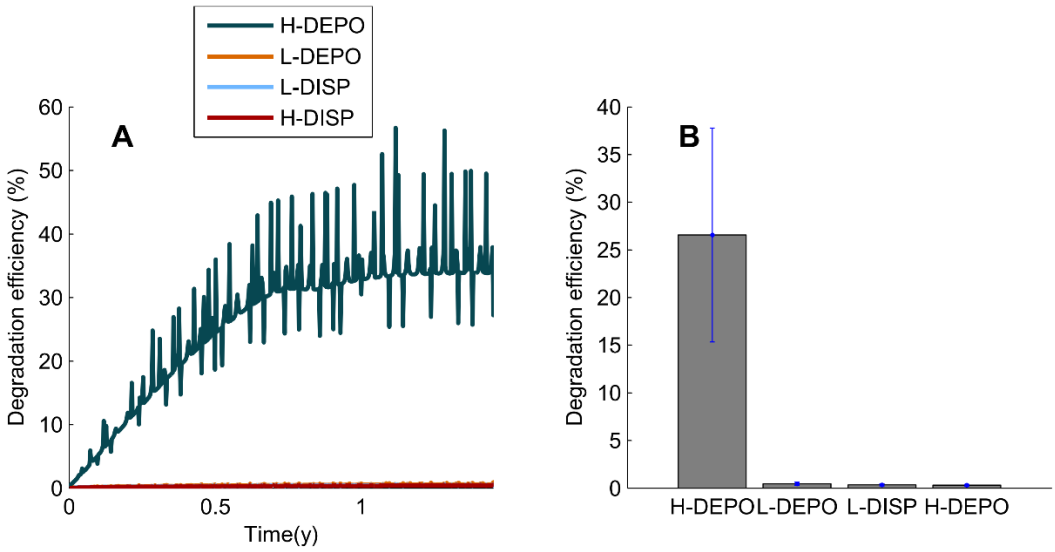

Figure 26: A. Evolution of degradation efficiency of pristine sediment exposed to organic wastes during a single fish farm production cycle according to parameters of **Table 8**. Simulations were carried out assuming a feed wastage of 3%, twice-per-day feeding (for 20 minutes each), and a constant water depth of 20 m below the fish cage (35 m in total). **B.** Mean degradation efficiency for each hydrodynamic scenario defined in **Table 10**. Degradation efficiency was calculated based on daily averaged organic waste degradation and gross deposition rates.

The degradation efficiency was specifically calculated from the daily accumulated rates of C_{org} degradation and gross deposition. This was required to eliminate strong variations in degradation efficiency caused by changes in organic waste deposition within the day (due to changes in currents, dispersion and feeding time). The remaining variations observed in **Figure 26A**, particularly in the DEPO scenarios, are caused by variations in daily accumulated C_{org} deposition rates due to tidal retardation.

Figure 27 shows the evolution of bacterial activity, which increased through the fish farm cycle, following the dynamic of the C_{org} concentration. Bacterial activity was predicted to enhance C_{org} degradation rates up to three times compared to simulations

without the bacterial sub model. This agrees with observations by Vezzulli et al. (2002) and La Rosa et al. (2001).

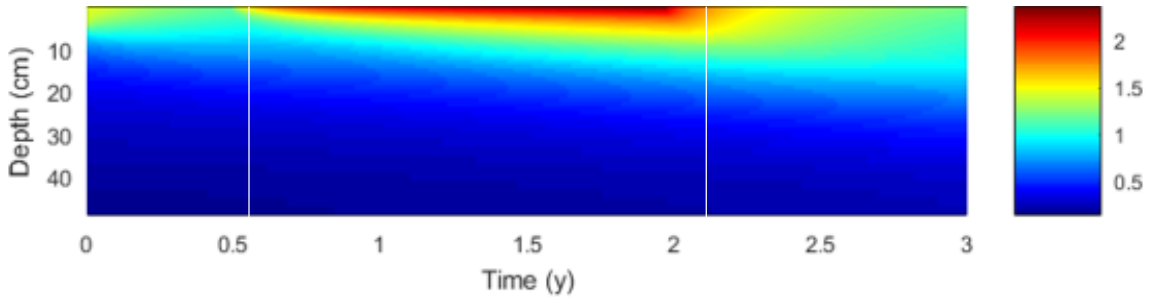

Figure 27: Bacterial activity in sediments exposed to organic enrichments according parameters of **Table 2** and assuming a feed wastage of 3%. Vertical white lines at 0.5 and 1.97 years delineates the farming cycle. This simulation corresponds to the high deposition case (H-DEPO) defined in the text.

4.4.3.2 **Integrated processes**

Similar patterns are observed when benthic processes are integrated over the entire farming cycle (18 months, **Figure 28**). The percent of organic wastes reaching sediments (gross values) varied between ~22 % in H-DEPO (2.3 Kg m^{-2}) to ~9.0 % in H-DISP (0.9 Kg m^{-2}). The total amount of waste generated throughout the farming cycle (540 days) when assumed a 3% feed wastage and parameters of **Table 8** was equal to 10.5 Kg m^{-2}. Ambient deposition in the same period was equal to 0.23 Kg C_{org} m^{-2} (**Eq. 8**, **Table A18**).

As observed in **Figure 28A**, the dispersion of organic wastes in the water column increase considerably with the increase in mean tidal current (higher at H-DISP). Mass erosion tended to decrease at both hydrodynamic extremes (H-DEPO and H-DISP), either because current speed was most of the time below critical current speed for resuspension (in H-DEPO), or because little organic material was available for resuspension (in H-DISP). Highest resuspension was predicted at the intermediate hydrodynamic scenarios (L-DEPO and L-DISP) where the exchange of solids at the sediment surface was the highest.

The dispersion of solid wastes in the water column was the major factor controlling the fate of solid wastes. Within the farming cycle, sediment burial at the lower boundary (50 cm) was negligible in all scenarios, and accumulation of organic wastes was

only predicted in L-DEPO (1.68 Kg m^{-2}). Resuspension played a significant role in the fate of solid wastes after deposition, particularly, in the most dispersive scenarios (L- and H-DISP). Hereafter, I do not discuss organic waste degradation in L- and H-DISP, as net deposition was negligible in both scenarios (Fig 28A). The later do not implies that at different farming regimes (e.g., higher density) or shallower depth the net deposition of organic wastes may have a significant impact on sediment geochemistry. Accumulated over the entire fish farm production cycle, 26.2%, and 0.5% of gross waste deposits were degraded locally within the farming cycle in H-DEPO and L-DEPO, respectively (**Figure 28A** and **4B**, and **Table 11**).

As observed in **Figure 28B**, sulfate reduction was the dominant pathway of organic waste degradation in non-dispersive conditions, accounting for 89% (H-DEPO) and 94% (L-DEPO) of total C_{org} degradation.

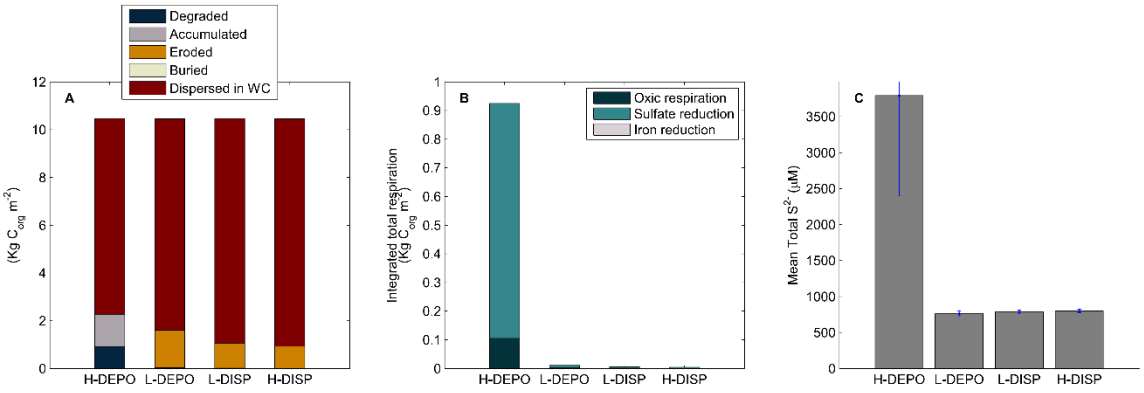

Figure 28: Integrated benthic processes calculated for a representative fish farm production cycle according to **Table 8**. Simulations were carried out assuming a feed wastage of 3%, twice-per-day feeding (for 20 minutes each), and a constant water depth of 20 m below the fish cage (35 m in total). Simulations are presented for four different hydrodynamic scenarios covering poorly- (H-DEPO) to well-flushed aquaculture sites (H-DISP) according **Table 10**. **A.** Fate of gross organic wastes deposits. **B.** Integrated total respiration and contribution of different degradation pathways to organic waste degradation (not ambient POC). **C.** Mean Total S^{2-} concentration throughout the farming cycle (±1 standard deviation).

4.4.4 Assimilative capacity

4.4.4.1 Constrained optimizations

Our estimates of the assimilative capacity of fish farm organic wastes, expressed as assimilable gross deposition, are site-specific, and dependent on hydrodynamics,

background (ambient) deposition, bioturbation and bacterial activity. Except for porosity, these variables are time-dependent in the model. Assimilative capacity was defined as the gross C_{org} deposition rate that prevented sulfide concentration above 1500 µM (AC-H_2S) in surface sediments (upper 2 cm). Suboxic conditions in surface sediments were predicted in all hydrodynamic scenarios exposed to ambient deposition. AC-H_2S increased from 0.49 g C_{org} m^{-2} d^{-1} in H-DEPO to 101.1 g C_{org} m^{-2} d^{-1} in H-DISP. The high assimilative capacity in H-DISP is due to significant dispersion of organic wastes predicted in this scenario (**Table 10**). As observed in the **Table 12**, the degradation efficiency at AC-H_2S decreased considerably from 41% in H-DEPO to 0.2% in H-DISP. The decrease in degradation efficiency toward H-DISP was mostly associated with the increased resuspension.

Net deposition represents the specific amount of organic material that remains in sediments after erosion, and therefore that is susceptible of degradation. The net deposition at AC-H_2S does not differ between scenarios as sediment properties do not differ among hydrodynamic scenarios, being equal to 0.61 ± 0.1 g C_{org} m^{-2} d^{-1}. This value represents the amount of organic carbon that can be degraded on top of ambient deposition without exceeding AC-H_2S.

Table 12: Assimilative capacity of organic wastes that prevent sulfide concentration above 1500 µM in surface sediments (upper 2 cm) (AC-H_2S). Corresponding culture density at AC-S_2^- was calculated assuming a feed wastage of 3%. Degradation efficiency represents how much is predicted to be locally degraded in sediments in relation to gross waste deposition, being the remaining fraction resuspended, buried or accumulated in sediments by the end of the fish farm cycle.

	H-DEPO	**L-DEPO**	**L-DISP**	**H-DISP**
Gross assimilative capacity, AC-H_2S (g C_{org} m^{-2} d^{-1})	0.5	22.7	81.9	101.1
Net deposition of organic wastes at AC-H_2S (g C_{org} m^{-2} d^{-1})	0.2	0.2	0.2	0.2
Ambient deposition (g C_{org} m^{-2} d^{-1})	0.42	0.42	0.42	0.42
Total respiration at AC-H_2S (g C_{org} m^{-2} d^{-1})	0.55	0.55	0.55	0.55
Degradation efficiency at AC-H_2S (%)	41.0	0.9	0.3	0.2
Waste contribution to C_{org} mineralization at AC-H_2S (%)	37.2	37.7	37.5	37.5
Culture density at AC-H_2S (Kg m^{-3})	<3.2	<4.6	ND	ND
Average dispersion coefficient (0-1)	0.78	0.84	0.90	0.91

4.4.4.2 **Scenario analysis**

In addition to constrained optimizations, the response of benthos (H-DEPO to H-DISP) to organic waste deposition was analyzed through scenario simulations, carried out in the four hydrodynamic scenarios described in **Table 10**, and assuming a fish farm cycle according **Table 8**, including twice per day feeding, and a percent feed wastage between zero (ambient deposition) and 8%. All simulations were initiated from ambient conditions, implying no previous exposure to organic wastes. **Figure 29** shows gross deposition rates and benthic processes as a function of the percent feed wastage for the different hydrodynamic scenarios described in **Table 10**.

Gross deposition rates increased with increases in percent feed wastage reaching up to 6.4 g C m^{-2} d^{-1} in H-DEPO when assuming an 8% feed wastage (**Figure 29A**). Net deposition for H-DEPO ranged between 2.5 g C m^{-2} d^{-1} (3% feed wastage) and 3.6 g C m^{-2} d^{-1} (8% feed wastage, **Figure 29B**). These values were considerably higher than net deposition predicted at AC-H_2S (0.61 g C m^{-2} d^{-1}, **Table 12**). Net deposition of organic wastes for L-DEPO to H-DISP was negligible regarding the variations in wastage rate. Fish density (8 kg m^{-3}) and digestive coefficients (80%) among other fish farm parameters in **Table 8** were constant in all simulations, so variations in these parameters may significantly affect predicted production and deposition of organic wastes.

Figure 29C shows the mean C_{org} degradation rate in sediments (H-DEPO to H-DISP) as a function of the percent feed wastage. C_{org} degradation rates increase with increases in the net deposition of organic wastes (up 1.4 g C m^{-2} d^{-1}, **Figure 29B**) plateauing when oxidant demand exceed supply within sediments (**Figure 29C**). Oxic respiration in fish farm sediments was lower than 10% in all hydrodynamic scenarios.

During fish culture, the non-dispersive scenarios showed significant increases in Total S^{2-} (**Figure 28C**), up to ~5800 µM in H-DEPO. This value is considered within the range of hypoxic to anoxic conditions according Hargrave et al. (2008). At this level of sulfide accumulation severe effects on sediment macroinfauna are expected in sediments. No increases above the ambient condition were predicted in sulfide concentration in the remaining hydrodynamic scenarios (**Table 3**).

As observed in **Figure 29C** and **D**, a slight decrease in C_{org} degradation rates was predicted in the L-DEPO scenario with increases in waste deposition (represented here by the percent feed wastage). Likewise, the maximum predicted sulfide concentration in surface sediments (upper 2 cm) followed a similar pattern decreasing from ~5800 µM when exposed to a 3% feed wastage to ~5050 µM when exposed to an 8% feed wastage. This pattern was caused by the different approaches (i.e., formulas) used in the model to simulate C_{org} degradation rates (based on Michaelis-Menten kinetics, R2, **Table A15**), and sulfide reoxidation (first order reaction linearly dependent on sulfide and oxygen concentration, R8, **Table A15**). The difference in model formulation results in relatively higher reoxidation rates of sulfide with O_2 compared to the C_{org} degradation rates when exposed to increasing levels of organic waste deposition.

Most of the produced sulfide in ambient conditions (non-farm) was reoxidized to SO_4^{2-} (R5, Table 1), while precipitation to elemental sulfur (R7, **Table S6**), and to FeS (R8, **Table S6**) was negligible. In sediments exposed to organic farm wastes, prediction shows that most of the sulfide was reoxidized with O_2 or diffused out of sediments in anoxic conditions. In fish farm sediments Fe^{2+} accumulated to concentrations up to 11.6 µM (H-DEPO, 8% feed wastage). FeS precipitation increased significantly with increases in organic waste deposition due to accumulation of reduced by-products (Fe^{2+} and Total S^{2-}). Escape of dissolved Fe^{2+} to bottom waters was also predicted in anoxic conditions due to low reoxidation rates.

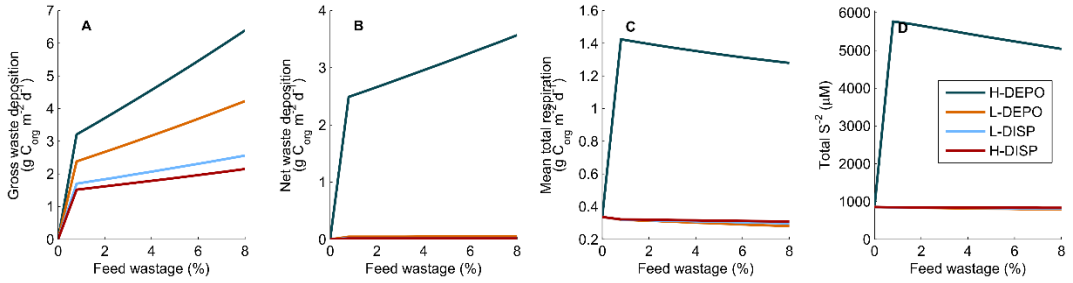

Figure 29: Prediction of benthic processes in fish farm sediments exposed for the first time to fish farm organic wastes according to parameters of **Table 8**, and assuming feed wastage between zero and 8%. Wastage rates were assumed constant, i.e., do not consider variations in feces and lost feed output from the fish cage. The color line represents different hydrodynamic scenarios (H- and L-DEPO, L-DISP, H-DISP). **A.** Gross waste deposition. **B.** Net waste deposition. **C.** Mean total respiration of ambient POC and fish

farm wastes. **D.** Maximum Total S^{2-} concentration predicted throughout the fish farm cycle. The break observed between 0% feed wastage and increasing values is caused by the transition from ambient deposition to farm deposition.

4.4.4.3 **Maximum wastage rates and culture densities**

According to model predictions, the maximum wastage rate assuming an 8% feed wastage was equal to 27.4 g C m^{-2} d^{-1}, however, it increased at higher culture densities (e.g., ~59 g C m^{-2} d^{-1} at 17 Kg m^{-3}). The predicted wastage rates at AC-H_2S are equal to 2.3, 148.4, 803.2 g C_{org} m^{-2} d^{-1} for H-DEPO, L-DEPO, and L-DISP, respectively. These values were calculated based on average dispersion coefficients (**Table 12**) estimated for each scenario (i.e., average fraction of produced wastes deposited out of the fish cage bottom area). Assuming a feed wastage of 3%, fish may be cultured in H-DEPO without exceeding AC-H_2S at culture densities as high as 3.2 Kg m^{-3}. On the other hand, and according to model predictions, fish production in L-DEPO to H-DISP is not limited by AC-H_2S (**Figure 30B**).

A traffic light model of local environmental sustainability of fish farm operations was developed based on scenario simulations and benthic response to organic enrichment (**Figure 30A** and **B**). The precautionary area (yellow) that separates sustainable (green) from unsustainable (red) aquaculture practices was established whenever a specific combination of wastage rate and hydrodynamic conditions leads to sulfide concentration in surface sediments (upper 2 cm) between 1500 and 3000 μM (**Figure 30A**). As expected, the area defining sustainable aquaculture practices (shown in green) decreases considerably with increased percent wastage rate, as well as toward the more depositional environments. As indicated above, H-DEPO provides less suitable conditions for fish farming, even at low culture density. On the contrary, the DISP scenarios are those that present lower local accumulation of organic wastes.

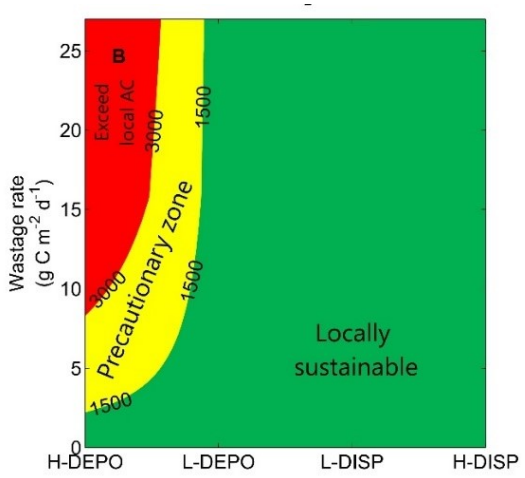

Figure 30: Traffic light model predicting environmental sustainability of aquaculture operations based on hydrodynamic conditions, the wastage rate at the base of the fish cage, and the predicted benthic response to organic enrichment. Environmental performance of aquaculture operations is considered successful if AC-H_2S is not exceeded throughout the fish farm cycle. The precautionary area (yellow) that separates sustainable (green) from unsustainable (red) aquaculture is defined based on the maximum sulfide concentration predicted in surface sediments (upper 2 cm) throughout the fish farm cycle. The precautionary limits are 1500 to 3000 µM Total S^{2-}. The traffic light model was developed considering twice-per-day feeding (20 minutes each), constant production of feces, a constant culture density of 8 Kg m^{-3}, and a wastage rate between 0 (ambient deposition) and 27.4 g C_{org} m^{-2} d^{-1} (0 to 8% feed wastage).

4.5 Discussion

4.5.1 Model performance and prediction

Although the simulations of transient sediment fluxes may be improved by a better representation of physical forcing (e.g., wave-driven porewater exchange), geochemical (e.g., different C_{org} pools), and biological processes (e.g., sediment irrigation), simple numerical models, such as the one presented here provide a cost-effective approach to study the behavior of sediments exposed to organic enrichment. Its simplicity relative to more sophisticated reaction-transport models facilitates the exploration of multiple scenarios (hydrodynamics, oxidant availability in bottom water, etc.), and more importantly, allows us to explore the effects of sustained accumulation of organic matter and metabolic by-products on assimilative capacity.

The introduction of an explicit formulation for bacterial activity, based on Talin et al. (2003), allowed us to speculate on the impact of bacterial dynamics on C_{org} degradation. Future considerations may consider the impact of chemotherapeutic (e.g., antibiotics) on bacterial activity, and of stochastic events (short-term hypoxia, storms) on C_{org} degradation rates.

The incorporation of optimization techniques as a complement to more traditional scenario analysis allows the prediction of the sediment assimilative capacity based on predefined environmental goals. Constrained optimizations were carried out by gradually increasing gross C_{org} deposition rates until assimilative capacity was reached. At assimilative capacity, all biological (bioturbation and bacterial activity) and geochemical (concentration of C_{org}, oxidants, and reduced by-products) variables reach equilibrium in sediments. This steady state condition is hardly met in real farm operations since sediments are usually exposed to highly variable organic deposition rates. This situation may increase the chance of early transition to suboxic conditions depending on the response time of macrofaunal and microbial communities to the changes in organic deposition. Despite the assumption of steady state conditions, model results showed close agreement between constrained optimizations and scenario analysis. This highlights the potential importance that other factors, beyond benthic adaptation play in assimilative capacity, specifically bottom oxidant renewal and associated hydrodynamic conditions.

These results provide confidence in the application of optimization techniques to the study of assimilative capacity at marine fish farms, despite implicit assumptions made in this analysis.

Also relevant for model predictions was the incorporation of husbandry practices at the fish farm. The model is forced by wastage rates and associated parameters (culture density, digestive coefficients, and feeding strategy). This allowed us to link benthic processes to the fish farm operation, an aspect missing in most approaches of environmental impact assessment of organic enrichment. A recent exception to this is provided by Brigolin et al. (2014).

The model uses analytical forcing (tidal current, waste deposition), and is not explicitly ground-truthed, although, an assessment of model performance is provided by comparing fluxes, rates and state variables (C_{org} and H_2S) with observations from Chapter 2 and others from literature. Based on sediment trap data (Abo & Yokoyama 2007, Brigolin et al. 2009), and model predictions (Chang et al. 2014), waste deposition rates to the seafloor may reach values as high as 25.4 g C_{org} m^{-2} d^{-1} under current fish farm practices. The model predicts waste deposition rates (total daily gross values) to sediments underlying the fish cage as high as 6.4 g C_{org} m^{-2} d^{-1} in the worst-case scenario considered in simulations (H-DEPO, 8% feed wastage). Despite the predicted accumulation of waste, H-DEPO does not represent the worst feasible scenario that can be produced by the model, as only ~22% of produced wastes were predicted to reach sediments immediately below the fish cage, the rest dispersed in the water column. A higher deposition may be predicted at lower depth or lower mean current speed.

Reported TOU for fish farm sediments reach up to ~100 mmol m^{-2} d^{-1} (Findlay & Watling 1997, Hargrave et al. 1997). The TOU predictions for the high-deposition scenario (H-DEPO, 3% feed wastage, **Figure 25**) averaged 10.7 mmol m^{-2} d^{-1} for the entire cycle, with a maximum of 15.8 mmol m^{-2} d^{-1}. These values are close to the average observed in similar fish farm cohesive sediments in southern Nova Scotia which averaged 13.5 ± 8.2 mmol m^{-2} d^{-1} (n = 55, maximum, 40.8 mmol m^{-2} d^{-1}, **Chapter 2**).

Similarly, maximum C_{org} concentration predicted in the simulations (1.5% dry weight, H-DEPO, 3% feed wastage, **Figure 25**)), was relatively low compared to reported

values for organically enriched sediments which may reach up to ~10% in heavily loaded conditions (pellet layer) (Hargrave et al. 1995). This value is also relatively low when expressed as percent organic matter (~5%) and compared to observations from fish farm sediments reported in **Chapter 2**, which range between 1.2 and 34% (20.4 ± 4.9 %). The former conversion was done assuming C_{org} contents of feces and feed according to **Table 8**, a waste composition of 10.1% feed and 89.8% feces for H-DEPO (3% feed wastage), and no significant changes in degradability of surface deposits (upper 2 cm). The relatively low O_2 consumption rates and organic matter concentrations predicted in the model suggest that the study fish farm may be exposed to higher loading rates than those simulated in H-DEPO. Nonetheless, further data, particularly hydrodynamic and gross deposition under the cages, is required for a direct comparison of scenario simulations and observations.

Our model predicts H-DEPO sulfide concentrations of ~6000 uM by the end of the fish farm cycle (3% feed wastage). Although observations by Hargrave et al. (1995) have shown sulfide concentration > 3000 µM at C_{org} concentrations as low as 1%, this is not necessarily the dominant pattern observed in organically-enriched sediments. The high predicted sulfide concentration compared to the relatively low C_{org} concentration suggest that the model might be overestimating sulfide concentration in surface sediments. Further adjustment of model parameters, particularly of those related to solid burial (w_{sed}) and reoxidation of sulfide ($k_{\text{Total } S_{SL}^{-2},ox1}$), are required to better reproduce dominant patterns observed at aquaculture sites.

4.5.2 Sediment assimilative capacity

Only a few estimates of sediment assimilative capacity have been reported in the literature. C_{org} loading rates causing marked anoxic conditions vary by an order of magnitude from 0.36 to 11.4 g C_{org} m^{-2} d^{-1} (Cranston 1994, Hargrave 1994, Findlay & Watling 1997, Fisheries and Oceans Canada 2004, Chamberlain & Stucchi 2007, Environment Canada 2009, Chang et al. 2012). Based on empirical observations, Findlay & Watling (1997) suggested that sedimentation rates in excess of 2.4 − 4.8 g C_{org} m^{-2} d^{-1} (200 − 400 mmol C m^{-2} d^{-1}) in areas exposed to bottom current lower than 10 cm s^{-1} may lead to anoxic conditions and formation of sulfur bacteria mats. Likewise, the Department

of Environment of New Brunswick, Canada, indicates that sulfide concentrations > 3000 μM, and C_{org} deposition rates > 2 g C_{org} m^{-2} d^{-1}, are the threshold level at which adverse environmental effects are expected in sediments (NBDENV 2012). These values agree with the site-specific maximum loading rates (gross values) predicted by the model, which ranges between 0.49 to 22.7 g C_{org} m^{-2} d^{-1} in poorly-flushed environments (H- and L-DEPO). According simulations, AC-H_2S do not limit farms production in environments exposed to mean tidal currents > 9.5 cm s^{-1} (DISP scenarios), where most fish farm organic wastes are dispersed to the far-field or resuspended after deposition.

In addition, model results show that ambient sediments initially exposed to organic wastes possess a higher assimilative capacity than sediments with an exposure history. The latter condition occurs when the oxidants have been partially or fully depleted, or when refractory organic wastes remain in sediments. This chronology, already emphasized in the literature (McGhie et al. 2000), needs to be considered in management strategies of finfish aquaculture sites, as it affect the transition to suboxic conditions and the recovery time of fallowed sediments.

Assimilative capacity of sediments to degrade organic wastes is expected to increase in well-flushed environments due to increased renewal of oxidants in bottom waters. In contrast, net C deposition is expected to decrease as flushing increases. As a result, benthic metabolism may be primarily defined by the balance between oxidant availability and net C_{org} deposition (deposition – erosion). Nonetheless, several additional factors add complexity to this relationship. First, animal-sediment relationships may play a major role in oxidant availability and C_{org} degradation rates in sediments. Two variables are emphasized in this model: bioturbation and bacterial activity. Sediment-water exchange of solutes is partially controlled by bioturbating activity, which in nature maximizes at intermediate C_{org} loading rates, and low concentration of reduced compounds such as sulfide. Only the effects of increase toxic sulfide concentration were incorporated in the model, not the effects of increase carbon availability, which should be included in future model developments. On the other hand, bacterial activity was represented explicitly, assuming growth rates directly proportional to C_{org} degradation rates (combined oxic and anoxic). This factor is not usually considered in traditional one-

dimensional diagenetic models, where C_{org} degradation is modelled as a function of oxidant availability and maximum degradation rates. According to model simulations, C_{org} degradation efficiency increases with exposure time to organic wastes as result of sustained increases in bacterial activity. However, this prediction needs to be contrasted with the loss of macrofaunal biomass/activity observed under heavily loaded conditions, and their impact on C_{org} degradation rates.

A second relevant aspect for modelling sediment C_{org} degradation is the accurate representation of transport mechanisms of solutes and particles across the sediment-water interface. Fish farms prefer sites with relatively high flushing rates to ensure adequate ventilation within cages, as well as to prevent excessive accumulation of organic wastes in beds underlying cages. Minimum current speed required for safe operation of fish farms varies according fish size and fish density within cages (Page et al. 2005, Solstorm et al. 2015). Page et al. (2005) predicted that threshold current speeds of ~2 cm s^{-1} for 40 minutes may induce O_2 depletion within fish cages stocked with pre-market salmon. This threshold varies with culture density but roughly indicates the lower current required for safe operation. Estimates of critical current speed causing fatigue to small and large post-smolts, and adults range between 80.6 and 99.5 cm s^{-1} (Remen et al. 2016). Sediment type may varies within this range of current speed, from cohesive muds to permeable sands, and consequently the dominant transport mechanisms within sediments. In high-energy environment, advection may play a significant role in the transport of solutes across the sediment-water interface, particularly, in sandy beds with permeabilities greater than 10^{-12} m^2 (Huettel et al. 1998). Permeability in coastal sediments ranges several orders of magnitude, from ~10^{-19} to ~10^{-9} m^2, depending on grain size and shape, porosity and tortuosity (Spinelli et al. 2004). According to Huettel et al. (2003), flow- and topography-induced advective fluxes can be enhanced by 50 times relative to molecular diffusion, and reach tens of centimeters within permeable sediments (Santos, Eyre, & Huettel 2012). This may significantly influence the capacity of sediments to degrade organic matter, particularly of dissolved compounds. Differences in porosity and permeability were not included in the model, nor porewater flows associated with tidal pumping, flow- or topography-induced pressure gradients, among other driving forces of porewater advection (Santos, Eyre, & Huettel 2012). Accounting for the differences in surface and

in-bed transport is important to improve modelled C_{org} degradation at fish farm sediments.

4.5.3 Concepts and models

Our model demonstrates that the balance of culture density, waste production, and hydrodynamics can be used to simulate benthic metabolic response to fish farm organic enrichment. Moreover, the model is used to formalize the definition of assimilative capacity in terms of a deposition rate (gross and net) which maintains predefined environmental quality criteria. I suggest that the model has significant applications to the regulatory environment, and fills a void in predicting benthic impacts of aquaculture, as well as in the planning new farm sites.

The concept of sediment assimilative capacity was initially adopted from Omori et al. (1994), who define it as "the capacity for oxygenic degradation [oxic respiration] of organic matter at the bottom of the system". In this conceptual model, oxic respiration is assumed to peak at some intermediate organic carbon loading rate, the higher extreme dominated by anaerobic degradation. This peak and corresponding sulfide concentration, represents the upper limit of oxic assimilative capacity, and of sustainable organic loading at fish farm sites. I build on this work and extend it to consider alternative sustainability criteria and some weaknesses associated with this definition and the modeling approach. The underlying assumption of steady state in Omori's work implies no accumulation of organic material over time, the opposite case of sediments exposed to aquaculture wastes, especially in poorly-flushed conditions. This assumption limits the capacity of the model to predict the temporal evolution of metabolic conditions in organically enriched sediments. Second, the occurrence of time lags in sulfide accumulation in relation to C_{org} deposition may prevents its utilization as indicator of assimilative capacity as proposed by Omori et al. (1994). The immediate accumulation of sulfide may not necessarily be expected in all sedimentary environments exposed to organic enrichment. A lagged increase in sediment sulfide may occurs if oxygen supply is greater than oxygen demand in the initial stages of organic loading. This was not observed in the simulations, as they represent diffusion-dominated environments (muddy sediments), but it may be expected in permeable sediments subject to porewater advection, and therefore higher O_2 renewal.

Evidence of time lags in ambient sediments has been documented by Luff & Moll (2004) and suggested as well by Chang et al. (2012).

We choose a transient approach to simulate C_{org} diagenesis below fish farm cages. Instead of determining organic carbon deposition at the point of maximum oxic respiration, I used diagenetic modeling to estimate the organic carbon deposition rate that maximizes total respiration while preventing sulfide concentration above 1500 µM (AC-H_2S). This approach allows us to consider the effects of C_{org} accumulation and the background deposition over which organic enrichment occurs. This is critical in that the history of mineralization, and trophic condition (from oligo- to eutrophic) control the capacity of benthos to deal with excess organic loading. Assimilative capacity is thus recognized as a finite and time-space dependent environmental threshold that may increase or decrease according to the history of mineralization, benthic composition, and sediment type.

We emphasize that C_{org} degradation rates predicted in the simulations are largely dominated by anaerobic degradation, even in sediments exposed to ambient deposition. This is due to the vertical extent covered by the model (50 cm) that include a large anoxic zone, as well as because sediments simulated here are of the muddy type, that is to say diffusion-dominated. In this case, as opposed to permeable sands, oxic respiration is largely restricted to the upper millimetres of sediments.

4.5.4 Application to regulation

Successful environmental management of marine fish farms requires assurance that production levels are within an area's capacity. This also implies maintaining ecosystem function and state within desired limits despite uncertainties in management systems and/or environmental conditions. The advancement of knowledge regarding sustainable limits of organic loading can promote the implementation of anticipatory rather than reactive management practices, decreasing the risk of self-pollution of aquaculture grounds. The combination of geochemical analysis and diagenetic modeling provides a valuable tool to accomplish this objective.

Monitoring of benthic health has been based on biological and geochemical parameters. Their integration has led to the development of multiple benthic condition

indices (Rhoads & Germano 1982, Findlay & Watling 1997, Nilsson & Rosenberg 1997, Fossing et al. 2004, Hargrave et al. 2008, Borja et al. 2009, Wilson & Vopel 2012, Simone & Grant 2017). Several studies has suggested that recovery of macrofaunal communities from eutrophicated conditions under salmon farms requires considerably more time than chemical recovery (Chang & Page (2011) and references therein), making biological indicators a better indicator of recovery. However, a drawback of macrofaunal analysis is that it requires considerably more time of analysis and expertise on the composition of local benthic communities (Wildish et al. 2001). In contrast, geochemical indicators such as sediment sulfide, redox potential (Eh), and C_{org} are widely applicable to any sedimentary environment, their response to organic enrichment well understood, and cost-effective methods are available for routine analysis.

Sulfide is considered one of the major regulatory variables in Canada and elsewhere, yet models predicting sediment concentration are sorely lacking. Modelling capability for these benthic variables and oxic state adds powerful capability to the regulatory regime. When linked to dispersion models and fish growth models, they can be used to predict fish biomass that relates to any given sulfide concentration in a particular sedimentary environment.

In this context, diagenetic models can serve as effective tools to predict (1) values of environmental regulatory variables such as sulfide concentration, (2) the transition to suboxic conditions, (3) sustainable C_{org} loading, and (4) recovery rates of organically enriched sediments. Applications cover the entire fish farm production cycle, including the a priori assessment of new aquaculture sites (e.g., license or lease applications), throughout operations (e.g., farm management plans, fallowing), and after complete cessation of aquaculture operations (e.g., site remediation plans).

4.5.5 Application to an Ecosystem Approach to Aquaculture

Our model has demonstrated its application to non-aquaculture conditions in the ‘ambient’ scenarios. This outcome means that the model capability can be extended to the far-field. The present model is one dimensional, but is readily extended to two or three dimensions when coupled with a circulation model. It incorporation in spatially-explicit simulations is expected to facilitate the development of spatial planning tools and the

incorporation of an ecosystem-oriented approach to salmon aquaculture (FAO 2010, Filgueira et al. 2014). This is particularly relevant for areas of rapid expansion of salmon aquaculture such as Nova Scotia (Canada) and Southern Chile. Applications include aquaculture siting optimization and the evaluation of interactions of finfish aquaculture with other human activities, ecosystem services, and sensitive biological communities (e.g., shellfish aquaculture, C and nutrient cycling, nursery grounds,). It is important to recognize that in a spatial mode, the model allows assessment of the distribution of sulfides, sediment carbon, etc. This spatial component allows scaling of potential impacts, and thus their interpretation in an appropriate context beyond merely local near-field effects.

CHAPTER 5. CONCLUSIONS

5.1 Major findings and summary of results

A combination of scientific and management-oriented objectives guide this thesis. The major findings of each research chapter are as follows:

In **Chapter 2**, the spatial variability in benthic metabolism, particularly of sediment fluxes across the sediment-water interface (O_2, DIC, TA, NH_3), was studied in relation to benthic habitat diversity (vegetated and aphotic sediments), sediment type (muddy to sandy sites), and in sediment underlying fish farm cages. Factors considered as explanatory variables of benthic fluxes were the organic matter content, porosity, salinity, temperature, depth, and light availability.

I found significant differences in metabolic activity and sediment properties among different sediment/habitat types (O_2 and DIC fluxes, O_2 consumption, and LOI). These differences highlight the significant role of habitat diversity and sediment-biological interactions (e.g., autotrophic activity) on diagenetic processes in coastal areas.

Results indicate that only a moderate fraction of the observed variability in benthic fluxes was accounted by the explanatory variables considered in the study (11.2% to 69.3%). The variables that mostly contributed to the observed variability were temperature, O_2 availability, irradiance, mud percent, and depth. LOI content only showed a significant explanatory power when data was disaggregated by habitat types.

Non-evaluated secondary processes that may help to explain observed patterns are NH_4^+ adsorption, organic matter quality, and alternative pathways of N_2 production. Future research should consider them into the evaluation of benthic processes.

Finally, fish farm sediments show a significantly higher LOI content compare to pristine sites. Nonetheless, exchange rates of oxidants (O_2) and reduced products (NH_3, and DIC) in fish farm sediments were not significantly higher than observed in pristine sediment. I suggest that the comparatively low exchange rates may be explained by the low to null infaunal activity (and therefore bioturbation and degradation) and by the fact

that the fish farm sediments were significantly muddier and therefore dominated by diffusion processes.

In **Chapter 3**, I used a diagenetic model to predict the contribution of sub-tidal sediments in photic and aphotic environments to C and N removal via C_{org} degradation and denitrification, respectively, in Shelburne Bay (SH), Nova Scotia, Canada.

Simulations suggest that subtidal sediments in SH play a significant role in nutrient cycling and C_{org} mineralization. On an annual basis, SH sediments behave as an active source of nutrient regeneration to the water column (NO_3, NH_3, Fe^{2+}), contributing specifically with 31.6 tonnes of NO_3 y^{-1} and 83.7 tonnes NH_3 y^{-1}. Denitrification was a significant sink of nitrogen in the bay, removing ~25% (37.9 tonnes N y^{-1}) of total particulate nitrogen inputs to sediments (153.2 tonnes y^{-1}). Total N inputs to SH from Roseway River, municipal discharges, and atmospheric deposition was estimated equal to 36.6 tonnes N y^{-1}. This value represented about 95 % of total N removal by sub-tidal SH sediments.

No sufficient information was available to build a complete the N budget of SH. Future research efforts should focus on incorporating N inputs associated with diffusive runoff, other secondary riverine inputs, industrial point sources, particularly from local fish farms, as well as on a more accurate estimations of bay-ocean N exchange. Model results also indicate that annual C_{org} recycling in SH subtidal sediments equal to 1816.9 tonnes C y^{-1}.

Finally, simulations indicate that benthic primary production was a significant driver of C and nutrient cycling at hour- to daily-scales. Nonetheless, the variability imposed by BMA activity on benthic processes was well within seasonal variability imposed by C_{org} deposition. As a result, benthic primary production does not affect significantly daily average rates and fluxes when compared to aphotic sediments.

The model lacks several factors that control C and N recycling efficiencies, such as advective transport within sandy sediments which compress ~54% of subtidal bay sediments (887.7 Ha), and alternative pathways of N_2 formation, and is therefore conservative in the prediction of C and N removal from SH sediments.

In **Chapter 4**, I built on the current state of the art by exploring a novel approach to define sustainable limits of fish farm operation based on waste production and their impacts on sediment quality.

The numerical model allows exploring the interactions of husbandry practices (fish density and percent feed lost to the environments), organic waste production, and sediment quality in a broad range of environmental conditions.

I formalized the concept of sediment assimilative capacity in the context of fish farm aquaculture as the gross C_{org} deposition rate (g m^{-2} d^{-1}), that can be degraded in a particular sedimentary environment while preventing accumulation of toxic sulfide above regulatory limits in Canada (> 1500 μM, upper 2 cm). Model results show that the assimilative capacity of organic wastes ranges between 0.49 and 101.1 g C_{org} m^{-2} d^{-1} in poorly- to well-flushed environments as defined in the methods.

Predicted net deposition at assimilative capacity, including ambient deposits and fish farm wastes, equal to 0.62 g C m^{-2} d^{-1} for the cohesive (muddy) sediment represented in the model. This result was consistent with empirical observations that range between 0.36 to 11.4 g C_{org} m^{-2} d^{-1} (Cranston 1994, Hargrave 1994, Findlay & Watling 1997, Gillibrand et al. 2002, Fisheries and Oceans Canada 2004, Chamberlain & Stucchi 2007, Environment Canada 2009, Chang et al. 2012).

Finally, based on sediment assimilative capacity, suitable combinations of fish density and percent feed wastage were estimated for multiple hydrodynamic scenarios. The explicit links between farming practices and environmental indicators mean the model can be used by farmers or managers to adapt farming practices with respect to environmental targets.

5.2 Research tools and novel approaches

In this thesis, a suite of experimental and observational tools, combined with statistical and dynamical models were used to study benthic metabolism and aquaculture – sediment interactions in coastal areas. A rigorous assessment of uncertainties in observation and model simulations was carried out and reported in each chapter, and suggestions to reduce them were provided. Model assumptions, limitations, and

parameter sensitivity were also communicated to ensure adequate use of results, and to guide further research.

In model experiments, forcing conditions were downscaled to the relevant scales at which coastal benthic processes and aquaculture operate. I emphasize that assuming steady state conditions was not possible, nor was it of interest to this research. The steady-state approximation can only be considered if the exchange flux between sediments and surface water is relatively constant, no accumulation of mass occur over time, or, alternatively, when changes in boundary conditions occur either on a much longer or a much shorter time scale than the characteristic response time of the sedimentary transport-reaction system. None of these conditions meet in coastal sediments exposed to daily to seasonal fluctuations in C_{org} deposition and boundary conditions (light irradiance, temperature, O_2 concentration in bottom water, etc.), nor in fish farm sediments exposed to organic enrichment. For this reason, I choose to simulate benthic processes assuming dynamic steady-state (**Chapter 3**) and transient conditions (**Chapter 4**).

In **Chapter 2**, in-situ and laboratory incubations, and benthic mapping techniques were combined to characterize the patterns of, and controls on the C and N cycling in shallow coastal sediments. In **Chapter 3**, sub-seasonal and meter to kilometer scales of variability in benthic processes at SH were studied using a time-dependent diagenetic model supported by observations of **Chapter 2** and time series of PAR irradiance, C_{org} deposition, and temperature reported for Southern Nova Scotia. To my knowledge, no diagenetic models have been developed and used to evaluate benthic metabolism in subtidal sediments at these scales, this being a novel aspect of this project.

In **Chapter 4**, deterministic models of fish growth, organic waste production, dispersion, and degradation were applied to produce indications of the suitability of fish farm operations. The links between farming practices (cultured densities and feeding practices/methods) and indicators of environmental performance (sediment sulfide) were explicitly modeled. The latter was a key aspect to define suitable conditions of fish farm operation, as well as to strengthen and expand the applicability of benthic indicators beyond monitoring, and into anticipatory practices. Model simulations were forced with

sub-hour variations in organic waste deposition in relation to farming practices (feeding time) and tidal current. The incorporation of this time scale of forcing was required to predict more accurately the fate of organic wastes produced at the fish farm (dispersion, deposition, resuspension, accumulation, and degradation).

We incorporate as well, for the first time to the knowledge, optimization techniques to determine sustainable levels of organic waste production and deposition in fish farm sediments. The algorithms of optimization sorted through numerous wastage rate, to reach predefined environmental goals based on sediment degradation efficiency and acceptable limits of sulfide accumulation in surface sediments.

5.3 Outlook and Perspectives

There is a growing body of literature focusing on increasing the use of marine ecosystem models and observations in decision-making and policy development for sustainable use marine resources (Hyder et al. 2015).

In this research project, significant attention was given to contribute to the development of tools and knowledge in support of the sustainable management of human activities in coastal areas.

The knowledge gained in modeling annual C and N cycling in SH sediments (Chapter 3) is expected to contribute to the development of bay-scale management strategies. This may be achieved through incorporation of sediment N cycling in the analysis of potential cumulative effects of nutrient inputs to SH, as well as in the definition of Total Maximum Daily Load (TMDL) of nutrients to maintain water quality standards.

In salmon aquaculture, various types of models of different complexity have been proposed to address multiple socioeconomic and ecological aspects associated with farm operation, including pen sitting, connectivity, waste dispersal, water quality, epidemiological risk, production potential, and economic viability, among others. For a full review of some of the different types of aquaculture models, I refer to Bjorndal et al. (2004), McKindsey et al. (2006), Pomeroy et al. (2008), Tapia & Giglio (2010) and Stigebrandt (2011).

The model developed in Chapter 4 looks to contribute to the understanding and management of one of the most significant aquaculture-environment interactions occurring in salmon farming; the organic enrichment of sediments underlying fish farm cages. I expect this model and associated concepts, may complement the battery of aquaculture models currently available, and help to expand the use of benthic indicators into monitoring and management of aquaculture activities and eutrophication of coastal areas.

References

Abo K, Yokoyama H (2007) Assimilative capacity of fish farm environments as determined by the benthic oxygen uptake rate: Studies using a numerical model. Bulletin of Fisheries Research Agency, Japan 19:79–87

Aitkenhead-Peterson J, Alexander J, Clair T (2005) Dissolved organic carbon and dissolved organic nitrogen export from forested watersheds in Nova Scotia: Identifying controlling factors. Global Biogeochem Cycles 19

Alber M (2000) Settleable and non-settleable suspended sediments in the Ogeechee River estuary, Georgia, USA. Estuar Coast Shelf Sci 50:805–816

An S, Joye SB (2001) Enhancement of coupled nitrification-denitrification by benthic photosynthesis in shallow estuarine sediments. Limnology and Oceanography 46:62–74

Bailey EM (2005) Measurements of nutrient and oxygen fluxes in estuarine and coastal marine sediments: Literature review and data report. University of Maryland Center for Environmental Science, Chesapeake Biological Laboratory

Bartoli M, Nizzoli D, Viaroli P (2003) Microphytobenthos activity and fluxes at the sediment-water interface: interactions and spatial variability. Aquatic Ecology 37:341–349

Bennett EM, Carpenter SR, Caraco NF (2001) Human Impact on Erodable Phosphorus and Eutrophication: A Global Perspective: Increasing accumulation of phosphorus in soil threatens rivers, lakes, and coastal oceans with eutrophication. AIBS Bulletin 51:227–234

Berelson W, Heggie D, Longmore A, Kilgore T, Nicholson G, Skyring G (1998) Benthic nutrient recycling in Port Phillip bay, Australia. Estuar Coast Shelf Sci 46:917–934

Berelson W, McManus J, Coale K, Johnson K, Burdige D, Kilgore T, Colodner D, Chavez F, Kudela R, Boucher J (2003) A time series of benthic flux measurements from Monterey Bay, CA. Cont Shelf Res 23:457–481

Berner RA (1971) Principles of chemical sedimentology. McGraw-Hill, New York, 240 pp.

Berner RA (1980) Early diagenesis: A theoretical approach. Princeton University Press

Bjorndal T, Lane DE, Weintraub A (2004) Operational research models and the management of fisheries and aquaculture: A review. European Journal of Operational Research 156:533–540

Borcard D, Legendre P (1994) Environmental control and spatial structure in ecological communities: an example using oribatid mites (Acari, Oribatei). Environmental and Ecological Statistics 1:37–61

Borja Á, Rodríguez JG, Black K, Bodoy A, Emblow C, Fernandes TF, Forte J, Karakassis I, Muxika I, Nickell TD, others (2009) Assessing the suitability of a range of benthic indices in the evaluation of environmental impact of fin and shellfish aquaculture located in sites across Europe. Aquaculture 293:231–240

Boudreau BP (1996) A method-of-lines code for carbon and nutrient diagenesis in aquatic sediments. Computers & Geosciences 22:479–496

Boudreau BP (1997) Diagenetic models and their implementation: modelling transport and reactions in aquatic sediments. 414 pp., Springer-Verlag, Berlin

Boudreau BP, Mucci A, Sundby B, Luther GW, Silverberg N (1998) Comparative diagenesis at three sites on the Canadian continental margin. Journal of Marine Research 56:1259–1284

Brady DC, Testa JM, Toro DM Di, Boynton WR, Kemp WM (2013) Sediment flux modeling: calibration and application for coastal systems. Estuar Coast Shelf Sci 117:107–124

Bravo F, Grant J (2017) Benthic habitat mapping and sediment fluxes in shallow coastal environments of Nova Scotia, Canada. In preparation

Brigolin D, Meccia VL, Venier C, Tomassetti P, Porrello S, Pastres R (2014) Modelling biogeochemical fluxes across a Mediterranean fish cage farm. Aquaculture Environment Interactions 5:71–88

Brigolin D, Pastres R, Nickell TD, Cromey CJ, Aguilera DR, Regnier P (2009) Modelling the impact of aquaculture on early diagenetic processes in sea loch sediments. Marine Ecology Progress Series 388:63–80

Brock TD (1981) Calculating solar radiation for ecological studies. Ecol Modell 14:1–19

Brock JC, Yates KK, Halley RB, Kuffner IB, Wright Cw, Hatcher BG (2006) Northern Florida reef tract benthic metabolism scaled by remote sensing. Marine Ecology Progress Series 312:123–129

Brooks KM (2001) An evaluation of the relationship between salmon farm biomass, organic inputs to sediments, physicochemical changes associated with those inputs and the infaunal response – with emphasis on total sediment sulfides, total volatile solids, and oxidation reduction potential as surrogate endpoints for biological monitoring. Final Report. 172 pp. Aquatic Environmental Sciences, 644 Old Eaglemount Road, Port Townsend, Washington, U.S.A.

Brooks KM, Mahnken CV (2003) Interactions of Atlantic salmon in the Pacific Northwest environment: II. Organic wastes. Fisheries Research 62:255–293

Brown KA, McGreer ER, Taekema B, Cullen JT (2011) Determination of total free sulphides in sediment porewater and artefacts related to the mobility of mineral sulphides. Aquatic geochemistry 17:821–839

Brown CJ, Smith SJ, Lawton P, Anderson JT (2011) Benthic habitat mapping: A review of progress towards improved understanding of the spatial ecology of the seafloor using acoustic techniques. Estuar Coast Shelf Sci 92:502–520

Bundy A, Themelis D, Sperl J, Heyer N den (2014) Inshore Scotian Shelf Ecosystem Overview Report: Status and Trends. DFO Can Sci Advis Sec Res Doc 2014/065 xii + 213 p

Burt W, Thomas H, Fennel K, Horne E (2013) Sediment-water column fluxes of carbon, oxygen and nutrients in Bedford Basin, Nova Scotia, inferred from 224 Ra measurements. Biogeosciences 10:53–66

Buschmann AH, Riquelme VA, Hernández-González MC, Varela D, Jiménez JE, Henríquez LA, Vergara PA, Guíñez R, Filún L (2006) A review of the impacts of salmonid farming on marine coastal ecosystems in the southeast Pacific. ICES Journal of Marine Science: Journal du Conseil 63:1338–1345

Cabello-Pasini A, Muñoz-Salazar R, Ward D (2004) Biochemical characterization of the eelgrass Zostera marina at its southern distribution limit in the North Pacific. Ciencias Marinas 30:21–34

Cabrita MT, Brotas V (2000) Seasonal variation in denitrification and dissolved nitrogen fluxes in intertidal sediments of the Tagus estuary, Portugal. Marine Ecology Progress Series 202:51–65

Canadian Council of Ministers of the Environment (2007) Canadian water quality guidelines for the protection of aquatic life: Nutrients: Canadian Guidance Framework for the Management of Nearshore Marine Systems. In: Canadian environmental quality guidelines, 1999, Canadian Council of Ministers of the Environment, Winnipeg

Canavan RW, Slomp CP, Jourabchi P, Cappellen P Van, Laverman AM, Berg GA Van den (2006) Organic matter mineralization in sediment of a coastal freshwater lake and response to salinization. Geochim Cosmochim Acta 70:2836–2855

Capone D (1993) Determination of nitrogenase activity in aquatic samples using the acetylene reduction procedure. In: Handbook of methods in aquatic microbial ecology. Boca Raton, FL, USA: Lewis Publishers, p 621–631

Cappellen P Van, Wang Y (1996) Cycling of iron and manganese in surface sediments; a general theory for the coupled transport and reaction of carbon, oxygen, nitrogen,

sulfur, iron, and manganese. American Journal of Science 296:197–243

Carrascal LM, Galván I, Gordo O (2009) Partial least squares regression as an alternative to current regression methods used in ecology. Oikos 118:681–690

Chamberlain J, Stucchi D (2007) Simulating the effects of parameter uncertainty on waste model predictions of marine finfish aquaculture. Aquaculture 272:296–311

Chang B, Page F (2011) Analysis of results from the Environmental Management Program Tier 1 monitoring of salmon farms in southwestern New Brunswick, Bay of Fundy: Relationships between sediment sulfide concentration and selected parameters, 2002-2008. Can. Tech. Rep. Fish. Aquat. Sci. 2936: v + 77 p.

Chang B, Page F, Losier R, McCurdy E (2012) Predicting organic enrichment under marine finfish farms in southwestern New Brunswick, Bay of Fundy: Comparisons of model predictions with results from spatially-intensive sediment sulfide sampling. DFO Can. Sci. Advis. Sec. Res. Doc. 2012/078. iv + 146 p.

Chang B, Page F, Losier R, McCurdy E (2014) Organic enrichment at salmon farms in the Bay of Fundy, Canada: DEPOMOD predictions versus observed sediment sulfide concentrations. Aquaculture Environment Interactions 5:185–208

Chanton JP, Martens CS, Kelley CA (1989) Gas transport from methane-saturated, tidal freshwater and wetland sediments. Limnology and Oceanography 34:807–819

Chapelle A, Ménesguen A, Deslous-Paoli J-M, Souchu P, Mazouni N, Vaquer A, Millet B (2000) Modelling nitrogen, primary production and oxygen in a Mediterranean lagoon. Impact of oysters farming and inputs from the watershed. Ecol Modell 127:161–181

Chen C-TA, Wang S-L (1999) Carbon, alkalinity and nutrient budgets on the East China Sea continental shelf. Journal of Geophysical Research: Oceans 104:20675–20686

Cloern JE (2001) Our evolving conceptual model of the coastal eutrophication problem. Marine ecology progress series 210:223–253

Cornwell JC, Kemp WM, Kana TM (1999) Denitrification in coastal ecosystems: methods, environmental controls, and ecosystem level controls, a review. Aquatic Ecology 33:41–54

Costanza R (1999) The ecological, economic, and social importance of the oceans. Ecological economics 31:199–213

Costanza R, Arge R d', Groot R De, Farber S, Grasso M, Hannon B, Limburg K, Naeem S, O'neill RV, Paruelo J, others (1998) The value of the world's ecosystem services and natural capital. Ecological economics 1:3–15

Couture R-M, Shafei B, Cappellen P Van, Tessier A, Gobeil C (2009) Non-steady state modeling of arsenic diagenesis in lake sediments. Environmental science & technology 44:197–203

Cranston R (1994) Dissolved ammonium and sulfate gradients in surficial sediment pore water as a measure of organic carbon burial rate. Chapter 6. Canadian technical report of fisheries and aquatic sciences/Rapport technique canadien des sciences halieutiques et aquatiques[CAN TECH REP FISH AQUAT SCI] 1994

Cromey C, Black K, Edwards A, Jack I (1998) Modelling the deposition and biological effects of organic carbon from marine sewage discharges. Estuar Coast Shelf Sci 47:295–308

Cromey CJ, Nickell TD, Black KD (2002) DEPOMOD—modelling the deposition and biological effects of waste solids from marine cage farms. Aquaculture 214:211–239

Cromey C, Nickell T, Black K, Provost P, Griffiths C (2002) Validation of a fish farm waste resuspension model by use of a particulate tracer discharged from a point source in a coastal environment. Estuaries 25:916–929

Cummings ME, Zimmerman RC (2003) Light harvesting and the package effect in the seagrasses Thalassia testudinum Banks ex König and Zostera marina L.: optical constraints on photoacclimation. Aquatic botany 75:261–274

Deutsch B, Forster S, Wilhelm M, Dippner J, Voss M (2010) Denitrification in sediments as a major nitrogen sink in the Baltic Sea: an extrapolation using sediment characteristics. Biogeosciences 7:3259–3271

DFO. (2009) Does eelgrass (Zostera marina) meet the criteria as an ecologically significant species? DFO Can. Sci. Advis. Sec. Sci. Advis. Rep. 2009/018.

Dias E, Morais P, Cotter AM, Antunes C, Hoffman JC (2016) Estuarine consumers utilize marine, estuarine and terrestrial organic matter and provide connectivity among these food webs. Marine Ecology Progress Series 554:21–34

Diaz RJ, Rosenberg R (2008) Spreading dead zones and consequences for marine ecosystems. Science (80-) 321:926–929

Duarte CM (2002) The future of seagrass meadows. Environmental conservation 29:192–206

Ducklow H, Kirchman D, Quinby H, Carlson C, Dam H (1993) Stocks and dynamics of bacterioplankton carbon during the spring bloom in the eastern North Atlantic Ocean. Deep Sea Research Part II: Topical Studies in Oceanography 40:245–263

Eldridge PM, Morse JW (2000) A diagenetic model for sediment-seagrass interactions. Marine Chemistry 70:89–103

Environment Canada (2009) Organic Waste and Feed Deposits on Bottom Sediments from Aquaculture Operations: Scientific Assessment and Guidance. Ecosystem Health: Science-based Solutions Report No. 1-14. National Guidelines and Standards Office, Environment Canada. pp. 68.

Environment Canada (2011) Water quality status and trends of nutrients in major drainage areas of Canada: Technical Summary.

Eppley RW (1972) Temperature and phytoplankton growth in the sea. Fishery Bulletin 70:1063–1085

EU (2009) Protocol on integrated coastal zone management in the Mediterranean. Official Journal of the European Union OJ L 34, 4.2.2009, p. 19–28

Eyre BD, Ferguson AJ (2009) Denitrification efficiency for defining critical loads of carbon in shallow coastal ecosystems. Hydrobiologia 629:137–146

Eyre BD, Ferguson AJ, Webb A, Maher D, Oakes JM (2011) Metabolism of different benthic habitats and their contribution to the carbon budget of a shallow oligotrophic sub-tropical coastal system (southern Moreton Bay, Australia). Biogeochemistry 102:87–110

Eyre BD, Maher D (2011) Mapping ecosystem processes and function across shallow seascapes. Cont Shelf Res 31:S162–S172

Eyre BD, Rysgaard S, Dalsgaard T, Christensen PB (2002) Comparison of isotope pairing and N_2: Ar methods for measuring sediment denitrification—Assumption, modifications, and implications. Estuaries 25:1077–1087

Eyre BD, Santos IR, Maher DT (2013) Seasonal, daily and diel N2 effluxes in permeable carbonate sediments. Biogeosciences 10:2601–2615

Faber P, Kessler A, Bull J, McKelvie I, Meysman F, Cook P (2012) The role of alkalinity generation in controlling the fluxes of CO_2 during exposure and inundation on tidal flats. Biogeosciences 9:4087–4097

FAO (2010) Aquaculture Development: Ecosystem approach to aquaculture. Technical Guidelines for Responsible Fisheries. No. 5, Suppl. 4. Rome, FAO. 53p.

Fennel K, Brady D, Toro D Di, Fulweiler RW, Gardner WS, Giblin A, McCarthy MJ, Rao A, Seitzinger S, Thouvenot-Korppoo M, others (2009) Modeling denitrification in aquatic sediments. Biogeochemistry 93:159–178

Ferguson AJ, Eyre BD (2007) Seasonal discrepancies in denitrification measured by isotope pairing and N_2:Ar techniques. MARINE ECOLOGY-PROGRESS SERIES-350:19

Filgueira R, Grant J, Strand O (2014) Implementation of marine spatial planning in shellfish aquaculture management: modeling studies in a Norwegian fjord. Ecological Applications 24:832–843

Findlay RH, Watling L (1997) Prediction of benthic impact for salmon net-pens based on the balance of benthic oxygen supply and demand. Marine Ecology Progress Series 155:147

Fisheries and Oceans Canada (2004) A scientific review of the potential environmental effects of aquaculture in aquatic ecosystems. Volume III. Near-field organic enrichment from marine finfish aquaculture (D.J. Wildish, M. Dowd, T.F. Sutherland and C.D. Levings); Environmental fate and effect of chemicals associated with Canadian freshwater aquaculture (R.J. Scott). Can. Tech. Rep. Fish. Aquat. Sci. 2450: ix + 117 p.

Fisheries NS, Aquaculture (2011) Environmental monitoring program framework for marine aquaculture in Nova Scotia. :19 p.

Fisheries, Canada O (2015) Aquaculture Monitoring Standard.

Folk RL (1957) Petrology of sedimentary rocks. Hemphill Publishing Company

Forja JM, Ortega T, DelValls TA, Gómez-Parra A (2004) Benthic fluxes of inorganic carbon in shallow coastal ecosystems of the Iberian Peninsula. Marine Chemistry 85:141–156

Forster S, Huettel M, Ziebis W (1996) Impact of boundary layer flow velocity on oxygen utilisation in coastal sediments. Marine Ecology Progress Series 143:173–185

Fossing H, Berg P, Thamdrup B, Rysgaard S, Sørensen HM, Nielsen K (2004) A model set-up for an oxygen and nutrient flux model for Aarhus Bay (Denmark). National Environmental Research Institute, Denmark. 65 pp. – NERI Technical Report No. 483

Fulweiler R, Nixon S, Buckley B, Granger S (2007) Reversal of the net dinitrogen gas flux in coastal marine sediments. Nature 448:180–182

Fulweiler RW, Nixon SW, Buckley BA, Granger SL (2008) Net sediment N_2 fluxes in a coastal marine system—experimental manipulations and a conceptual model. Ecosystems 11:1168–1180

Gaetano P De, Doglioli AM, Magaldi MG, Vassallo P, Fabiano M (2008) FOAM, a new simple benthic degradative module for the LAMP3D model: an application to a

Mediterranean fish farm. Aquaculture Research 39:1229–1242

Galloway JN, Dentener FJ, Capone DG, Boyer EW, Howarth RW, Seitzinger SP, Asner GP, Cleveland C, Green P, Holland E, others (2004) Nitrogen cycles: past, present, and future. Biogeochemistry 70:153–226

Galparsoro I, Borja A, Uyarra MC (2014) Mapping ecosystem services provided by benthic habitats in the European North Atlantic Ocean. Frontiers in Marine Science 1:1–14

Gao Y, Kennish MJ, Flynn AM (2007) Atmospheric nitrogen deposition to the New Jersey coastal waters and its implications. Ecological Applications 17:S31–S41

Garcia HE, Gordon LI (1992) Oxygen solubility in seawater: Better fitting equations. Limnology and oceanography 37:1307–1312

Garwood JC, Hill PS, Law BA (2013) Biofilms and size sorting of fine sediment during erosion in intertidal sands. Estuaries and coasts 36:1024–1036

GESAMP (2001) A sea of troubles. Rep. Stud. GESAMP No. 70, 35 pp.

Gillibrand P, Gubbins M, Greathead C, Davies I (2002) Scottish executive locational guidelines for fish farming: predicted levels of nutrient enhancement and benthic impact. Scottish Fisheries Research Report 63:2002

Glud RN (2008) Oxygen dynamics of marine sediments. Marine Biology Research 4:243–289

Grant J, Filgueira R (2011) The application of dynamic modeling to prediction of production carrying capacity in shellfish farming. In: Shellfish aquaculture and the environment. Wiley Online Library, p 135–154

Grant J, Mills EL, Hopper CM (1986) A chlorophyll budget of the sediment-water interface and the effect of stabilizing biofilms on particle fluxes. Ophelia 26:207–219

Gregory D, Petrie B, Jordan F, Langille P (1993) Oceanographic, geographic and hydrological parameters of Scotia-Fundy and southern Gulf of St. Lawrence inlets. Can. Tech. Rep. Hydrogr. Ocean Sci. No. 143: viii + 248 pp.

Groffman PM, Butterbach-Bahl K, Fulweiler RW, Gold AJ, Morse JL, Stander EK, Tague C, Tonitto C, Vidon P (2009) Challenges to incorporating spatially and temporally explicit phenomena (hotspots and hot moments) in denitrification models. Biogeochemistry 93:49–77

Groot RS de, Wilson MA, Boumans RMJ (2002) A typology for the classification, description and valuation of ecosystem functions, goods and services. Ecological

Economics 41:393–408

Gudasz C, Sobek S, Bastviken D, Koehler B, Tranvik LJ (2015) Temperature sensitivity of organic carbon mineralization in contrasting lake sediments. Journal of Geophysical Research: Biogeosciences 120:1215–1225

Gunderson LH (2000) Ecological resilience—in theory and application. Annual review of ecology and systematics 31:425–439

Hamme RC, Emerson SR (2004) The solubility of neon, nitrogen and argon in distilled water and seawater. Deep Sea Research Part I: Oceanographic Research Papers 51:1517–1528

Hammond DE, Fuller C (1979) The use of radon-222 to estimate benthic exchange and atmospheric exchange rates in San Francisco Bay. In: T.J. Conomos (ed.), San Francisco Bay: The Urbanized Estuary. Pacific Div. Am. Ass. Adv. Sci., San Francisco: 213-230 (ed)

Harborne AR, Mumby PJ, Micheli F, Perry CT, Dahlgren CP, Holmes KE, Brumbaugh DR (2006) The functional value of Caribbean coral reef, seagrass and mangrove habitats to ecosystem processes. Advances in Marine Biology 50:57–189

Hardison AK, Algar CK, Giblin AE, Rich JJ (2015) Influence of organic carbon and nitrate loading on partitioning between dissimilatory nitrate reduction to ammonium (DNRA) and N_2 production. Geochim Cosmochim Acta 164:146–160

Hargrave B (1978) Seasonal changes in oxygen uptake by settled particulate matter and sediments in a marine bay. Journal of the Fisheries Board of Canada 35:1621–1628

Hargrave B (1980) Factors affecting the flux of organic matter to sediments in a marine bay. Marine benthic dynamics 11:243–263

Hargrave B (1994) Modeling benthic impacts of organic enrichment from marine aquaculture. Can Tech Rep Fish Aquat Sci 1949:1–125

Hargrave B (1995) Past and future studies with sediment traps in Canadian east coast waters. In: S. Floderus, A.-S. Heiskanen, M. Olesen and P. Wassmann (ed) Sediment Trap Studies in the Nordic Countries, Nurmi Print Oy, Helsinki.p 10–27

Hargrave B (2001) Benthic metabolism and carbon storage in coastal sediments. In: Kepkay P. (ed) Proceedings of the Workshop on “Carbon storage in the coastal zone.” Can. Sci. Adv. Sec. Pro. Ser. 2001/027

Hargrave B (2010) Empirical relationships describing benthic impacts of salmon aquaculture. Aquaculture Environment Interactions 1:33–46

Hargrave B, Holmer M, Newcombe C (2008) Towards a classification of organic enrichment in marine sediments based on biogeochemical indicators. Marine Pollution Bulletin 56:810–824

Hargrave BT, Phillips G, Doucette L, White M, Milligan T, Wildish D, Cranston R (1995) Biogeochemical observations to assess benthic impacts of organic enrichment from marine aquaculture in the Western Isles region of the Bay of Fundy, 1994. Canadian technical report of fisheries and aquatic sciences/Rapport technique canadien des sciences halieutiques et aquatiques 1995

Hargrave B, Phillips G, Doucette L, White M, Milligan T, Wildish D, Cranston R (1997) Assessing benthic impacts of organic enrichment from marine aquaculture. Water Air and Soil Pollution:641–650

Hargrave B, Phillips GA, Taguchi S (1976) Sedimentation measurements in Bedford Basin, 1973-1974. Fish. Mar. Servo Res. Dev. Tech. Rep. 608, 147 p.

Hargrave B, Taguchi S (1978) Origin of deposited material sedimented in a marine bay. Journal of the Fisheries Board of Canada 35:1604–1613

Hatcher A, Grant J, Schofield B (1994) Effects of suspended mussel culture (Mytilus spp.) on sedimentation, benthic respiration and sediment nutrient dynamics in a coastal bay. Marine Ecology Progress Series 115:219–219

Heiri O, Lotter AF, Lemcke G (2001) Loss on ignition as a method for estimating organic and carbonate content in sediments: reproducibility and comparability of results. Journal of paleolimnology 25:101–110

Hensen C, Zabel M, Schulz HN (2006) Benthic cycling of oxygen, nitrogen and phosphorus. In: Marine Geochemistry. Springer, p 207–240

Hewitt J, Thrush S, Legendre P, Funnell G, Ellis J, Morrison M (2004) Mapping of marine soft-sediment communities: integrated sampling for ecological interpretation. Ecological Applications 14:1203–1216

Hoch MP, Kirchman DL (1993) Seasonal and inter-annual variability in bacterial production and biomass in a temperate estuary. Marine ecology progress series 98:283–295

Hochard S, Pinazo C, Grenz C, Evans JLB, Pringault O (2010) Impact of microphytobenthos on the sediment biogeochemical cycles: A modeling approach. Ecol Modell 221:1687–1701

Hochard S, Pinazo C, Rochelle-Newall E, Pringault O (2012) Benthic pelagic coupling in a shallow oligotrophic ecosystem: Importance of microphytobenthos and physical forcing. Ecol Modell 247:307–318

Holling CS (1973) Resilience and stability of ecological systems. Annual review of ecology and systematics 4:1–23

Holm-Hansen O, Lorenzen CJ, Holmes RW, Strickland JD (1965) Fluorometric determination of chlorophyll. Journal du Conseil 30:3–15

Holmer M, Wildish D, Hargrave B (2005) Organic enrichment from marine finfish aquaculture and effects on sediment biogeochemical processes. In: Environmental effects of marine finfish aquaculture. Springer, p 181–206

Hooper DU, Chapin F, Ewel J, Hector A, Inchausti P, Lavorel S, Lawton J, Lodge D, Loreau M, Naeem S, others (2005) Effects of biodiversity on ecosystem functioning: a consensus of current knowledge. Ecological monographs 75:3–35

Hopkinson CS, Giblin AE, Tucker J, Garritt RH (1999) Benthic metabolism and nutrient cycling along an estuarine salinity gradient. Estuaries 22:863–881

Hou L, Liu M, Jiang H, Xu S, Ou D, Liu Q, Zhang B (2003) Ammonium adsorption by tidal flat surface sediments from the Yangtze Estuary. Environmental Geology 45:72–78

Howarth RW (2007) Atmospheric deposition and nitrogen pollution in coastal marine ecosystems. In: Acid in the Environment. Springer, p 97–116

Huber C, Shafei B, Parmigiani A (2014) A new pore-scale model for linear and non-linear heterogeneous dissolution and precipitation. Geochim Cosmochim Acta 124:109–130

Huettel M, Berg P, Kostka JE (2014) Benthic exchange and biogeochemical cycling in permeable sediments. Ann Rev Mar Sci 6:23–51

Huettel M, Røy H, Precht E, Ehrenhauss S (2003) Hydrodynamical impact on biogeochemical processes in aquatic sediments. In: The interactions between sediments and water. Springer, p 231–236

Huettel M, Ziebis W, Forster S, Luther G (1998) Advective transport affecting metal and nutrient distributions and interfacial fluxes in permeable sediments. Geochim Cosmochim Acta 62:613–631

Hyder K, Rossberg AG, Allen JI, Austen MC, Barciela RM, Bannister HJ, Blackwell PG, Blanchard JL, Burrows MT, Defriez E, others (2015) Making modelling count-increasing the contribution of shelf-seas community and ecosystem models to policy development and management. Marine Policy 61:291–302

Jager HI, King AW (2004) Spatial uncertainty and ecological models. Ecosystems 7:841–847

Jahnke RA (1996) The global ocean flux of particulate organic carbon: Areal distribution and magnitude. Global Biogeochem Cycles 10:71–88

Jahnke RA (2005) Transport processes and organic matter cycling in coastal sediments. In: The global coastal ocean-Multi-scale interdisciplinary processes, edited by: Robinson, AR and Brink, KH.p 163–191

Jickells TD, Rae JE (2005) Biogeochemistry of intertidal sediments (Jickells, Tim D and Rae, Joy E, Ed.). Cambridge University Press

Johnson K, Wills K, Butler D, Johnson W, Wong C (1993) Coulometric total carbon dioxide analysis for marine studies: maximizing the performance of an automated gas extraction system and coulometric detector. Marine Chemistry 44:167–187

Johnston K, Hoef JM Ver, Krivoruchko K, Lucas N (2001) Using ArcGIS geostatistical analyst. Esri Redlands

Jones CG, Lawton JH, Shachak M (1994) Organisms as ecosystem engineers. Oikos:373–386

Jørgensen BB (1977) The sulfur cycle of a coastal marine sediment (Limfjorden, Denmark). Limnology and Oceanography 22:814–832

Jørgensen SE, Bendoricchio G (2001) Fundamentals of ecological modelling. Elsevier

Jørgensen BB, Sørensen J (1985) Seasonal cycles of O_2, and reduction in estuarine sediments: the significance of an reduction maximum in spring. Marine Ecology Progress Series:65–74

Joseph V, Schmidt A, Gregory R (2013) Use of eelgrass habitats by fish in eastern Canada. DFO, Ottawa, ON

Joye SB, Anderson IC (2008) Nitrogen cycling in coastal sediments. In: Nitrogen in the marine environment, 2nd edn. Academic Press, Amsterdam.p 868–915

Kana TM, Darkangelo C, Hunt MD, Oldham JB, Bennett GE, Cornwell JC (1994) Membrane inlet mass spectrometer for rapid high-precision determination of N2, O2, and Ar in environmental water samples. Analytical Chemistry 66:4166–4170

Kana TM, Sullivan MB, Cornwell JC, Groxzkowski KM (1998) Denitrification in estuarine sediments determined by membrane inlet mass spectrometry. Limnology and Oceanography 43:334–339

Karle I-M, Hall PO, Dahllof I (2007) Biogeochemical response of an intact coastal sediment to organic matter input: a multivariate approach. Marine Ecology Progress Series 342:15–25

Katsev S, Rancourt D, L'Heureux I (2004) dSED: A database tool for modeling sediment early diagenesis. Computers & geosciences 30:959–967

Kaushik S (2013) Feed management and on-farm feeding practices of temperate fish with special reference to salmonids. In: M.R. Hasan and M.B. New. (ed) On-farm feeding and feed management in aquaculture. FAO Fisheries and Aquaculture. Technical Paper No. 583. Rome, FAO, p 519–551

Kostylev VE, Todd BJ, Fader GB, Courtney R, Cameron GD, Pickrill RA (2001) Benthic habitat mapping on the Scotian Shelf based on multibeam bathymetry, surficial geology and sea floor photographs. Marine Ecology Progress Series 219:121–137

Kostylev V, Todd B, Shaw J (2008) Benthic habitat mapping in Canada—a perspective. J Ocean Technol 2:7–12

Kristensen E (2005) Interactions between macro-and microorganisms in marine sediments. American Geophysical Union

Krumins V, Gehlen M, Arndt S, Cappellen P Van, Regnier P (2013) Dissolved inorganic carbon and alkalinity fluxes from coastal marine sediments: model estimates for different shelf environments and sensitivity to global change. Biogeosciences 10:371–398

LaMontagne MG, Astorga V, Giblin AE, Valiela I (2002) Denitrification and the stoichiometry of nutrient regeneration in Waquoit Bay, Massachusetts. Estuaries 25:272–281

Lecours V, Devillers R, Schneider DC, Lucieer VL, Brown CJ, Edinger EN (2015) Spatial scale and geographic context in benthic habitat mapping: review and future directions. Marine Ecology Progress Series 535:259

Liu J, Zhang P, Guo D, Niu S, Zhang X (2011) Annual change in photosynthetic pigment contents of Zostera marina L. in Swan Lake. African Journal of Biotechnology 10:18194–18199

Luff R, Moll A (2004) Seasonal dynamics of the North Sea sediments using a three-dimensional coupled sediment-water model system. Cont Shelf Res 24:1099–1127

Luther GW, Sundby B, Lewis BL, Brendel PJ, Silverberg N (1997) Interactions of manganese with the nitrogen cycle: alternative pathways to dinitrogen. Geochim Cosmochim Acta 61:4043–4052

MacIntyre HL, Geider RJ, Miller DC (1996) Microphytobenthos: the ecological role of the "secret garden" of unvegetated, shallow-water marine habitats. I. Distribution, abundance and primary production. Estuaries 19:186–201

Mackin JE, Aller RC (1984) Ammonium adsorption in marine sediments. Limnology and Oceanography 29:250–257

Martin W, Sayles F (2004) Organic matter cycling in sediments of the continental margin in the northwest Atlantic Ocean. Deep Sea Research Part I: Oceanographic Research Papers 51:457–489

Mazzola A, Mirto S, Rosa Ti La, Fabiano M, Danovaro R (2000) Fish-farming effects on benthic community structure in coastal sediments: analysis of meiofaunal recovery. ICES Journal of Marine Science 57:1454–1461

McGhie TK, Crawford CM, Mitchell IM, O'Brien D (2000) The degradation of fish-cage waste in sediments during fallowing. Aquaculture 187:351–366

McKindsey CW, Thetmeyer H, Landry T, Silvert W (2006) Review of recent carrying capacity models for bivalve culture and recommendations for research and management. Aquaculture 261:451–462

MEA MEA (2005) Ecosystems and human well-being: synthesis. Island, Washington, DC

Meyer-Reil L-A, Köster M (2000) Eutrophication of marine waters: effects on benthic microbial communities. Marine Pollution Bulletin 41:255–263

Meyercordt J, Meyer-Reil L-A (1999) Primary production of benthic microalgae in two shallow coastal lagoons of different trophic status in the southern Baltic Sea. Marine Ecology Progress Series 178:179–191

Middelburg JJ, Duarte CM, Gattuso J-P (2005) Respiration in coastal benthic communities. Respiration in aquatic ecosystems Oxford, New York

Middelburg JJ, Klaver G, Nieuwenhuize J, Wielemaker A, Hass W de, Vlug T, Nat JF van der (1996) Organic matter mineralization in intertidal sediments along an estuarine gradient. Marine Ecology Progress Series:157–168

Middelburg J, Levin L (2009) Coastal hypoxia and sediment biogeochemistry. Biogeosciences 6:1273–1293

Middelburg JJ, Soetaert K, Herman PM (1997) Empirical relationships for use in global diagenetic models. Deep Sea Research Part I: Oceanographic Research Papers 44:327–344

Middelburg JJ, Soetaert K, Herman PM, Heip CH (1996) Denitrification in marine sediments: A model study. Global Biogeochem Cycles 10:661–673

Mitchell MR, Harrison G, Pauley K, Gagné A, Maillet G, Strain P (2002) Atlantic zonal monitoring program sampling protocol. Can. Tech. Rep. Hydrogr. Ocean Sci. 223: iv +

23 pp.

Miyajima T, Suzumura M, Umezawa Y, Koike I (2001) Microbiological nitrogen transformation in carbonate sediments of a coral-reef lagoon and associated seagrass beds. Marine Ecology Progress Series 217:273–286

Morse JW, DiMarco SF, Hebert AB, Sell KS (2003) A scaling approach to spatial variability in early diagenetic processes. Hydrobiologia 494:25–29

Muller-Karger FE, Varela R, Thunell R, Luerssen R, Hu C, Walsh JJ (2005) The importance of continental margins in the global carbon cycle. Geophysical Research Letters 32

Mulsow S, Krieger Y, Kennedy R (2006) Sediment profile imaging (SPI) and micro-electrode technologies in impact assessment studies: example from two fjords in Southern Chile used for fish farming. Journal of Marine Systems 62:152–163

NBDENV (2012) Environmental management program for the marine finfish cage aquaculture Industry in New Brunswick V 3.0.

New Brunswick Department of Agriculture A, DAAF) F (NB (2012) Standard Operating Practices for the Environmental Monitoring of the Marine Finfish Cage Aquaculture Industry in New Brunswick.

Newell RI, Koch EW (2004) Modeling seagrass density and distribution in response to changes in turbidity stemming from bivalve filtration and seagrass sediment stabilization. Estuaries 27:793–806

Nilsson H, Rosenberg R (1997) Benthic habitat quality assessment of an oxygen stressed fjord by surface and sediment profile images. Journal of Marine Systems 11:249–264

Nilsson HC, Rosenberg R (2000) Succession in marine benthic habitats and fauna in response to oxygen deficiency: analysed by sediment profile-imaging and by grab samples. Marine Ecology Progress Series 197:139–149

Nixon SW (1995) Coastal marine eutrophication: a definition, social causes, and future concerns. Ophelia 41:199–219

Noss RF (1990) Indicators for Monitoring Biodiversity: A Hierarchical Approach. Conservation Biology 4:355–364

Nova Scotia Department of Natural Resources 1:10,000 Nova Scotia Watersheds. Available at: https://data.novascotia.ca/Environment-and-Energy/1-10-000-Nova-Scotia-Watersheds/569x-2wnq.

Nowicki BL, Kelly JR, Requintina E, Keuren D van (1997) Nitrogen losses through sediment denitrification in Boston Harbor and Massachusetts Bay. Estuaries 20:626–

639

NSDFA (2014) Standard Operating Procedures for the Environmental Monitoring of Marine Aquaculture in Nova Scotia. Nova Scotia Fisheries & Aquaculture (NSDFA)

Omori K, Hirano T, Takeoka H (1994) The limitations to organic loading on a bottom of a coastal ecosystem. Marine Pollution Bulletin 28:73–80

Ontario Clean Water Agency (2016) Annual report for the Shelburne waste water treatment facility.

Orth RJ, Carruthers TJ, Dennison WC, Duarte CM, Fourqurean JW, Heck KL, Hughes AR, Kendrick GA, Kenworthy WJ, Olyarnik S, others (2006) A global crisis for seagrass ecosystems. Bioscience 56:987–996

Page F, Losier R, McCurdy P, Greenberg D, Chaffey J, Chang B (2005) Dissolved oxygen and salmon cage culture in the southwestern New Brunswick portion of the Bay of Fundy. Handbook of Environmental Chemistry 5:1–28

Paraska DW, Hipsey MR, Salmon SU (2014) Sediment diagenesis models: Review of approaches, challenges and opportunities. Environmental Modelling \& Software 61:297–325

Pastor L, Cathalot C, Deflandre B, Viollier E, Soetaert K, Meysman F, Ulses C, Metzger E, Rabouille C (2011) Modeling biogeochemical processes in sediments from the Rhône River prodelta area (NW Mediterranean Sea). Biogeosciences 8:1351–1366

Pätsch J, Kühn W (2008) Nitrogen and carbon cycling in the North Sea and exchange with the North Atlantic—a model study. Part I. Nitrogen budget and fluxes. Cont Shelf Res 28:767–787

Pearson T, Rosenberg R (1978) Macrobenthic succession in relation to organic enrichment and pollution of the marine environment. Oceanography and Marine Biology - An Annual Review 16:229–311

Petersen S, Sutherland T, Higgs D (2005) Physical and chemical characterization of salmonid feed pellets. Can. Data. Rep. Fish. Aquat. Sci. 1159

Petrie B, Strain P, Yeats P (1999) Nitrate, silicate and phosphate atlas for the Scotian Shelf and the Gulf of Maine. Fisheries \& Oceans Canada, Maritimes Region, Ocean Sciences Division, Bedford Institute of Oceanography

Pickrill R, Kostylev V (2007) Habitat mapping and national seafloor mapping strategies in Canada. Mapping the seafloor for habitat characterization Geological Association of Canada, Special Paper 47:483–495

Piehler M, Smyth A (2011) Habitat-specific distinctions in estuarine denitrification affect both ecosystem function and services. Ecosphere 2:art12

Platt T, Prakash A, Irwin B (1972) Phytoplankton nutrients and flushing of inlets on the coast of Nova Scotia. Le Naturaliste Canadien 99:253–261

Pomeroy R, Bravo-Ureta BE, Solis D, Johnston RJ (2008) Bioeconomic modelling and salmon aquaculture: an overview of the literature. International Journal of Environment and Pollution 33:485–500

Precht E, Huettel M (2004) Rapid wave-driven advective pore water exchange in a permeable coastal sediment. Journal of Sea Research 51:93–107

Reid M, Tripathee R, Schäfer K, Jaffé P (2013) Tidal marsh methane dynamics: Difference in seasonal lags in emissions driven by storage in vegetated versus unvegetated sediments. Journal of Geophysical Research: Biogeosciences 118:1802–1813

Remen M, Solstorm F, Bui S, Klebert P, Vågseth T, Solstorm D, Hvas M, Oppedal F (2016) Critical swimming speed in groups of Atlantic salmon Salmo salar. Aquaculture Environment Interactions 8:659–664

Revsbech NP, Nielsen J, Hansen PK (1988) Benthic primary production and oxygen profiles. In: T. H. Blackburn and J. Sørensen (ed) Nitrogen cycling in coastal marine Environments. John Wiley Chichester, UK, p 69–114

Rhoads DC, Germano JD (1982) Characterization of organism-sediment relations using sediment profile imaging: an efficient method to remote ecological monitoring on the seafloor (REMOTS'system). Marine Ecology Progress Series 8:115–128

Riley GA, Bumpus DF (1946) Phytoplankton-zooplankton relationships on Georges Bank. Journal of Marine Research 6:33–47

Rosa T La, Mirto S, Mazzola A, Danovaro R (2001) Differential responses of benthic microbes and meiofauna to fish-farm disturbance in coastal sediments. Environmental Pollution 112:427–434

Rudnick DT (1989) Time lags between the deposition and meiobenthic assimilation of phytodetritus. Marine ecology progress series Oldendorf 50:231–240

Rudnick DT, Oviatt CA (1986) Seasonal lags between organic carbon deposition and mineralization in marine sediments. Journal of Marine Research 44:815–837

Santos IR, Eyre BD, Glud RN (2012) Influence of porewater advection on denitrification in carbonate sands: Evidence from repacked sediment column experiments. Geochim Cosmochim Acta 96:247–258

Santos IR, Eyre BD, Huettel M (2012) The driving forces of porewater and groundwater flow in permeable coastal sediments: A review. Estuar Coast Shelf Sci 98:1–15

Schrum HN, Spivack AJ, Kastner M, D'Hondt S (2009) Sulfate-reducing ammonium oxidation: a thermodynamically feasible metabolic pathway in subseafloor sediment. Geology 37:939–942

Seiter K, Hensen C, Zabel M (2005) Benthic carbon mineralization on a global scale. Global Biogeochem Cycles 19

Seitzinger SP (1988) Denitrification in freshwater and coastal marine ecosystems: ecological and geochemical significance. Limnology and Oceanography 33:702–724

Seitzinger S, Harrison JA, Böhlke J, Bouwman A, Lowrance R, Peterson B, Tobias C, Drecht GV (2006) Denitrification across landscapes and waterscapes: a synthesis. Ecological Applications 16:2064–2090

Shafei B (2012) Reactive transport in natural porous media: Contaminant sorption and pore-scale heterogeneity. Georgia Institute of Technology

Silverberg N, Sundby B, Mucci A, Zhong S, Arakaki T, Hall P, Landén A, Tengberg A (2000) Remineralization of organic carbon in eastern Canadian continental margin sediments. Deep Sea Research Part II: Topical Studies in Oceanography 47:699–731

Silvert W, Sowles J (1996) Modelling environmental impacts of marine finfish aquaculture. Journal of Applied Ichthyology 12:75–81

Simone M, Grant J (2017) Visual assessment of redoxcline compared to electron potential in coastal marine sediments. Estuar Coast Shelf Sci 188:156–162

Smith VH (2003) Eutrophication of freshwater and coastal marine ecosystems a global problem. Environmental Science and Pollution Research 10:126–139

Soetaert K, Herman PM, Middelburg JJ (1996) A model of early diagenetic processes from the shelf to abyssal depths. Geochim Cosmochim Acta 60:1019–1040

Solstorm F, Solstorm D, Oppedal F, Fernö A, Fraser T, Olsen RE (2015) Fast currents reduce production performance of post-smolt Atlantic salmon. Aquaculture Environment Interactions 7:125–134

Soulsby R (1997) Dynamics of marine sands: a manual for practical applications. Thomas Telford

Spilmont N, Migné A, Seuront L, Davoult D (2007) Short-term variability of intertidal benthic community production during emersion and the implication in annual budget calculation. Marine Ecology Progress Series 333:95–101

Spinelli GA, Giambalvo ER, Fisher AT (2004) Sediment permeability, distribution, and influence on fluxes in oceanic basement. In: Davis E and Elderfield H (ed) Hydrogeology of the oceanic lithosphere. Cambridge University Press, New York, p 151–188

Ståhl H, Tengberg A, Brunnegård J, Bjørnbom E, Forbes T, Josefson A, Kaberi H, Hassellöv I, Olsgard F, Roos P, others (2004) Factors influencing organic carbon recycling and burial in Skagerrak sediments. Journal of Marine Research 62:867–907

Stead SM, Laird L (2002) The handbook of salmon farming. Springer Science & Business Media

Stewart PL, White L (2001) A review of contaminants on the Scotian Shelf and in adjacent coastal waters: 1970 to 1995. Can Tech Rep Fish Aquat Sci/Rapp Tech Can Sci Halieut Aquat:176

Stigebrandt A (2011) Carrying capacity: general principles of model construction. Aquaculture Research 42:41–50

Stigebrandt A, Aure J, Ervik A, Hansen PK (2004) Regulating the local environmental impact of intensive marine fish farming: III. A model for estimation of the holding capacity in the Modelling-Ongrowing fish farm-Monitoring system. Aquaculture 234:239–261

Stucchi D, Sutherland T-A, Levings C, Higgs D (2005) Near-field depositional model for salmon aquaculture waste. In: Environmental effects of marine finfish aquaculture. Springer, p 157–179

Sturtevant C, Ruddell BL, Knox SH, Verfaillie J, Matthes JH, Oikawa PY, Baldocchi D (2016) Identifying scale-emergent, nonlinear, asynchronous processes of wetland methane exchange. Journal of Geophysical Research: Biogeosciences 121:188–204

Su J, Tian T, Krasemann H, Schartau M, Wirtz K (2015) Response patterns of phytoplankton growth to variations in resuspension in the German Bight revealed by daily MERIS data in 2003 and 2004. Oceanologia 57:328–341

Sundbäck K, Miles A, Göransson E (2000) Nitrogen fluxes, denitrification and the role of microphytobenthos in microtidal shallow-water sediments: an annual study. Marine Ecology Progress Series 200:59–76

Taguchi S, Hargrave B (1978) Loss rates of suspended material sedimented in a marine bay. Journal of the Fisheries Board of Canada 35:1614–1620

Talin F, Tolla C, Rabouille C, Poggiale J (2003) Relations between bacterial biomass and carbon cycle in marine sediments: An early diagenetic model. Acta biotheoretica 51:295–315

Tapia F, Giglio S (2010) Fjord carrying capacity assessment models applicable to ecosystems in Southern Chile. Valdivia, Chile:1–22

Tromp T, Cappellen P Van, Key R (1995) A global model for the early diagenesis of organic carbon and organic phosphorus in marine sediments. Geochim Cosmochim Acta 59:1259–1284

Tuominen L, Heinänen A, Kuparinen J, Nielsen LP (1998) Spatial and temporal variability of denitrification in the sediments of the northern Baltic Proper. Marine Ecology Progress Series 172:13–24

Ullman WJ, Aller RC (1982) Diffusion coefficients in nearshore marine sediments. Limnology and Oceanography 27:552–556

Vance-Harris C, Ingall E (1999) Denitrification pathways and rates in the sandy sediments of the Georgia continental shelf, USA. Geochem Trans 6:12

Vezzulli L, Chelossi E, Riccardi G, Fabiano M (2002) Bacterial community structure and activity in fish farm sediments of the Ligurian sea (Western Mediterranean). Aquaculture International 10:123–141

Wal D van der, Wielemaker-van den Dool A, Herman PM (2010) Spatial synchrony in intertidal benthic algal biomass in temperate coastal and estuarine ecosystems. Ecosystems 13:338–351

Walker B, Holling CS, Carpenter S, Kinzig A (2004) Resilience, adaptability and transformability in social-ecological systems. Ecology and society 9

Wang X, Olsen LM, Reitan KI, Olsen Y (2012) Discharge of nutrient wastes from salmon farms: environmental effects, and potential for integrated multi-trophic aquaculture. Aquaculture Environment Interactions 2:267–283

Water Survey of Canada National Hydrometric Real-time website. Real-Time Hydrometric Data Graph for Roseway River at Lower Ohio (01EC001) [NS].

Webster IT, Harris GP (2004) Anthropogenic impacts on the ecosystems of coastal lagoons: modelling fundamental biogeochemical processes and management implications. Marine and Freshwater Research 55:67–78

Webster T, Paranjape MA, Mann K (1975) Sedimentation of organic matter in St. Margaret's Bay, Nova Scotia. Journal of the Fisheries Board of Canada 32:1399–1407

Welschmeyer NA (1994) Fluorometric analysis of chlorophyll a in the presence of chlorophyll b and pheopigments. Limnology and Oceanography 39:1985–1992

Welsh DT (2000) Nitrogen fixation in seagrass meadows: regulation, plant-bacteria interactions and significance to primary productivity. Ecology Letters 3:58–71

Welsh D, Bourgues S, Wit R De, Herbert R (1996) Seasonal variations in nitrogen-fixation (acetylene reduction) and sulphate-reduction rates in the rhizosphere of *Zostera noltii*: nitrogen fixation by sulphate-reducing bacteria. Marine Biology 125:619–628

Westrich JT, Berner RA (1984) The role of sedimentary organic matter in bacterial sulfate reduction: The G model tested. Limnology and oceanography 29:236–249

Whitehead ML (2012) The role of benthic nitrogen fixation as a source of new nitrogen to the New River Estuary, NC

Wilding TA, Cromey CJ, Nickell TD, Hughes DJ (2012) Salmon farm impacts on muddy-sediment megabenthic assemblages on the west coast of Scotland. Aquaculture Environment Interactions 2:145–156

Wildish D, Hargrave B, Pohle G (2001) Cost-effective monitoring of organic enrichment resulting from salmon mariculture. ICES Journal of Marine Science: Journal du Conseil 58:469–476

Wilson RF, Fennel K, Mattern JP (2013) Simulating sediment-water exchange of nutrients and oxygen: A comparative assessment of models against mesocosm observations. Cont Shelf Res 63:69–84

Wilson PS, Vopel K (2012) Estimating the in situ distribution of acid volatile sulfides from sediment profile images. Limnology and Oceanography: Methods 10:1070–1077

Woelfl S, Mages M, Encina F, Bravo F (2006) Trace metals in microcrustaceans and Brazilian waterweed from a contaminated Chilean wetland using total reflection X-ray fluorescence spectrometry. Microchimica Acta 154:261–268

Wolfstein K, Colijn F, Doerffer R (2000) Seasonal dynamics of microphytobenthos biomass and photosynthetic characteristics in the northern German Wadden Sea, obtained by the photosynthetic light dispensation system. Estuar Coast Shelf Sci 51:651–662

Wong MC, Vercaemer B, others (2012) Effects of invasive colonial tunicates and a native sponge on the growth, survival, and light attenuation of eelgrass (Zostera marina). Aquatic Invasions 7:315–326

Zimmerman RC, Reguzzoni JL, Wyllie-Echeverria S, Josselyn M, Alberte RS (1991) Assessment of environmental suitability for growth of Zostera marina L.(eelgrass) in San Francisco Bay. Aquatic Botany 39:353–366

Zirino A, Neira C, Maicu F, Levin LA (2013) Comments on and implications of a steady-state in coastal marine ecosystems. Chemistry and Ecology 29:86–99

Appendix A

Table A13: Mean benthic fluxes for summer (May to September) according to habitat types, and minimum and maximum observed values for the entire study area. Daily averaged fluxes are reported in mmol m^{-2} d^{-1}, while net and gross fluxes are reported in µmol m^{-2} h^{-1}. Nitrogen fluxes are reported as mmol-N (DIN, NH_3, NO_3). Positive values denote efflux from sediments, while negative values denote influx.

		Mean ± STD					Min	Max	Samples	Literature range	Reference
		SH-FF	SH-BP	SH-BA	PJ-BP	PJ-SB					
Daily average flux											
O_2		-14.1 ± 8.2	-28.2 ± 21.7	-12.1 ± 12.9	-44.2 ± 33.3	-16.3 ± 16.0	-115.8	5.9	105	-9.23 ± 0.7	(1)
DIC		13.2 ± 10.1	NA	15.7 ± 10.6	86.5 ± 94.4	93.6 ± 137.0	-4.8	291.9	28	18.8 ± 1.4	(1)
TA		2.9 ± 6.7	NA	9.4 ± 8.8	53.3 ± 73.2	16.0 ± 11.3	-7.1	211.3	28	-8 – 192	(2)
NH_3		0.3 ± 1.3	0.0 ± 0.2	0.9 ± 2.3	1.4 ± 1.4	2.2 ± 2.2	-4.1	5.8	82	0.63 ± 0.08	(1)
NO_3		0.8 ± 1.5	NA	-0.4 ± 3.2	0.3 ± 0.7	1.2 ± 2.7	-6.3	6.0	46	0.16 ± 0.04	(1)
Net exchange rate											
O_2	**dark**	-578.9 ± 334.7	-1547.3 ± 819.8	-503.8 ± 538.0	-1863.0 ± 1217.3	-2100.5 ± 1429.2	-5097.3	51.4	129	0 – -18041	(3)
	light	NA	-868.4 ± 1042.2	NA	-1107.3 ± 1451.1	534.7 ± 1085.2	-5616.7	2544.7	45	0 – 4310	(4)
DIC	**dark**	549.5 ± 420.4	NA	655.7 ± 440.0	2777.1 ± 1764.7	1368.0 ± 1588.3	-614.1	6313.9	35	0 – 30500	(5)
	light	NA	NA	NA	4081.5 ± 7350.3	9056.5 ± 11497.3	-1141.4	21829.1	12		
TA	**dark**	122.4 ± 279.2	NA	391.6 ± 366.5	1752.8 ± 1599.0	236.7 ± 683.5	-707.2	5180.3	35		
	light	NA	NA	NA	2486.5 ± 5655.7	2745.9 ± 3845.5	-862.9	16061.4	12		
NH_3	**dark**	14.0 ± 54.3	-1.9 ± 9.2	38.7 ± 95.8	46.3 ± 52.4	62.1 ± 108.0	-169.7	385.3	93	-83.33 – +2708	(6)
	light	NA	2.1 ± 7.2	NA	47.1 ± 83.9	63.6 ± 119.7	-59.2	343.8	32	-33.3 – +40.9	(6)
NO_3	**dark**	32.6 ± 60.8	NA	-15.7 ± 134.0	20.1 ± 35.0	83.8 ± 206.6	-261.6	584.6	50	-44.3 – -104.2	(7)
	light	NA	NA	NA	20.3 ± 35.9	0.7 ± 29.9	-64.1	90.0	18	-6.4 – -132.0	(7)
N_2	**dark/light (DNF)**	-161.6 ± 483.0	NA	-455.2 ± 1271.9	172.4 ± 436.6	-290.2 ± 501.0	-4872.6	773.3	70	1.93-0.1	(1)
N_2	**fixation**	NA	133.7 ± 41.1	174.3 ± 0	NA	NA	93.7	184.5	7		
Gross benthic O_2 production		NA	678.9 ± 622.1	NA	744.3 ± 1102.2	3811.9 ± 1945.7	-1570.6	6681.1	31	0 - 27000	
Gross benthic CO_2 fixation		NA	NA	NA	2586.2 ± 6850.1	474.6 ± 1702.7	-2302.1	14538.2	7	-9922.3 – -13946.7	(8)

[1] An & Joye (2001)
[2] Eyre et al. 2011, Silverberg et al. 2000.
[3] Glud (2008), Soetaert et al. (1996), LaMontagne et al. (2002), Bartoli et al. (2003), Forja et al. (2004), Hopkinson et al. (1999).
[4] Bartoli et al. (2003)
[5] An & Joye (2001), Eldridge & Morse (2000), Ståhl et al. (2004), Eyre et al. (2011), Silverberg et al. (2000), Karle et al. (2007), Forja et al. (2004).
[6] Bailey (2005), Bartoli et al. (2003)
[7] Bartoli et al. (2003), Revsbech et al. (1988)
[8] Brock et al. (2006)

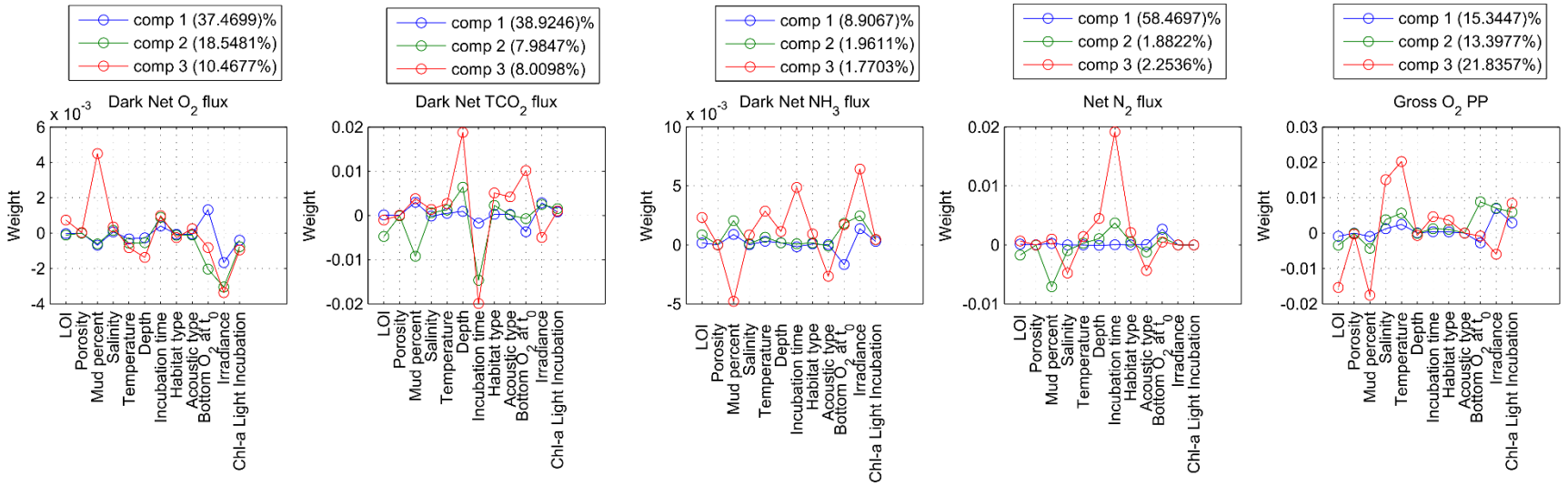

Figure A31: Partial least squares (PLS) regression analysis of benthic fluxes in relation to control variables. The plots show the PLS weights describing how strongly each component in the PLS depends on the original predicting variables, and in what direction. In the upper right corner, the percent of the variance explained by each component is specified.

Appendix B

Table A14: Model equations summary. Production-consumption rates of solid and dissolved compounds in µmol cm^{-3} solid d^{-1} and in µmol cm^{-3} porewater d^{-1}, respectively.

Reaction	Eq.
$\sum \mathrm{R(POC)} = -(\mathrm{R2a} + \mathrm{R3a} + \mathrm{R4a})$	12
$\sum \mathrm{R(Waste)} = -(\mathrm{R2b} + \mathrm{R3b} + \mathrm{R4b})$	13
$\sum \mathrm{R(O_2)} = \frac{\varphi_S}{\varphi} * \mathrm{R2} * \gamma \mathrm{OR}_{\mathrm{O_2}}^{\mathrm{POC}} - \mathrm{R5} * \gamma \mathrm{RO}_{\mathrm{O_2}}^{\mathrm{Total\ S^{2-}}} - \mathrm{R6}$	14
$\sum \mathrm{R(SO_4)} = \mathrm{R5} - \frac{\varphi_S}{\varphi} * \mathrm{R3} * \gamma \mathrm{SR}_{\mathrm{SO_4^{=}}}^{\mathrm{POC}}$	15
$\sum \mathrm{R(Fe(OH)_3)} = \frac{\varphi}{\varphi_S} * \mathrm{R6} * \gamma \mathrm{RO}_{\mathrm{O_2}}^{\mathrm{Fe^{2+}}} - \mathrm{R4} * \gamma \mathrm{IR}_{\mathrm{Fe(OH)_3}}^{\mathrm{POC}} - \mathrm{R7}$	16
$\sum \mathrm{R(Total\ S^{-2})} = \frac{\varphi_S}{\varphi} * \left(\mathrm{R3} * \gamma \mathrm{SR}_{\mathrm{SO_4^{=}}}^{\mathrm{POC}} - \mathrm{R7} * \gamma \mathrm{RO}_{\mathrm{Fe(OH)_3}}^{\mathrm{H_2S}} - \mathrm{R8}\right) - \mathrm{R5}$	17
$\sum \mathrm{R(Fe^{2+})} = \frac{\varphi_S}{\varphi} * (\mathrm{R4a} + \mathrm{R4b}) * \gamma \mathrm{IR}_{\mathrm{Fe(OH)_3}}^{\mathrm{POC}} + \frac{\varphi_S}{\varphi} * (\mathrm{R7} - \mathrm{R8}) - \mathrm{R6} * \gamma \mathrm{RO}_{\mathrm{O_2}}^{\mathrm{Fe^{2+}}}$	18
$\sum \mathrm{R(FeS)} = R8 - \mathrm{R9}$	19
$\sum \mathrm{R(Bact)} = \alpha_{\mathrm{BAC}}(\mathrm{R2} + \mathrm{R3} + \mathrm{R4}) * \mathrm{Bact} * \left(1 - \frac{\mathrm{Bact}}{\lambda_{\mathrm{BAC}} * \left(\left[\mathrm{C_{org}}\right] + [\mathrm{Waste}]\right)}\right)$	20

Table A15: Reactions terms. R1 in µmol $cm^{-2}d^{-1}$ and R2 to R9 in µmol $cm^{-3}d^{-1}$.

Water column – Partially stratified layer (TL)		
(R1)	POC consumption by oxic respiration	$R_{OR,TL} * [POC_{WC}]$
Sediment – Oxic/Anoxic layer (SL)		
(R2a)	POC consumption by oxic respiration	$R_{OR,SL} * [POC_{SL}] * [B_{SL}] * PF_{Bact,OR}$
(R3a)	POC consumption by SO_4^{2-} reduction	$R_{SR,SL} * [POC_{SL}] * [B_{SL}] * PF_{Bact,SR}$
(R4a)	POC consumption by Fe(III) reduction	$R_{IR,SL} * [POC_{SL}] * [B_{SL}] * PF_{Bact,IR}$
(R2b)	Organic waste consumption by oxic respiration	$R_{OR,SL} * [Waste_{SL}] * [B_{SL}] * PF_{Bact,OR}$
(R3b)	Organic waste consumption by SO_4^{2-} reduction	$R_{SR,SL} * [Waste_{SL}] * [B_{SL}] * PF_{Bact,SR}$
(R4b)	Organic waste consumption by Fe(III) reduction	$R_{IR,SL} * [Waste_{SL}] * [B_{SL}] * PF_{Bact,IR}$
(R5)	SO_4^{2-} production by Total S^{2-} reoxidation with O_2	$k_{Total\ S^{-2}_{SL,ox1}} * [Total\ S^{-2}_{SL}] * [O_{2,SL}]$
(R6)	Fe^{2+} reoxidation with O_2	$k_{Fe,ox} * [Fe^{2+}_{SL}] * [O_{2,SL}]$
(R7)	Total S^{2-} reoxidation with iron oxides	$k_{Total\ S^{-2}_{SL,ox2}} * [Total\ S^{-2}_{SL}] * [Fe^{2+}_{SL}]$
(R8)	Total S^{2-} precipitation to FeS	$k_{FeSppt} * ([Fe^{2+}_{SL}] * [Total\ S^{-2}_{SL}] - K_{sp}FeS)$
(R9)	FeS precipitation to FeS_2	$k_{FeS_2} * [FeS_{SL}]$

Table A16: Transport processes in bottom water.

Bottom water (WC)		
(T1)	Bottom water O_2 renewal	$u_{WC} * ([O_{2,WC,BC}] - [O_{2,WC}])$
(T2)	Bottom water SO_4^{2-} renewal	$u_{WC} * ([SO^{2-}_{4,WC,BC}] - [[SO^{2-}_{4,WC}])$
(T3)	Bottom water Total S^{2-} renewal	$u_{WC} * ([Total\ S^{-2}_{WC,BC}] - [Total\ S^{-2}_{WC}])$

Table A17: Kinetic terms. Notice that all reactions are adjusted by a dimensionless temperature factor.

Kinetic terms
$R_{OR,TL} = R^{max}_{OR,ML} * ([O_2] - [O_{2,min}])$
$R_{OR,SL} = R^{max}_{OR,SL} * \frac{[O_2]}{K_{s,OR} + [O_2]}$
$R_{SR,SL} = R^{max}_{SR,SL} * \frac{[SO_4^{2-}]}{K_{s,SR} + [SO_4^{2-}]} * \frac{K_{in,SR}}{K_{in,SR} + [O_2]}$
$R_{IR,SL} = R^{max}_{IR,SL} * \frac{[Fe(OH)_{3,SL}]}{K_{s,IR} + [Fe(OH)_{3,SL}]} * \frac{K_{in,IR}}{K_{in,IR} + [O_2]}$

Table A18: Forcing functions.

Forcing functions	
Free-flow bottom current (u_{WC}): $u_{WC} = u_{WC,mean} * 1.025 * cos\left(1 + \left(\frac{2\pi * day\ of\ year}{tidal\ period} + \frac{\pi}{2}\right)\right)$	21
Shear or frictional velocity at the sea bed: $u_* = u_{WC} * \frac{\kappa}{\ln \frac{z_{BBL}}{z_0}}$	22
Shear stress exerted by u_{WC}: $\tau_u = \rho_{SW} * u_*^2$	23
Dispersion area (m^2) of organic waste in the water column: $D_{Waste} = Z_{WC} * \frac{u_{WC,mean}}{w_{pellet\ and\ feces}}$	24
Gross deposition of organic wastes ($\tau_u < \tau_c$): $Waste_{flux,SWI} = Waste_{dep} * \left(1 - \frac{\tau_u}{\tau_{cd}}\right)$	25
Erosion rate of organic wastes ($\tau_u > \tau_c$): $Waste_{flux,SWI} = k_{waste} * \left(\frac{\tau_u}{\tau_{ce}} - 1\right)$	26
Attenuation of bio-transport: $K_v = 1 - \frac{[Total\ S^{-2}]}{[Total\ S^{-2}_{ref}]}$	27
Partitioning factor of bacterial activity: $f_{OR} = \frac{[O_2]}{K_{s,OR} + [O_2]}$	28
$f_{SR} = \frac{[SO_4^=]}{K_{s,SR} + [SO_4^=]} * \frac{K_{in,SR}}{K_{in,SR} + [O_2]}$	29
$f_{IR} = \frac{[Fe(OH)_{3,SL}]}{K_{s,IR} + [Fe(OH)_{3,SL}]} * \frac{K_{in,IR}}{K_{in,IR} + [O_2]}$	30
$PF_{Bact,OR} = \frac{f_{OR}}{f_{OR} + f_{SR} + f_{IR}}$	31
$PF_{Bact,SR} = \frac{f_{SR}}{f_{OR} + f_{SR} + f_{IR}}$	32
$PF_{Bact,IR} = \frac{f_{IR}}{f_{OR} + f_{SR} + f_{IR}}$	33

Table A19: Model parameters.

Parameter	Description / Name	Values	Units	References
κ	Von Kárman constant.	0.4	dimensionless	(–)
$k_{Total\ S_{SL}^{-2},ox1}$	Sulphide oxidation reaction velocity with O_2	164.4	$cm^3 \mu mol^{-1} d^{-1}$	Boudreau (1996)
$k_{Total\ S_{SL}^{-2},ox2}$	Sulphide oxidation reaction velocity with $Fe(OH)_3$	274.0	$cm^3 \mu mol^{-1} d^{-1}$	Boudreau (1996)
$k_{Fe,ox}$	Oxidation rate of Fe^{2+} by reaction with O_2	109.6	$cm^3 \mu mol^{-1} d^{-1}$	Boudreau (1996)
k_{FeS_2}	Rate constant for FeS_2 formation from FeS	2.73e-6	d^{-1}	Boudreau et al. (1998)
k_{FeSppt}	Rate constant for FeS precipitation from Fe^{2+}	0.821	$cm^3 \mu mol^{-1} d^{-1}$	Boudreau et al. (1998)
k_{waste}	Erosion rate coefficient of organic C associated to fish farm wastes	194.2	$\mu mol\ C\ cm^{-2} d^{-1}$	Cromey, Nickell, & Black (2002)
u_{WC}	Bottom water velocity	0 – 23	$cm\ s^{-1}$	Specific for this study
w_s	Settling velocity of suspended POC	520	$cm\ d^{-1}$	Alber (2000)
w_{feed}	Sinking speed of feed pellets	10.89	$cm\ s^{-1}$	Stucchi et al. (2005)
w_{feaces}	Sinking speed of feces	3	$cm\ s^{-1}$	Stucchi et al. (2005)
z_{BBL}	Height above the bottom	100	cm	Specific for this study.
z_0	Bed roughness length	0.013-0.1	cm	Soulsby (1997)
Z_{WC}	Water column depth below fish cage	20	m	Specific for this study.
$D_{Total\ S^{-2}}$	Diffusion coefficient of dissolved sulfide in sediment at 14 °C.	0.78	$cm^2 d^{-1}$	Fossing et al. (2004)
$D_{Fe^{2+}}$	Diffusion coefficient of iron in sediment at 14 °C.	0.32	$cm^2 d^{-1}$	Fossing et al. (2004)
D_{O_2}	Diffusion coefficient of oxygen in sediment at 14 °C.	1.04	$cm^2 d^{-1}$	Fossing et al. (2004)
D_{SO_4}	Diffusion coefficient of sulfate in sediment at 14 °C.	0.48	$cm^2 d^{-1}$	Fossing et al. (2004)
D_b	Biodiffusion coefficient	0.15	$cm^2 d^{-1}$	Middelburg et al. (1997)
$Fe(OH)_{3,dep}$	$Fe(OH)_3$ deposition rate	0.0177	$\mu mol\ cm^{-2} d^{-1}$	Fossing et al. (2004)
$K_{s,OR}$	HSC for O_2 limitation in OM	0.004	$\mu mol\ cm^{-3}$	Pastor et al. (2011)
$K_{s,SR}$	HSC for $SO_4^=$ limitation in SR	1.6	$\mu mol\ cm^{-3}$	Shafei (2012)
$K_{s,IR}$	HSC for $Fe(OH)_3$ limitation in SR	2.45	$\mu mol\ cm^{-3}_{solid}$	Specific for this study
$K_{in,SR}$	HSC for O_2 inhibition in SR	0.01	$\mu mol\ cm^{-3}$	Specific for this study
$K_{in,IR}$	HSC for O_2 inhibition in IR	0.01	$\mu mol\ cm^{-3}$	Soetaert et al. (1996)
$K_{sp}FeS$	Solubility product constant of .FeS	0.0523	$(\mu mol\ cm^{-3})^2$	Boudreau (1996)
$POC_{flux,SWI}$	Natural POC deposition rate	2	$\mu mol\ C\ cm^{-2} d^{-1}$	Specific for this study
$R_{OR,ML}^{max}$	The aerobic decomposition coefficient in the water column	0.00524	$cm^4 \mu mol^{-1} d^{-1}$	Omori et al. (1994)
$R_{POC,SL}^{max}$	Maximum decay rate or particulate organic matter	2.73E-4	d^{-1}	Brigolin et al. (2009)
$R_{Waste,SL}^{max}$	Maximum decay rate or organic waste	0.0027	d^{-1}	Brigolin et al. (2009)
TAU_{ce}	Critical shear stress for resuspension of POC and fish farm wastes	0.0179	$N\ m^{-2}$	Cromey, Nickell, & Black (2002)
TAU_{cd}	Critical shear stress for deposition of POC and fish farm wastes	0.004	$N\ m^{-2}$	Cromey, Nickell, & Black (2002)
$[O_{2,min}]$	Limiting O_2 concentration for oxic mineralization in the water column	0.0625	$\mu mol\ cm^{-3}$	Specific for this study.
$[Total\ S_{ref}^{-2}]$	Toxic H_2S concentration for macrofauna	5	$\mu mol\ cm^{-3}$	Brigolin et al. (2009)
α_{BAC}	Transformation rate of POC into bacterial biomass	0.3	$cm^3\ (umol\ C)^{-1}$	Talin et al. (2003)
w_{sed}	Burial rate of POC and solids	7.123e-4	$cm\ d^{-1}$	Omori et al. (1994)
λ_{BAC}	Bacteria biomass to POC ratio	2.52e-4	$cm^3\ (umol\ C)^{-1}$	Talin et al. (2003)
$\gamma OR_{O_2}^{POC}$	Mole O_2 reduced per mole of POC oxidized	1.3	$mol\ O_2\ (mol\ C)^{-1}$	Pastor et al. (2011), Soetaert et al. (1996)
$\gamma RO_{O_2}^{Total\ S^{2-}}$	Mole of O_2 reduced per mole of Total S^{2-} oxidized	2	$mol\ O_2\ (mol\ Total\ S^{2-})^{-1}$	Pastor et al. (2011), Soetaert et al. (1996)
$\gamma RO_{O_2}^{Fe^{2+}}$	Mole of Fe^{2+} oxidized per mole of O_2 reduced	4	$mol\ Fe^{2+}\ (mol\ O_2)^{-1}$	Pastor et al. (2011), Soetaert et al. (1996)
$\gamma SR_{SO_4^=}^{POC}$	Mole of $SO_4^=$ reduced per mole of POC oxidized	0.5	$mol\ SO_4^=\ (mol\ C)^{-1}$	Pastor et al. (2011), Soetaert et al. (1996)
$\gamma IR_{Fe^{2+}}^{POC}$	Mole of $Fe(OH)_3$ reduced per mole of POC oxidized	4	$mol\ Fe^{2+}\ (mol\ C)^{-1}$	Specific for this study
$\gamma RO_{Fe(OH)_3}^{H_2S}$	Mole of Total S^{2-} oxidized per mole of $Fe(OH)_3$ reduced to particulate S (S^0)	0.5	$mol\ Total\ S^{2-}\ (mol\ Fe(OH)_3)^{-1}$	Specific for this study
φ	Sediment porosity	0.8	dimensionless	Specific for this study
ρ	Sediment density	2.45	$g\ cm^{-3}$	Specific for this study
ρ_{SW}	Seawater density	1.027	$g\ cm^{-3}$	Specific for this study
ν	Exchange velocity of solutes due to bioturbation	3	$cm\ d^{-1}$	Hammond & Fuller (1979)

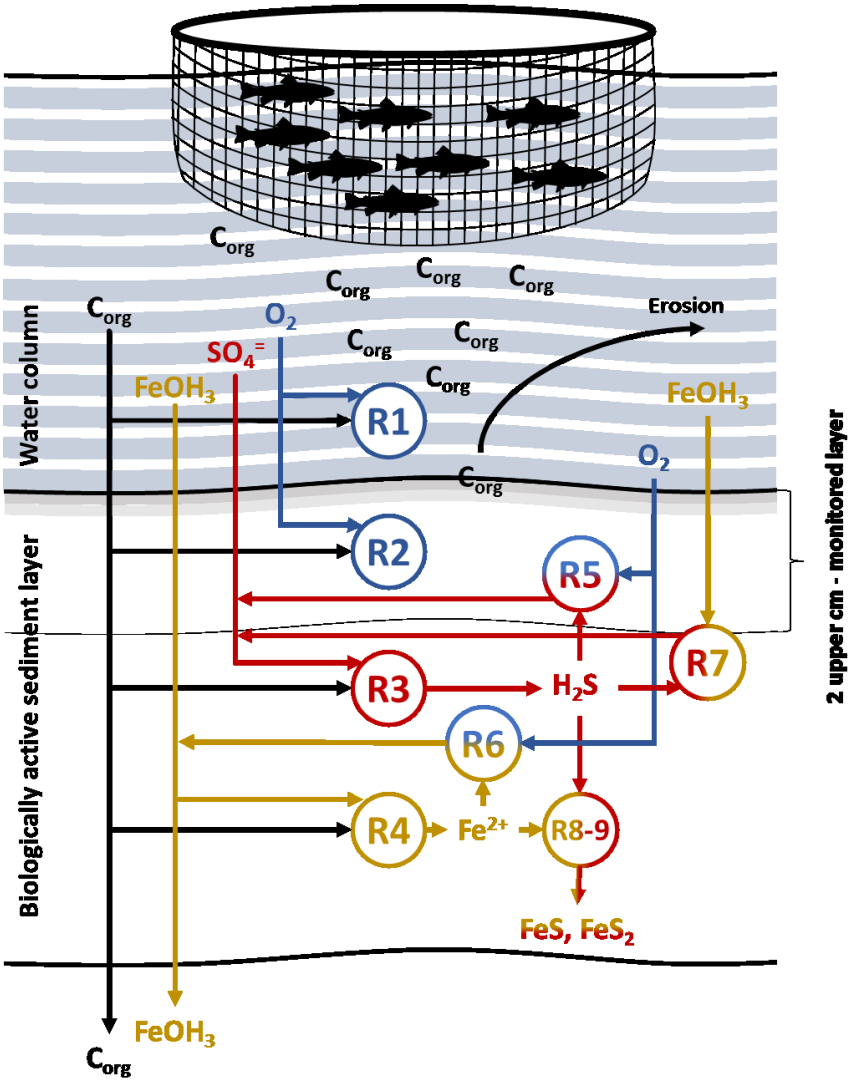

Figure A32: Conceptual model representation.

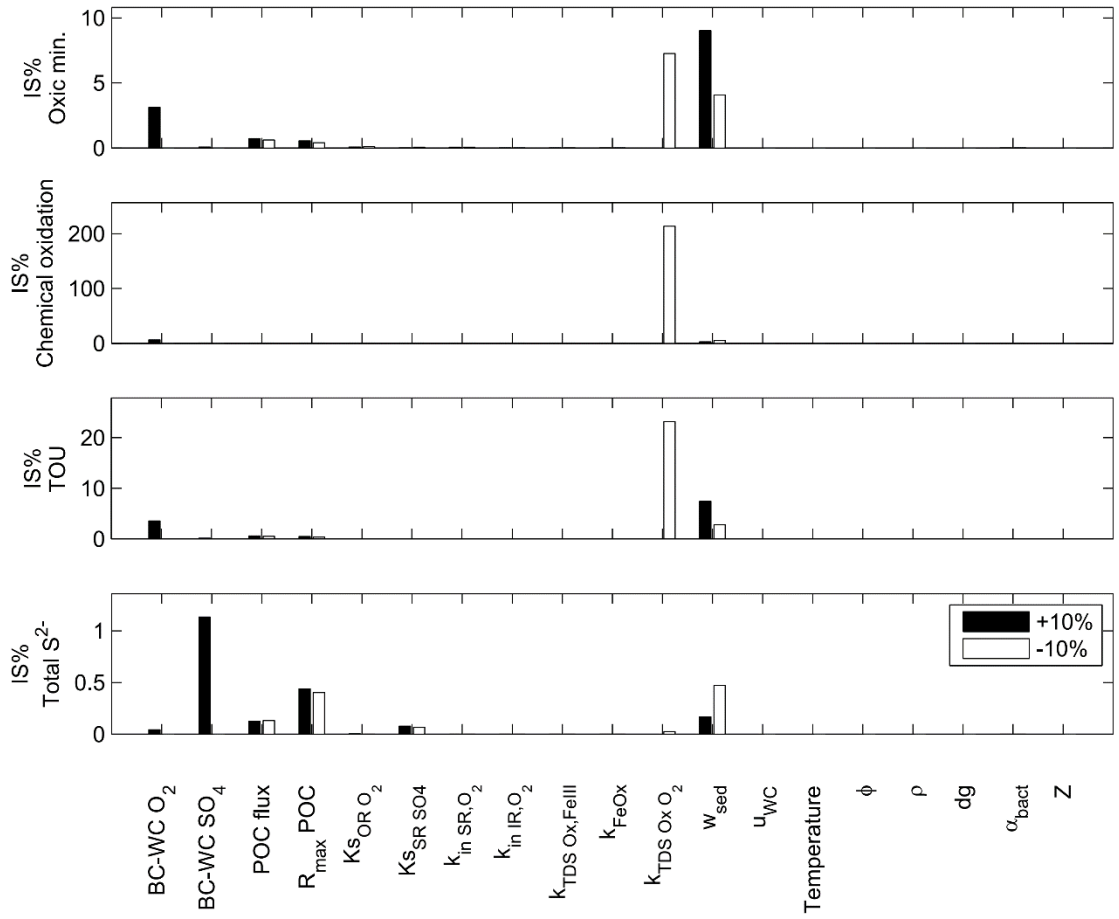

Figure A33: Sensitivity of state variables to +/- 10% changes in model parameters. Positive IS% values means that changes in model parameter increase state variable, and vice versa. Increase in state variable is observed.

Table A20. Model parameters tested for sensitivity. Ranges of variation of model parameters were defined from literature and natural ranges of oscillation in coastal waters (solute concentrations and POC deposition).

Parameter	Min	Max	Range	Units	Description
O_2 BC-WC	0	300	300	umol cm^{-3}	Far field O_2 in water column
SO_4 BC-WC	0	28	28	umol cm^{-3}	Far field O_2 in water column
POC flux	0	13.68	13.68	umol cm^{-2} d^{-1}	Ambient POC deposition
R_{max} POC	2.74E-06	0.0002	0.0003	d^{-1}	Degradation rate POC
Ks_{OR} O_2	1.00E-03	0.01	0.009	umol cm^{-3}	HSC for O_2 limitation in oxic respiration.
Ks_{SR} SO_4	0.05	1.6	1.55	umol cm^{-3}	HSC for SO_4 limitation in SR.
$K_{in,SR}$ O_2	1.00E-03	0.01	0.009	umol cm^{-3}	HSC for O_2 inhibition of SR
$K_{in,IR}$ O_2	1.00E-03	0.01	0.009	umol cm^{-3}	HSC for O_2 inhibition of IR
$k_{TDS,Ox}$ FeIII	2.74E-02	273.79	273.76	cm^3 $umol^{-1}$ d^{-1}	Rate constant for sulfide oxidation by FeIII
k_{FeOx}	273.90	2739.70	2465.8	cm^3 $umol^{-1}$ d^{-1}	Rate constant for Fe^{2+} oxidation by O_2
$k_{TDS,Ox}$ O_2	0.8767	4.38E+03	4382.72	cm^3 $umol^{-1}$ d^{-1}	Rate constant for sulfide oxidation by O_2
w	0.0002	0.0275	0.0271	cm d^{-1}	Burial rate at the sediment water interface
u_{WC}	259200	950400	691200	cm d^{-1}	Free-stream bottom current
Temperature	5	15	10	°C	Temperature
ρ	0.5	0.9	0.4	-	Sediment porosity
ρ	1.5	2.5	1	g of sediment cm^{-3} of dry sediment	Sediment density
dg	0.044	0.35	0.306	mm	Grain size diameter
α_{bact}	0.2	0.4	0.2	cm^3 $(umol\ C)^{-1}$	Transformation rate of POC into bacterial biomass
Z	50	100	50	cm	Height of BBL